Interaction of Ln(III) and An(III/IV/V/VI) with borate in dilute to concentrated NaCl, $CaCl_2$ and $MgCl_2$ solutions

Zur Erlangung des akademischen Grades eines

DOKTORS DER NATURWISSENSCHAFTEN

(Dr. rer. nat.)

Fakultät für Chemie und Biowissenschaften

Karlsruher Institut für Technologie (KIT)-Universitätsbereich

genehmigte

DISSERTATION

von

Dipl. Chem. Katja Hinz

aus

Karlsruhe, Deutschland

Dekan: Prof. Dr. Willem Klopper

Referent: Prof. Dr. Horst Geckeis

Korreferent: Prof. Dr. Petra Panak

Tag der mündlichen Prüfung: 23.10.2015

Erklärung / Declaration of Originality

Hiermit versichere ich, dass ich die vorliegende Arbeit selbstständig verfasst und keine anderen als die angegebenen Quellen und Hilfsmittel verwendet habe. Darüber hinaus versichere ich, dass alle Stellen der Arbeit, die wörtlich oder sinngemäß aus anderen Quellen übernommen wurden, als solche kenntlich gemacht sind und dass die Arbeit in gleicher oder ähnlicher Form noch keiner Prüfungsbehörde vorgelegt wurde. Die Satzung des Karlsruher Instituts für Technologie (KIT) zur Sicherung guter wissenschaftlicher Praxis wurde in der jeweils gültigen Fassung beachtet.

Datum, Ort Unterschrift

Acknowledgement/ Danksagung

Die vorliegende Dissertation wurde im Zeitraum von April 2012 bis Oktober 2015 unter der Leitung von Herrn Prof. Dr. Horst Geckeis am Institut für Nukleare Entsorgung am Karlsruher Institut für Technologie durchgeführt. Ich möchte Prof. Dr. Horst Geckeis für die interessante Themenstellung, die zahlreichen fachlichen Diskussionen und die wissenschaftliche Unterstützung und Betreuung meiner Arbeit danken.

Bei Prof. Dr. Petra Panak möchte ich mich für die Übernahme des Korreferats bedanken.

Dr. Marcus Altmaier danke ich für die hervorragende fachliche Betreuung, produktive Kritik und experimentellen Ideen, welche diese Arbeit ermöglicht haben.

Weiterhin möchte ich mich besonders bei Dr. Xavier Gaona für die großartige Unterstützung, zahlreichen fachlichen Diskussionen, Ratschläge und Hilfsbereitschaft bedanken.

Dr. David Fellhauer danke ich sehr für die fachliche Unterstützung dieser Arbeit. Dr. Thomas Rabung möchte ich für die Diskussionsbereitschaft, Ratschläge und konstruktive Kritik danken.

Für praktische und theoretische Unterstützung möchte ich mich weiterhin insbesondere bei Dr. Marika Vespa und Dr. Kathy Dardenne (stellvertretend für die EXAFS-Gruppe des KIT-INE), Dr. Dieter Schild, Dr. Nicolas Finck, Christian Adam (alle KIT-INE), Dr. Peter Kaden (HZDR), sowie Dr. Donald T. Reed und Dr. Michael Richmann (LANL-CO/USA) und Dr. Evgeny Alekseev (FZJ) bedanken.

Für ihre Hilfsbereitschaft und die Durchführung chemischer Analysen danke ich weiterhin Melanie Böttle, Stephanie Heck, Frank Geyer, Tanja Kisely, Cornelia Walschburger, Annika Kaufmann (KIT-INE) und der Werkstatt des KIT-INE.

Besonderer Dank geht an alle Mitglieder der aquatischen Chemie und Thermodynamik von Actiniden für ihre Unterstützung bei experimentellen Arbeiten, fachlichen und nicht fachlichen Diskussionen sowie einer sehr angenehmen Arbeitsatmosphäre.

Gerd Christill, Thorsten Hoffmann und Ilonca Bachmann danke ich für die Unterstützung bei Arbeiten im Kontrollbereich.

Zuletzt möchte ich mich bei meiner Familie, meinen Freunden und besonders bei meinem Freund Andreas für die große Unterstützung bedanken.

Abstract

In this PhD thesis, the interaction of borate with lanthanides (III) and actinides (III, IV, V, VI) is investigated in dilute to concentrated saline solutions. An accurate knowledge of the aquatic chemistry and solubility of these systems is highly relevant for the long-term performance assessment of repositories for nuclear waste disposal. The investigation of lanthanide and actinide behaviour in concentrated brines (besides dilute solutions) provides key inputs for the assessment of nuclear waste disposal in salt rock formations, but also allows deriving more accurate thermodynamic and activity models to be used in geochemical calculations.

Boron can be present as component of the emplaced waste in a nuclear waste repository. In certain rock salt formations, high boron concentrations can also occur in the intruding brine solutions. In this framework, it is very relevant to understand the impact of borate in the chemical behaviour of actinides (e. g. complexation, solubility phenomena or redox processes) under repository relevant conditions. In spite of this, only a limited number of studies on the interaction of borate with lanthanides and actinides are reported in the literature. This is also reflected by the absence of any thermodynamic data selection for actinide–borate aqueous complexes or solid compounds in the current NEA–TDB reviews. In order to gain a better understanding of the processes taking place in the Ln(III)– and An(III, IV, V, VI)–borate systems, comprehensive solubility experiments in combination with spectroscopic studies and a detailed solid phase characterization were performed in this PhD work under repository-relevant conditions.

The interaction Ln(III)– and An(III, IV, V, VI) with borate is investigated with a comprehensive series of solubility experiments in dilute to concentrated NaCl, $CaCl_2$ and $MgCl_2$ solutions, in combination with a detailed solid phase characterization using XPS, XRD, SEM–EDS and synchrotron-based spectroscopic techniques (XANES and EXAFS). These are also complemented with a characterization of the aqueous phase with spectroscopic techniques such as TRLFS and UV–Vis/NIR. Nd(III)/Cm(III), Th(IV), Np(V) and U(VI) have been taken as representatives of actinides in oxidation states +III, +IV, +V and +VI to assess the influence of borate. The study of Pu(III/IV) under near-neutral pH conditions has been purposely targeted to assess the impact of borate on a redox-sensitive radionuclide under repository-relevant conditions.

Cm(III)–TRLFS confirms the unequivocal formation of weak Cm(III)–borate complexes under near-neutral pH-conditions and $[B]_{tot} \geq 0.04$ M. In spite of this, no significant increase in the Nd(III) solubility occurs in any of the investigated systems up to $[B]_{tot} = 0.4$ M. On the contrary, a significant decrease in the solubility of Nd(III) is observed at $pH_m \leq 9$ in NaCl and $MgCl_2$ systems with $[B]_{tot} \geq 0.16$ M. This observation together with a clear change in the slope of the solubility curve indicates the transformation of $Nd(OH)_3$(am) into a so far unknown Nd(III)–borate secondary phase. SEM–EDS and XPS confirm that this solid phase is formed on the surface of the $Nd(OH)_3$(am)

particles and has a stoichiometric contribution of boron (Nd / B ratio of 1:4.5 – 1:1 depending on background electrolyte and concentration).

As for Ln(III)/An(III), UV–vis/NIR clearly indicates the formation of weak Np(V)–borate complexes under weakly alkaline pH-conditions, with the likely participation of $B(OH)_4^-$ in the complex formation. Similarly to Nd(III), the formation of Np(V)–borate complexes has only a minor impact on the solubility of Np(V) under near-neutral to weakly alkaline pH-conditions. On the contrary, a very significant drop in the Np(V) solubility (3 to 4 orders of magnitude) is observed in NaCl and dilute $MgCl_2$ solutions with $[B]_{tot} = 0.16$ M and $pH_m \leq 9$. The drop in the solubility is accompanied by a clear change in the colour of the solid phase (from green to white). XRD, XPS, SEM–EDS and EXAFS confirm the formation of the previously unreported solid phases $NpO_2[B_5O_6(OH)_4]\cdot 2NaOH(cr)$ and $(NpO_2)_2[B_5O_6(OH)_4]_2\cdot 3Mg(OH)_2(cr)$. The absence of precipitation in concentrated $MgCl_2$ solutions is rationalized with the competition of Mg^{2+} and NpO_2^+ for the complexation with borate.

Additional solubility experiments with Th(IV) and U(VI) were performed in dilute to concentrated saline solutions in NaCl and $MgCl_2$ solution with various boron concentrations at $6.5 \leq pH_m \leq 9$. Hence, borate has a minor impact on the solubility of Th(IV) in the investigated systems, especially in view of the large overall uncertainties affecting the solubility of this actinide under alkaline pH conditions, both in the absence and presence of borate. In concentrated NaCl and $MgCl_2$ solutions, a slight increase of the Th(IV) solubility is found with high boron concentrations and a minor effect of borate on Th(IV) speciation cannot be excluded. The lesser influence of borate on Th(IV) compared to tri- or pentavalent actinides is explained by the high tendency of tetravalent actinides towards hydrolysis, which outcompetes borate complexation under most of the investigated experimental conditions.

Borate increases the solubility of U(VI) in NaCl solutions with $pH_m \geq 9$ and (in lesser extent) in $MgCl_2$ solutions with $pH_m \approx 7.5$ due to the formation of U(VI)–borate aqueous complexes. No complexation phenomena are observed at $pH_m \leq 6.5$ where $B(OH)_3(aq)$ prevails in solution, in line with the consideration of $B(OH)_4^-$ as ligand counterpart in the U(VI)–borate complex formation. In contrast to Nd(III) and Np(V), no solubility decrease caused by a solid phase transformation is observed in the U(VI) system in the presence of borate over the investigated timescale. This observation is explained by the significantly lower solubility, i.e. higher stability, of $Na_2U_2O_7\cdot H_2O(cr)$ compared to $Nd(OH)_3(am)$ and $NpO_2OH(am,fresh)$ at $pH_m = 7–8$, which makes unlikely its transformation into a hypothetical U(VI)-borate solid phase. In line with the experimental observations collected for Nd(III)/Cm(III) and Th(IV), borate has a minor impact on the chemistry of Pu under redox conditions where Pu(IV) prevails. In those redox conditions where Pu(III) forms, the decreased solubility with respect to $Pu(OH)_3(s)$ combined with the predominance of Pu(III) in the solid phase confirmed by XPS hint towards the formation of a Pu(III)–borate coating or solid phase transformation similar to the findings obtained for Nd(III) under analogous experimental conditions.

The comprehensive work undertaken within this PhD thesis provides key inputs for the source term estimation of An(III, IV, V, VI) in the presence of borate under repository-relevant conditions. In the case of Ln(III)/An(III) and An(V), preliminary thermodynamic models have been also derived. These are clearly restricted by the several assumptions taken in the model development, which affect not only An–borate interaction but also reflect the relevant uncertainties holding for the aquatic chemistry of borate. These models provide a first workable tool for a rough thermodynamic estimation of An–borate interactions in waste disposal scenarios.

Kurzfassung

Im Rahmen dieser Dissertation wurden erstmals systematische Untersuchungen zur Wechselwirkung von Actiniden (III, IV, V, VI) und Lanthaniden(III) mit Borat in verdünnt bis konzentrierten aquatischen Salzlösungen durchgeführt. Bor kann über zutretendes Wasser, den endgelagerten Abfall oder als Bestandteil des Wirtsgesteins selbst in ein Endlager eingebracht werden und stellt einen potentiell komplexbildenden Liganden für Radionuklide dar. Untersuchungen in konzentrierten Salzlösungen mit Actiniden sind von hoher Relevanz hinsichtlich eines möglichen Endlagers in Salzgesteinsformationen, bzw. in Salztonformationen. Es ist somit von großer Bedeutung den Einfluss von Borat auf das chemische Verhalten von Actiniden unter endlagerrelevanten Bedingungen zu untersuchen und spezifische Rückhaltemechanismen zu identifizieren und quantifizieren. Im Rahmen der hier vorliegenden Doktorarbeit konnte der Kenntnisstand zu dieser relevanten Thematik, wie nachfolgend dargestellt, endscheidend erweitert und ein signifikant verbessertes wissenschaftliches Prozessverständnis entwickelt werden.

Trivalente Actiniden: TRLFS Messungen mit Cm(III) bestätigen die Bildung schwacher Ln(III)/An(III)-Boratkomplexe in der wässrigen Phase bei pH_m = 8 und $[B]_{tot} \geq 0.04$ M. Ungeachtet dessen wurde keine deutliche Löslichkeitserhöhung in den untersuchten Systemen mit Nd(III) mit $[B]_{tot}$ bis zu 0.4 M beobachtet. Es trat hingegen ein deutliches Absinken der initial durch $Nd(OH)_3(am)$ kontrollierten Nd(III)-Löslichkeit in NaCl und $MgCl_2$-Lösungen bei $pH_m \leq 9$ und $[B]_{tot} \geq 0.16$ M auf. SEM-EDS und XPS bestätigen die Bildung einer neuen borathaltigen Nd(III)-Festphase auf der Oberfläche der $Nd(OH)_3(am)$-Festphase, was einen bisher nicht erkannten, neuen potentiellen Retentionsmechanismus für trivalente Radionuklide darstellt.

Pentavalente Actiniden: Mithilfe von UV-Vis/NIR Messungen wurde die Bildung schwacher Np(V)-Boratkomplexe, mit $B(OH)_4^-$ als wahrscheinlichem Liganden, bei pH_m = 8-9 und $[B]_{tot} \geq 0.04$ M nachgewiesen. Wie im Falle der Untersuchungen mit Ln(III)/An(III) haben diese jedoch keinen signifikanten Einfluss auf die Np(V)-Löslichkeit im untersuchten pH-Bereich. Ein deutliche Abnahme der Np(V)-Löslichkeit zusammen mit einer sichtbaren Umwandlung der ursprünglichen löslichkeitskontrollierenden Np(V)-Festphase trat in NaCl- und verdünnten $MgCl_2$-Lösungen bei $pH_m \leq 9$ und $[B]_{tot}$ = 0.16 M auf. XRD, XPS, SEM–EDS und EXAFS Untersuchungen bestätigen die Bildung von zwei neuen Np(V)-Boratfestphasen mit der Stöchiometrie $NpO_2[B_5O_6(OH)_4]\cdot 2NaOH(cr)$ und $(NpO_2)_2[B_5O_6(OH)_4]_2\cdot 3Mg(OH)_2(cr)$. Aufgrund dieser bisher unbekannten Umwandlung des löslichkeitsbestimmenden Np(V)-Bodenkörpers in eine wesentlich weniger lösliche sekundäre Np(V)-borat-Festphase kann es in bestimmten endlagerrelevanten Systemen potentiell zu deutlich niedrigeren Np(V) Löslichkeiten kommen als bisher angenommen.

Tetravalente Actiniden: Löslichkeitsexperimente mit Th(IV), durchgeführt in NaCl- und $MgCl_2$-Lösungen und $[B]_{tot}$ = 0.16 M, zeigten im untersuchten pH_m-Bereich 6.5.-11keinen eindeutigen Effekt

von Borat auf die Th(IV) Löslichkeit. Lediglich in hochkonzentrierten NaCl- und $MgCl_2$-Lösungen wurde auf Basis der neuen experimentellen Daten ein geringer Löslichkeitsanstieg in Gegenwart von $[B]_{tot}$ = 0.16 M diskutiert, was ggf. eine schwache Wechselwirkung zwischen Borat und Th(IV) unter diesen speziellen Bedingungen nahelegt.

Hexavalente Actiniden: Ein Anstieg der U(VI)-Löslichkeit wurde in NaCl-Lösungen in Gegenwart von $[B]_{tot}$ = 0.16 bei $pH_m \geq 9$ und (weniger ausgeprägt) in $MgCl_2$-Lösungen bei $pH_m \approx 7.5$ beobachtet und mit der Bildung aquatischer U(VI)–Boratkomplexe korreliert. Eine Verringerung der U(VI)-Löslichkeit aufgrund einer Festphasentransformation in Gegenwart von Borat, analog zu Untersuchungen mit Nd(III) und Np(V), wurde im Rahmen des Untersuchungszeitraums nicht beobachtet.

Plutonium: Erste Untersuchungen im komplexen Plutonium-System zeigen, dass unter Redoxbedingungen, in welchen Pu(IV) vorliegt, Borat keinen eindeutigen Einfluss auf die Pu-Löslichkeit hat, übereinstimmend mit den Untersuchungen mit Th(IV) in dieser Arbeit. In stärker reduzierendem Milieu, in welchem Pu(III) gebildet wird, deutet die in Bezug auf $Pu(OH)_3(s)$ niedrige Pu-Löslichkeit bei Anwesenheit von Borat sowie und das Vorliegen von hauptsächlich Pu(III) in der löslichkeitsbestimmenden Festphase auf die Bildung einer neuen Pu(III)-Boratfestphase analog zu Untersuchungen mit Nd(III) in dieser Arbeit hin. Auf Basis dieses Befundes wird ein neuer potentieller Retentionsmechanismus für Plutonium in stark reduzierenden borathaltigen aquatischen Systemen wahrscheinlich.

Radionuklid-Quelltermableitungen: Die durchgeführten Arbeiten dieser Dissertation liefern für verschiedene Ionenstärken und verschiedene endlagerrelevanten wässrige Systeme belastbare experimentelle Daten zur An(III, IV, V, VI)–Löslichkeiten in Gegenwart von Borat. Auf Basis der in dieser Arbeit erarbeiteten empirischen Löslichkeitsdaten in aquatischen Systemen bei Anwesenheit von Borat, sind Radionuklid-Quelltermableitungen für entsprechende Szenarien in Zukunft auf einem eindeutig verbesserten wissenschaftlichen Niveau möglich. Für trivalente und pentavalente Actiniden konnte zudem erstmalig ein löslichkeitserniedrigender Prozess basierend auf einer bisher nicht bekannten Festphasenumwandlung im aquatischen borathaltigen System aufgedeckt werden. Für Ln(III)/An(III) und An(V) wurden erste vorläufige thermodynamische Modelle erstellt, welche perspektivisch eine modellbasierte, verbesserte Beschreibung der Actinid-Borat-Wechselwirkung in wässrigen Systemen erlauben.

Table of Contents

1 Introduction

1.1 Background of the work

Radioactive waste containing long-lived radionuclides is mainly generated in nuclear power plants, but also in the fabrication of nuclear fuel, reprocessing plants, dismantling of nuclear weapons, medical applications and nuclear research. The composition of this waste is strongly dependent on the source, and eventually includes actinides (U, Np, Pu, Am, etc.), fission products (^{99}Tc, ^{79}Se, etc.) and activation products (^{59,63}Ni, ^{60}Co, etc.). This radioactive waste needs to be safely disposed to avoid any exposure to humans and the environment.

Deep geological repositories are generally accepted by the international scientific community as the safest option for the disposal of radioactive waste. These repositories are normally planned within 250–1000 m underground in stable host rock formations. Three well established options are considered: crystalline (granite), clay rock and salt rock. The selection of the host rock material varies among countries depending on natural availability [1-3].

Crystalline formations are the most common rock formation. The advantages of granite include its mechanical stability, low solubilites of rock forming minerals and low heat sensitivity. On the other hand, its fractured structure provides natural pathways for the migration of solutions and gases to the environment, thus emphasizing the need for technical barriers. In several countries (e.g. Sweden, Finland) granite has been chosen as host rock formation for the disposal of radioactive waste [2].

Clay formations and clay minerals are considered as host rock material because of their high sorption capacity and sealing properties in contact with water. Hence, the swelling of clay minerals in contact with water prevents the intrusion and migration of water in and out of the nuclear waste repository. Several countries have selected clay formations as host rock for deep geological disposal like Switzerland, France and Belgium [2].

Salt rock formations provide many advantages such as self-sealing features, high temperature resistance and good self-healing properties. A nuclear waste repository located in salt rock is expected to be dry. On the other hand salt rock provides a limited actinide retention capacity, in case of water access and thus the knowledge of the solubility and sorption processes onto secondary mineral phases occurring in saline systems is needed for the safety assessment of a nuclear waste repository in salt rock. Repositories in salt rock formations are under consideration or already in operation in Germany (Morsleben) and USA (WIPP, Carlsbad New Mexico).

The assessment of the long-term safety of a nuclear waste repository requires the evaluation of the potential scenario of water intrusion and the consequent contact of the intruding water with the emplaced waste. Such a scenario may lead to the mobilization of radionuclides into the biosphere, and consequently needs to be properly investigated. The knowledge of the solution processes taking place in the geochemical conditions found in a nuclear waste repository is especially important. The speciation of actinides, redox transformations, colloid formation, sorption/precipitation and desorption/dissolution phenomena are strongly dependent upon composition of the intruding water, host rock material and waste forms, and need to be properly understood for the long term performance assessment of a repository for radioactive waste disposal.

Groundwater and the pore water resulting after its interaction with geotechnical barriers and the waste containers contain dissolved salts. In the particular case of rock salt formations, highly saline brines (mainly NaCl and $MgCl_2$ with 5 M < I < 15 M) can potentially form. In cementitious environments, the corrosion of cement in concentrated $MgCl_2$ brines can also lead to highly concentrated $CaCl_2$ solutions [4]. Whereas the pH in NaCl dominated brines is not limited, in $MgCl_2$ and $CaCl_2$ the maximum pH is limited to pH_{max} = 9 and 12 due to the precipitation and consequent pH buffering of magnesium and calcium hydroxides or hydroxo-chlorides, respectively [5].

The aqueous chemistry of actinides in these high saline conditions is significantly altered and cannot be derived from diluted systems. Hence, ion interaction processes influence the stability of actinides in solution. Furthermore, the presence of high concentrations of background cations and anions can lead to complexation or precipitation phenomena therefore resulting in a very different chemical behavior. To understand and predict the behavior of actinides under these conditions, systematic experiments in well-defined saline solutions are needed.

Corrosion of iron steel canisters, emplaced as storage canisters in a repository is expected to cause strongly reducing conditions and production of H_2(g) affecting the oxidation state of actinides. The released Fe(II)(aq) and the formation of Fe(II)-bearing solid phases will buffer the Eh in a repository to very reducing conditions. Fe(II)(aq) and the corresponding secondary phases have a very significant impact on redox transformations and sorption processes and therefore have to be considered in the prediction of the migration behavior of actinides.

Boron can be present in repositories for radioactive waste disposal as component of the emplaced waste inventory. In repositories in rock salt formations, boron can further be a component of the intruding brine solutions. Large borax ($Na_2[B_4O_5(OH)_4]\cdot 8H_2O$) deposits are found at the Salado rock-salt formation in New Mexico leading to relatively high boron concentrations (up to 0.045 M) [6] relevant for the WIPP project. Although the aqueous chemistry of actinides under repository-relevant conditions is mostly dominated by hydrolysis reactions, the role of other inorganic and organic ligands in complexing (and thus potentially mobilizing) actinides needs to be assessed properly. In contrast to

carbonate, phosphate or sulphate, little attention has been dedicated so far to the possible complexation of borate species with actinides.

1.2 Basic knowledge and aquatic chemistry of An(III/IV/V/VI)

The chemical elements with the atomic numbers Z = 90–103 are referred to as actinides. The elements in this series are characterized by the occupancy of the 5f orbitals, starting with thorium (Z = 90). All actinides are radioactive and have no stable isotopes. In contrast to the lanthanides which are mainly present in the trivalent oxidation state, actinides have various thermodynamically stable oxidation states. The aquatic chemistry of actinides has been intensively studied over the last decades including fundamental studies, actinide coordination chemistry, complex formation with inorganic and organic ligands, structural investigations of aqueous and solid An phases, migration and retention reactions, among others [7-10]. The aquatic chemistry of actinides is mainly controlled by three key processes:

- Actinide redox processes that define the dominant oxidation state in solution.
- Solubility phenomena: solid actinide phases can form under given boundary conditions, thus defining upper limit concentrations for this actinide.
- Complexation reactions with inorganic or organic ligands in solution can influence the stability of a given actinide and redox state, and consequently impact its solubility and alter its sorption properties.

These key processes must be properly understood to adequately describe the chemistry of An in aqueous systems. Furthermore, the impact of additional parameters such as ionic strength or temperature, among others, or the effect of kinetics and microbial activity need to be assessed.

In aqueous systems, actinides are stable in oxidized forms and therefore lose electrons from their highest orbitals 5f, 6d and 7s. The most stable electron configuration is that of the closest rare gas, radon for actinides. With the same electron configuration as radon, actinides are found as Th(IV), Pa(V) and U(VI), respectively. Np(VII) is extremely oxidized and it is not stable in aqueous solution, except in highly alkaline and oxidizing conditions. Th(IV) is the only stable oxidation state for thorium in water and this actinide is redox-insensitive. Heavier actinides can also be stable in their trivalent and tetravalent states with more electrons in their outer shell than radon, and with a partial occupation of the 5f and 6d atomic orbitals. Oxidation states stabilized in aqueous systems for the most relevant actinides in the context of waste disposal are summarized in Table 1.1. The table also highlights the most stable redox state for each actinide.

Table 1.1. *Oxidation states stable in aqueous systems for a selection of actinides relevant in the context of waste disposal. Numbers highlighted in red correspond to the most stable oxidation state of each actinide. Numbers in brackets indicate less stable oxidation states.*

Th	Pa	U	Np	Pu	Am	Cm
		6	**(6)**	**6**		
	5	**(5)**	**5**	**5**	**5**	
4	**4**	**4**	**4**	**4**	**(4)**	**(4)**
		(3)		**3**	**3**	**3**

While An(III) and An(IV) form aquo ions An^{3+} and An^{4+}, An(V) and An(VI) are not stable as simple cations in solution. On the contrary, both redox states form dioxocations AnO_2^+ and AnO_2^{2+}, the so called actinyl ions. This applies to U, Np, Pu and Am but not to Pa(V), for which PaO_3^+ is defined as most stable species under acidic conditions [11, 12]. The actinyl ions are linear as a consequence of the covalent An=O double bond. Charge density transfer from the metal cation to the oxygen atoms in this structures leads to an effective charge (Z_{eff}) of 2.3 and 3.3 for AnO_2^+ and AnO_2^{2+}, respectively [13, 14]. All An cations can be considered as hard Lewis acids and are therefore strong electron acceptors [15]. They tend to interact with strong electron donors as hydroxide or carbonate in solution. The strength of an actinide complex is thus correlated with on the effective charge of the An cation with An(IV) forming the most stable complexes and An(V) the weakest

An(IV) > An(VI) > An(III) > An(V)

The oxidation state of an actinide is one of the most relevant factors determining its chemistry in aqueous solution. In this respect, actinides in the same oxidation state show similar chemical behavior and are often considered as analogs. These analogies can be used to assess thermodynamic properties of actinides with more complex aqueous chemistry such as plutonium. For instance, Am(III) or the lanthanides Eu(III) and Nd(III) are often used as analogs of Pu(III), which shows a much complex redox chemistry. Cm(III) is also often used as a relevant probe for the investigation of An(III) due to its very favorable fluorescence properties which allow speciation studies at very low concentrations (10^{-8} M and below, depending upon matrix composition). With this analogy concept, it is possible to estimate activity coefficients and also complex formation constants for aqueous species. On the contrary, thermodynamic data for solid phases cannot be derived (or only with very large uncertainties) based on the analogy concept. This is mainly due to the fact that small changes in the

ionic radii can lead to pronounced changes in the stability of a solid and therefore the solubility product.

Some actinides (especially U, Np and Pu) are characterized by the possible coexistence of several oxidation states in aqueous solutions. In the case of plutonium, up to four oxidation states can simultaneously exist under acidic conditions. Redox processes are also affected by kinetic effects. Some redox reactions e.g. between An^{3+}/An^{4+} or AnO_2^{+}/AnO_2^{2+} are very fast, whereas the transformation between An^{4+}/AnO_2^{+} is slow due to required breaking/formation of the actinyl bond.

In aqueous solution americium is mainly stable as Am(III). Am(V) is only stabilized in alkaline solutions under oxidizing conditions [16]. In aqueous systems, neptunium is mainly stable in tetravalent and pentavalent redox states with Np(V) as the most stable oxidation state. Tri- and hexavalent Np species are not relevant in the conditions expected in deep underground repositories for radioactive waste disposal. Uranium is mainly stable as U(IV) and U(VI). In slightly acidic and weakly reducing conditions, U(V) has a small stability field but a long term stability of U(V) is under discussion [17-20]. Compared to Np(IV), stronger reducing conditions are needed for the stabilization of U(IV). In the case of Pu, all oxidation states from three to six are present and have relatively large stability fields within the stability field of water. Under conditions in environmental aqueous systems, tetravalent and pentavalent Pu species are dominating. Under strongly reducing conditions as expected in most nuclear waste disposal concepts, Pu(III) becomes also relevant under near-neutral to weakly alkaline pH-conditions.

1.2.1 Solubility and hydrolysis of actinides

In the absence of other complexing ligands, the aquatic chemistry of actinides is dominated by hydrolysis species and oxy-hydroxide solid phases. An(IV) show the strongest hydrolysis and form sparingly soluble amorphous oxy-hydroxides, whereas An(V) have the weakest hydrolysis and form amorphous oxy-hydroxides with significantly higher solubility. An(III) and An(VI) lie in between regarding strength of hydrolysis and solubility of the corresponding oxy-hydroxides, principally due to the very similar effective charge of An^{3+} (Z_{eff} = 3) and AnO_2^{2+} (Z_{eff} = 3.2). Both An(V) and An(VI) show an amphoteric behavior (formation of positively and negatively charged hydrolysis species), whereas $An(OH)_3(aq)$ and $An(OH)_4(aq)$ are the most stable hydrolysis species of An(III) and An(IV), respectively, under alkaline to hyperalkaline pH conditions.

Solubility of An oxy-hydroxides and hydrolysis equilibria can be described as a function of H^+/H_2O or OH^-. In the NEA-TDB (Thermochemical Database project of the Nuclear Energy Agency,

explained in detail in section 1.6.1) equilibrium constants formulated in terms of H^+/H_2O are marked with * [21, 22]. Both formulations are connected by the ion product of water K_w:

$$H_2O \leftrightharpoons H^+ + OH^- \tag{1.1}$$

with

$$log\, K'_w = log\, [H^+] + log[OH^-] \tag{1.1a}$$

$$log\, K^o_w = log\, (H^+) + log(OH^-) - log\, a_w \tag{1.1b}$$

$$= log\, K'_w + log\, \gamma_{H^+} + log\, \gamma_{OH^-} - log a_w$$

with $\log K^o_w$ = -14.00 ± 0.01 [21]. Notation (‘) stands for a conditional equilibrium constant at a given ionic strength (and temperature), whereas (°) corresponds to an equilibrium constant in the standard state (I = 0, T = 298.15 K, P = 1 bar). [X] is the concentration, (X) the activity and γ_X the activity coefficient of the species X in given solution. a_w is the activity of water.

The dissolution of an actinide oxy-hydroxide can be formulated as:

$$An(OH)_n(s) + nH^+ \rightleftharpoons An^{n+} + nH_2O \tag{1.2}$$

with the solubility constant

$$log\, {}^*K'_{s,0} = log\, [An^{n+}] - n\, log[H^+] \tag{1.2a}$$

$$log\, {}^*K^0_{s,O} = log\, (An^{n+}) - n\, log(H^+) + n\, log\, a_w \tag{1.2b}$$

$$= log\, {}^*K'_{s,0} + log\gamma_{An^{n+}} - n\ log\, \gamma_{H^+} + n\ log a_w$$

Similarly, the hydrolysis of actinides can be formulated as:

$$An^{z+} + nH_2O \rightleftharpoons An(OH)_n^{(z-n)} + nH^+ \tag{1.3}$$

with

$$log\ \beta'_{(1,n)} = log\, [An(OH)_n^{(z-n)}] + n\, log[H^+] - log[M^{z+}] \tag{1.3a}$$

$$log\, \beta^o_{(1,n)} = log\ \beta'_{(1,n)} + log\, \gamma_{An(OH)_n^{(z-n)}} + n\, log\, \gamma_{H^+} - log\, \gamma_{M^{z+}} - n\, log a_w \tag{1.3b}$$

The conditional solubility constants $\log {}^*K'_{s,0}$ and $\log {}^*K'_{s,(1,n)}$ ($= \log {}^*K'_{s,0} + \log {}^*\beta'_{(1,n)}$) can be determined with comprehensive experimental studies and extrapolated to standard state conditions

$\log {}^{*}K^{\circ}_{s,0}$ and $\log {}^{*}K^{\circ}_{s,(1,n)}$ using a given activity model. This extrapolation also allows the quantification of ion interaction parameters according with the activity model used. Both SIT (specific ion interaction theory) and Pitzer activity models are introduced in section 1.2.4.

In the absence of other complexing ligands, the total An concentration in solution in equilibrium with a given oxy-hydroxide solid phase with solubility product $\log {}^{*}K^{\circ}_{s,0}$ can be easily calculated as a function of pH if all equilibrium constants and ion interaction coefficients are available:

$$[An]_{tot} = [An^{z+}] + \sum [M(OH)_y^{(z-y)}] \quad (1.4a)$$

$$[An]_{tot} = [\,{}^{*}K'_{s,0}[H^+]^n + \sum {}^{*}K'_{s,0}[H^+]^n\ {}^{*}\beta'_{1,n}[H^+]^{-y} \quad (1.4b)$$

1.2.1.1 Solubility and hydrolysis of Ln(III) and An(III)

Ln(III) and An(III) cations are strong Lewis acids and therefore they are expected to form relatively strong hydrolysis complexes in solution. Lanthanides and the actinides Am and Cm form predominantly complexes and compounds in their +III redox state. On the other hand, Pu, Np and U are only stabilized in the +III redox state under strongly reducing conditions. Although the stability field of U(III) and Np(III) is far from the Eh-pH conditions relevant in the context of waste disposal, Pu(III) does become relevant under near-neutral and weakly alkaline pH conditions, and therefore deserves close attention. Note that most of the available experimental studies focus on Am(III), Cm(III) and analogue lanthanides such as Nd(III) or Eu(III).

There are only limited studies of the solubility and hydrolysis of Pu(III). Systematic experimental studies are very difficult due to the high tendency of this actinide and redox state to oxidize. The solubility of $Pu(OH)_3$(s) was investigated by Felmy et al. in chloride solutions at pH 6–13 with iron powder as reducing agent [23]. Because of the low solubility of this solid phase, only data below pH ~8 was used in their thermodynamic interpretation. The authors were able to determine the $\log {}^{*}K^{\circ}_{s,0}$ of the solid phase, but no hydrolysis species were considered to form within the evaluated pH-range. Hence, very limited information on the solubility and hydrolysis of Pu(III), and the use of thermodynamic data gained for the analogs Am(III), Cm(III) and the trivalent lanthanides Nd(III) and Eu(III) is often considered. Neck et al. investigated the solubility of Nd(III) in dilute to concentrated NaCl, $CaCl_2$ and $MgCl_2$ solutions in the pH_m range 6–14 [24]. In NaCl solutions, the solubility behavior of Nd(III) was properly described with the aquo ion Nd^{3+} and the formation of mononuclear hydrolysis species $Nd(OH)_n^{3-n}$ (n= 1–3). No solubility increase was observed in the alkaline pH region due to the formation of anionic hydrolysis species. On the contrary, a significant increase in the solubility of $Nd(OH)_3$(am) was observed in concentrated $CaCl_2$ solutions within the pH-region 11–12. TRLFS experiments with Cm(III) confirmed the formation of ternary An(III) complexes

($Ca_p[M(OH)_n]^{2p+3n}$ stabilized with Ca^{2+} cations, in excellent agreement with observations made in the solubility experiments [25]. Wood et al. investigated the solubility of $Nd(OH)_3$(cr) in non-complexing sodium trifluoromethanesulfonate (NaTr) from 30°C up to 290°C. The authors reported a decreasing Nd(III) solubility with increasing temperature in the pH region where Nd^{3+} is dominant, although also observed that Nd^{3+} hydrolyses readily with increasing temperatures [26].

In the absence of complexing ligands other than hydroxide, the solubility of Ln(III) and An(III) is determined by the dissolution of $Ln(OH)_3$(s) and $An(OH)_3$(s), respectively. Different degrees of crystallinity (and consequently particle size) are defined in the literature for these solid phases. This has a direct impact on the solubility product, with smaller particle sized solids leading to greater solubility products. Amorphous solid phases (am) are expected to form in the context of radioactive waste disposal, and thus this crystallinity degree and consequent notation have been preferred in the following. Hence, the solubility product of $Ln(OH)_3$(am) and $An(OH)_3$(am) can be defined according with:

$$Ln/\,An(OH)_3(am) + 3H^+ \leftrightharpoons\ Ln/An^{3+} + 3H_2O \tag{1.5}$$

With

$$log\ {}^*K'_{s,0} = log\ [Ln/An^{3+}] - 3\ log[H^+] \tag{1.5a}$$

$$log\ {}^*K^o_{s,0} = log\ (Ln/An^{3+}) + 3\ log\ a_w - 3\ log(H^+) \tag{1.5b}$$

$$= log\ {}^*K'_{s,0} + log\ \gamma_{Ln/An^{3+}} + 3\ log\ a_w - 3\ log\ \gamma_{H^+}$$

Above pH ~6 (depending upon background electrolyte and ionic strength), Ln^{3+} and An^{3+} cations hydrolyze and the species $Ln/An(OH)_n^{3-n}$ become predominant in solution. Analogously to the solubility product, the hydrolysis of Ln^{3+} and An^{3+} can be described as:

$$Ln/An^{3+} + nH_2O \leftrightharpoons Ln/An(OH)_n^{3-n} + nH^+; n = 1,2,3 \tag{1.6}$$

with

$$log\ {}^*\beta'_n = log\ [Ln/An(OH)_n^{3-n}] + n\ log[H^+] - log\ [Ln/An^{3+}] \tag{1.6a}$$

$$log\ {}^*\beta^o_n = log\ (Ln/An(OH)_n^{3-n}) + n\ log(H^+) - log\ (Ln/An^{3+}) - n\ log\ a_w \tag{1.6b}$$

$$= log\ {}^*\beta'_n + log\ \gamma_{Ln/An(OH)_n^{3-n}} + n\ log\ \gamma_{H^+} - n\ log\ \gamma_{Ln/An^{3+}} - n\ log\ a_w$$

Hence, the overall aqueous concentration of Ln(III) and An(III) in equilibrium with $Ln(OH)_3$(am) and $An(OH)_3$(am), respectively, can be determined as the sum of Ln^{3+}/An^{3+} ions and corresponding hydrolysis species

$$[Ln/An(III)]_{tot} = [Ln/An] + \sum[Ln/An(OH)_n^{3-n}] \quad (1.7a)$$

$$[Ln/An(III)]_{tot} = ({}^*K'_{sp}\,[H^+]^n + \sum {}^*K'_{sp}\,[H^{\mp}]^n\,{}^*\beta'_{(1,n)}[H^+]^{-n} \quad (1.7b)$$

Based on the thermodynamic data selection reported in Neck et al. (2009) for Nd(III) (mostly consistent with the NEA–TDB selection for Am(III)) [22], Fig. 1.1 (a) and (b) show the solubility curve of $Am(OH)_3$(am) within $5 \leq pH_m \leq 13$ in 0.1 M NaCl, and the corresponding predominance diagram for the Am species prevailing in solution for 1 < pH < 13 and 25< pe < -17.

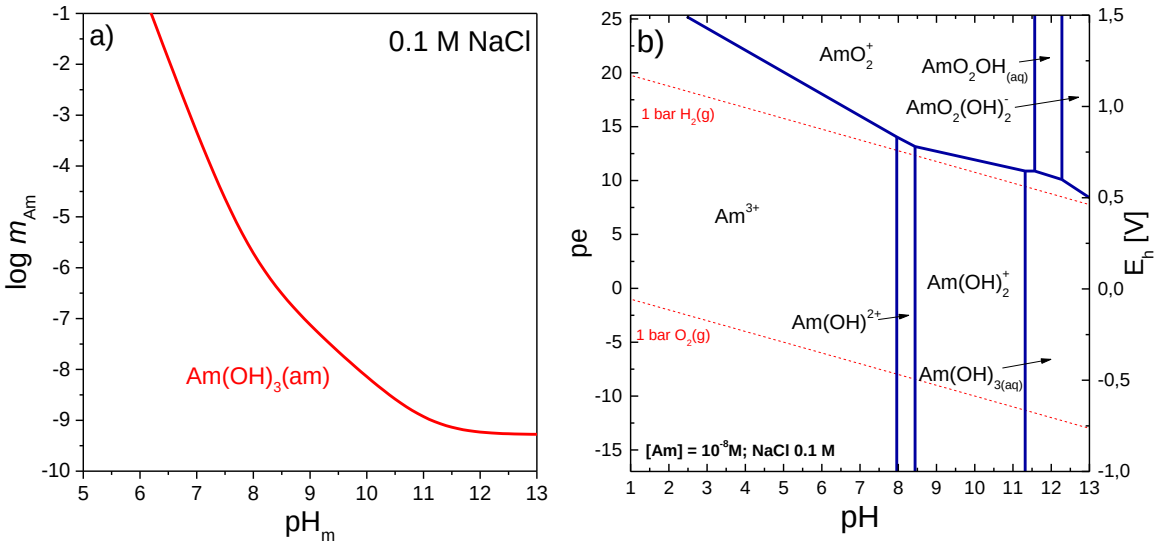

Figure 1.1. *(a) Solubility of $Am(OH)_3$(am) and (b) Pourbaix diagram for americium calculated for 10^{-8} M Am in 0.1 M NaCl solution. Calculations with SIT approach according to* [22, 24].

1.2.1.2 Solubility and hydrolysis of An(IV)

In aqueous solution thorium is only stable in the +IV oxidation state. U and Np can be stabilized in the +IV redox state under reducing conditions, whereas Pu(IV) shows a very large stability field extending from very reducing to oxidizing conditions. Considering the reducing conditions expected in a nuclear waste repository accurate knowledge of the behavior of tetravalent actinides is of high importance.

In the absence of complexing ligands other than hydroxide, the solubility of An(IV) (with An = Th, U, Np and Pu) is controlled by sparingly soluble amorphous oxy-hydroxide solid phases [22, 27].

Tetravalent actinides have a strong tendency towards hydrolysis. In the acidic pH region (pH < 5, depending upon actinide and ionic strength conditions) the aqueous speciation of Th(IV) is mainly dominated by monomeric hydroxide complexes, $Th(OH)_n^{4-n}$ with n= 1–3. In contrast to U(IV), Np(IV) and Pu(IV), several oligomeric cationic hydrolysis species of Th(IV) have been also described and are currently selected by the NEA–TDB [22, 27, 28]. Above this pH, the neutral species $Th(OH)_4(aq)$ is dominating the aqueous speciation of Th(IV), and defines a very low solubility limit in equilibrium with the corresponding $ThO_2(am,hyd)$.

Thorium has been considered in this work to assess the chemistry of An(IV) in borate-bearing solutions. Previous solubility experiments with Th(IV) often show higher solubility or a large scattering in near-neutral and alkaline pH conditions, especially in the absence of a solid phase separation involving ultracentrifugation or ultrafiltration. This solubility increase has been attributed to the formation of neutral Th(IV) (intrinsic) colloids of the type $Th_mO_{mx}(OH)_{m(4-2x)}\cdot(H_2O)_n$. The equilibrium of these colloids with the amorphous solid phase controlling the solubility, $AnO_2(am,hyd) \rightleftharpoons AnO_2(coll,hyd)$, imposes a significantly higher upper limit concentration of Th in the aqueous phase [29] (log $[ThO_2(coll,hyd)] = -6.3 \pm 0.5$), which is about 2 orders of magnitude higher than the concentration of the neutral monomeric species $Th(OH)_4(aq)$ [29].

The solubility and speciation of Th(IV) in alkaline dilute to concentrated $CaCl_2$ solutions was investigated by Altmaier et al. and Brendebach et al. [30, 31]. In contrast to analogous experiments in NaCl solutions at comparable ionic strength, a significant increase of the Th(IV) solubility was observed in concentrated $CaCl_2$ solutions ($pH_m > 10.5$). EXAFS investigation at $pH_m = 12.2$ in 4.5 M $CaCl_2$ solution identified a hitherto unknown ternary complex $Ca_4[Th(OH)_8]^{4+}$. Analogously to the ternary complexes determined for Nd(III) and Cm(III) in alkaline $CaCl_2$ solutions, the highly hydrolyzed $[Th(OH)_8]^{4-}$ needs to be charge-balanced by several Ca^{2+} ions. Later, Fellhauer et al. reported the formation of similar ternary complexes forming in alkaline $CaCl_2$ solutions with Np(IV) and Pu(IV) at $pH_m > 11$ [32].

Solubility studies with $Th(OH)_4(am,fresh)$ showed a significant decrease in the Th(IV) solubility at long equilibration times ($t > 100$ days), indicating a slow transformation of $Th(OH)_4(am,fresh)$ to the more stable Th(OH)(am,aged) [33]. Both solid phases are currently selected in the NEA-TDB review dedicated to thorium [27].

The solubility product of $Th(OH)_4(am)$ can be defined according with:

$$Th(OH)_4(am) + 4H^+ \leftrightharpoons Th^{4+} + 4H_2O \quad (1.8)$$

With

$$log\ {}^*K'_{s,0} = log\ [Th^{4+}] - 4\ log[H^+] \quad (1.8a)$$

$$log\ {}^{*}K^{o}_{s,0} = log\ (Th^{4+}) + 4\ log\ a_w - 4\ log(H^{+}) \quad (1.8b)$$

$$= log\ {}^{*}K'_{s,0} + log\ \gamma_{Th^{4+}} + 4\ log\ a_w - 4\ log\ \gamma_{H^{+}}$$

The hydrolysis of Th^{4+} can be described as:

$$mTh^{4+} + nH_2O \leftrightharpoons Th_m(OH)_n^{4m-n} + nH^{+}; n = 1-4;\ m = 1-6 \quad (1.9)$$

with

$$log\ {}^{*}\beta'_n = log\ [Th_m(OH)_n^{4m-n}] + n\ log[H^{+}] - m\ log\ [Th^{4+}] \quad (1.9a)$$

$$log\ {}^{*}\beta^{o}_n = log\ (Th_m(OH)_n^{4m-n}) + n\ log(H^{+}) - m\ log\ (Th^{4+}) - n\ log\ a_w \quad (1.9b)$$

$$= log\ {}^{*}\beta'_n + log\ \gamma_{Th_m(OH)_n^{4m-n}} + n\ log\ \gamma_{H^{+}} - m\ log\ \gamma_{Th^{4+}} - n\ log\ a_w$$

Based on the NEA–TDB selection for Th(IV) [27], Fig. 1.2 (a) and (b) show the solubility curve of $Th(OH)_4$(am,fresh) and $Th(OH)_4$(am,aged) within $3 \le pH_m \le 12$ in 0.1 M NaCl, and the corresponding predominance diagram for the Th species prevailing in solution for 1 < pH < 13 and 25 < pe < -17.

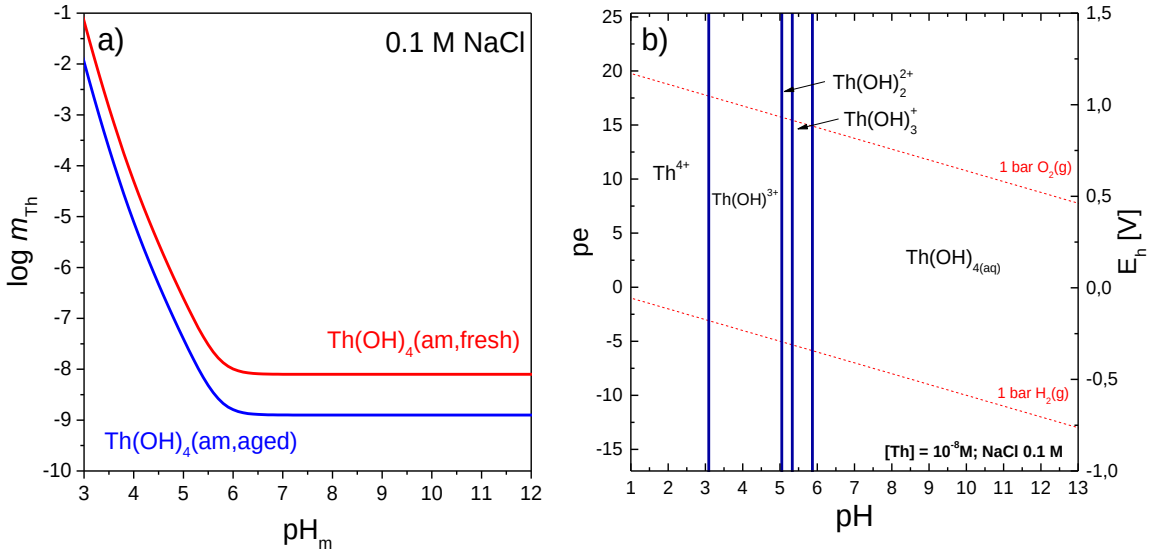

Figure 1.2. (*a) Solubility of $Th(OH)_4$(am, fresh). $Th(OH)_4$(am,aged) and (b) Pourbaix diagram for thorium calculated for 10 $^{-8}$ M Th in 0.1 M NaCl solution. Calculations with SIT considering ion interaction parameters selected in [27].*

1.2.1.3 Solubility and hydrolysis of An(V)

U, Np, Pu and Am form aqueous complexes and solid compounds in their +V redox state with the actinyl moiety $[O=An=O]^{+}$. Among these, Np(V) has the largest stability field and is very often

considered in experimental studies due to its redox stability under a large variety of pH and Eh conditions. The solubility of Np(V) in dilute systems is mostly controlled by the amorphous $NpO_2OH(am)$. The solubility of this solid phase was investigated in several studies, mainly in NaCl and $NaClO_4$ systems with various ionic strengths [34-36]. Solubility studies were further complemented with vis/NIR spectroscopy [36]. Neck et al. [36] and Runde [34] observed an aging effect of the fresh amorphous Np hydroxide together with a decreased solubility of about 0.6 log-units in 1.0 and 3.0 M $NaClO_4$, as well as in 5.0 M NaCl, respectively. Consequently, the authors defined two solid phases with the same stoichiometry but slightly different solubility products, namely $NpO_2OH(am,fresh)$ and $NpO_2OH(am,aged)$. Note that none of the solid phases was characterized (mainly because of their amorphous nature), and thus the main conclusions derived from this work can be considered not sufficiently sound (see for instance the discussion between Neck and Rao in [37-39]). The NEA–TDB review relied in the interpretation of these authors and considered both solid phases in their final selection. A recent study by Petrov and co-workers reported the formation of ternary Na–Np(V)–OH solid phases under hyperalkaline conditions (pH ≥ 11.5) and concentrated NaCl solutions (≥ 1.0 M). These solid phases appear to have a solubility significantly lower than $NpO_2OH(am,fresh)$, and thus can play a relevant role in saline and cementitious environments [40].

Solubility studies showed that the aquo ion NpO_2^+ is the dominant aqueous species in acidic, neutral and slightly alkaline region and that no hydrolysis species form until pH = 10. At pH 11-12 first the neutral $NpO_2OH(aq)$ complex and later $NpO_2(OH)_2^-$ are forming. Note that a combined potentiometric, spectrophotometric and calorimetric study conducted afterwards by Rao and co-workers suggested an earlier hydrolysis of Np(V) [37]. The presence of carbonate contamination in this study cannot be completely ruled out, and thus we retain in the discussion of this PhD work the thermodynamic data selection proposed by the NEA–TDB.

Fellhauer investigated the solubility of Np(V) in dilute to concentrated $CaCl_2$ solutions at pH_m = 8-12. Three new Ca–neptunate solid phases were found, with $Ca_{0.5}NpO_2(OH)_2 \cdot 1.3H_2O$ as the most stable and solubility-limiting phase. Analogously to An(III) and An(IV), the solubility of Np(V) in $CaCl_2$ solution is increased compared to NaCl solutions due to the formation two ternary Ca–Np(V)-(OH) complexes at pH > 10.5 [41].

Based on the discussion above and focusing on the binary system Np(V)-H_2O, the conditional solubility product of $NpO_2OH(am)$ ($\log {}^*K'_{s,0}$) and the corresponding $\log {}^*K^{\circ}_{s,0}$ can be written as:

$$NpO_2OH(am) + H^+ \leftrightharpoons NpO_2^+ + H_2O \tag{1.10}$$

with

$$log\ {}^*K'_{s,0} = log\ [NpO_2{}^+] - log[H^+] \tag{1.10a}$$

$$log\ {}^{*}K^{o}_{s,0} = log\ (NpO_2{}^{+}) + log\ a_w - log(H^{+}) \quad (1.10b)$$

$$= log\ {}^{*}K'_{s,0} + log\ \gamma_{NpO_2{}^{+}} + log\ a_w - log\ \gamma_{H^{+}}$$

The hydrolysis of Np(V) can be formulated as:

$$NpO_2^{+} + n\ H_2O \leftrightharpoons NpO_2\ (OH)_n^{1-n} + n\ H^{+};\ n= 1,2 \quad (1.11)$$

with

$$log\ {}^{*}\beta'_n = log\ [NpO_2(OH)_n^{1-n}] + n\ log[H^{+}] - log\ [NpO_2^{+}] \quad (1.11a)$$

$$log\ {}^{*}\beta^{o}_n = log\ (NpO_2(OH)_n^{1-n}) + n\ log(H^{+}) - log\ (NpO_2^{+}) - n\ log\ a_w \quad (1.11b)$$

$$= log\ {}^{*}\beta'_n + log\ \gamma_{NpO_2\ (OH)_n^{1-n}} + n\ log\ \gamma_{H^{+}} - n\ log\ \gamma_{NpO_2^{+}} - n\ log\ a_w$$

Based on the NEA–TDB selection for Np(V) [22], Fig. 1.3 (a) and (b) show the solubility curve of NpO_2OH(am,fresh) and NpO_2OH(am,aged) within $6 \le pH_m \le 13$ in 0.1 M NaCl, and the corresponding predominance diagram for the Np species prevailing in solution for 1 < pH < 13 and 25< pe < -17.

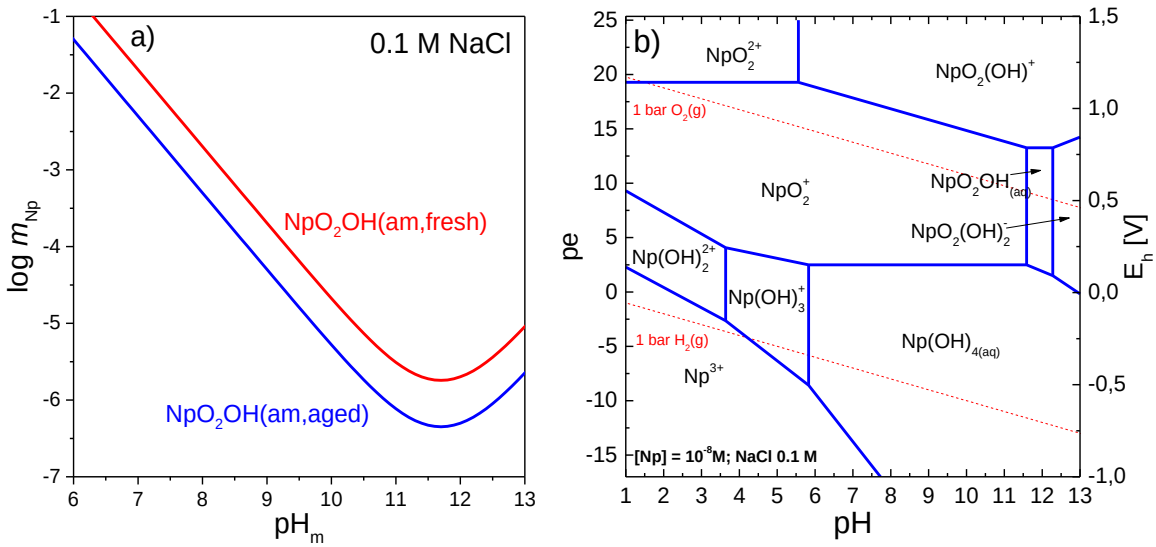

Figure 1.3. (a) *Solubility of NpO_2OH $(am, fresh)$, NpO_2OH $(am, aged)$ and (b) Pourbaix diagram for Neptunium calculated for 10 $^{-8}$ M Np in 0.1 M NaCl solution. Calculations with SIT approach according to NEA-TDB selection [22].*

1.2.1.4 Solubility and hydrolysis of An(VI)

U(VI) is the most relevant hexavalent actinide in the context of radioactive waste disposal. Pu(VI) and Np(VI) show also a predominant region within the stability field of water, although only under oxidizing acidic and relatively alkaline pH conditions [22]. Recent studies conducted at KIT–INE have shown the increased stability of Np(VI) under hyperalkaline pH conditions relevant in cementitious systems [42, 43].

A number of binary U(VI) oxo-hydroxides have been reported in the literature, reflecting different crystallinity and number of hydration waters ($UO_2(OH)_2$(s), $UO_3 \cdot 0.9H_2O$(cr), $UO_3 \cdot 2H_2O$(cr), among others) [21, 22, 44, 45]. At room temperature and dilute solutions with $4 \leq pH \leq 9$ (depending upon ionic strength and background electrolyte), the solubility limiting U(VI) oxo-hydroxides phase is meta-schoepite ($UO_3 \cdot 2H_2O$(cr)) [21, 46-48].

Solubility experiments with meta-schoepite in NaCl solutions showed that above pH = 9 a transformation of meta-schoepite into sodium uranate $Na_2U_2O_7 \cdot H_2O$(cr) takes place [21, 22]. Such a transformation has been also reported to take place in dilute to concentrated $CaCl_2$ solutions leading to the formation of $CaU_2O_7 \cdot 3H_2O$(cr) [49]. On the contrary, no transformation takes place in dilute to concentrated $MgCl_2$ solutions and thus metaschoepite remains as solubility-limiting solid phase in these systems.

Monomeric and oligomeric positively charged hydrolysis species of U(VI) are reported to occur in the literature [21, 22, 50, 51]. Negatively-charged monomeric hydrolysis species of U(VI) form under alkaline to hyperalkaline pH conditions. $UO_2(OH)_4^{2-}$ is widely accepted as the limiting hydrolysis species, although the formation of $UO_2(OH)_5^{3-}$ under very alkaline pH conditions has been hinted by several experimental and theoretical studies [52].

Dissolution equilibria of $UO_3 \cdot 2H_2O$(cr) and $Na_2U_2O_7 \cdot H_2O$(cr) can be described according with equations (1.12) and (1.13):

$$UO_3 \cdot 2H_2O(cr) + 2H^+ \leftrightharpoons UO_2^+ + 3H_2O \tag{1.12}$$

with

$$log\ {}^*K'_{s,0} = log\ [UO_2^+] - 2\ log[H^+] \tag{1.12a}$$

$$log\ {}^*K^o_{s,0} = log\ (UO_2^+) + 3\ log\ a_w - 2\ log(H^+) \tag{1.12b}$$

$$= log\ {}^*K'_{s,0} + log\ \gamma_{UO_2^+} + 3\ log\ a_w - 2\ log\ \gamma_{H^+}$$

and

$$\frac{1}{2}Na_2U_2O_7 \cdot H_2O(cr) + 3\,H^+ \leftrightharpoons\ UO_2^+ + Na^+ + 2\,H_2O \tag{1.13}$$

with

$$log\ {}^*K'_{s,0} = log\ [UO_2^+] - 3\,log[H^+] + log[Na^+] \tag{1.13a}$$

$$log\ {}^*K^o_{s,0} = log\ (UO_2^+) + log\ (Na^+) + 2\,log\ a_w - 3\,log(H^+) \tag{1.13b}$$

$$= log\ {}^*K'_{s,0} + log\ \gamma_{UO_2^+} + log\ \gamma_{Na^+} + 2\,log\ a_w - 3\,log\ \gamma_{H^+}$$

The hydrolysis reactions can be formulated as follows:

$$mUO_2^+ + n\mathrm{H_2O} \leftrightharpoons\ (UO_2^+)_m(OH)_n^{2m-n} + n\mathrm{H^+}; n = 1,2,3 \tag{1.14}$$

with

$$log\ {}^*\beta'_n = log\ [(UO_2^+)_m(OH)_n^{2m-n}] + n\,log[H^+] - m\,log[UO_2^+] \tag{1.14a}$$

$$log\ {}^*\beta^o_n = log\ ((UO_2^+)_m(OH)_n^{2m-n}) + n\,log(H^+) - m\,log\ (UO_2^+) - n\,log\ a_w \tag{1.14b}$$

$$= log\ {}^*\beta'_n + log\ \gamma_{(UO_2^+)_m(OH)_n^{2m-n}} + n\,log\ \gamma_{H^+} - m\,log\ \gamma_{UO_2^+} - n\,log\ a_w$$

Based on the thermodynamic data reported in Altmaier et al. (2003) for U(VI) [53] in combination with the current NEA-TDB selection [22], Fig. 1.4 (a) and (b) show the solubility curves of $UO_3{\cdot}2H_2O$(cr) and $Na_2U_2O_7{\cdot}H_2O$(cr) within $4 \le pH_m \le 12$ in 0.1 M NaCl, and the corresponding predominance diagram for the U species prevailing in solution for $1 < pH < 13$ and $25 < pe < -17$.

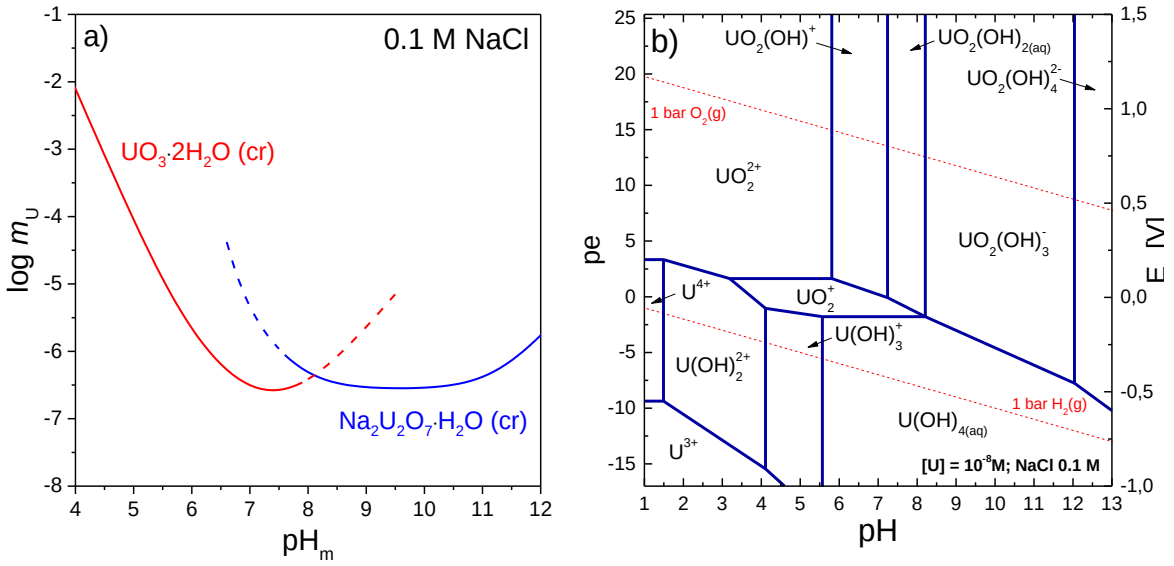

Figure 1.4. (a) *Solubility of $UO_3{\cdot}2H_2O$(cr) and $Na_2U_2O_7{\cdot}H_2O$(cr) and (b) Pourbaix diagram for uranium calculated for 10^{-8} M U in 0.1 M NaCl solution. Calculations with SIT approach according to with ion interaction coefficients reported elsewhere [22, 53].*

1.2.2 Definition of redox equilibrium

To describe the behavior of actinides in solution the redox state is of high importance. The formation/predominance of different oxidation states, depending upon pH, Eh and composition of the aqueous solution will cause very significant changes in the chemical behavior of the considered actinide.

The redox reaction of a redox couple in equilibrium is given by:

$$Ox + ne^- \leftrightharpoons Red \tag{1.15}$$

The Nernst equation defines the electrode (half-cell) potential of a redox couple:

$$E = E^0 + \frac{RT\ ln(10)}{nF}\ log(\frac{a_{ox}}{a_{red}}) \tag{1.16}$$

With E: the redox potential for a given medium, E°: the redox potential under standard conditions, n: the number of electrons participating in the reaction, R: the ideal gas constant, T: Temperature in K and F the Faraday constant.

Since the absolute electrode potential cannot be measured experimentally, the electrode potential is determined as the redox potential relative to the standard hydrogen electrode (equal to zero by

definition) and referred to as Eh value. The redox potential of a system can be also defined as the negative logarithm of the electron activity (analogue to the pH) as pe:

$$pe = -log(a_e{}^-) \tag{1.17}$$

Eh and pe can be correlated via:

$$Eh = -\frac{RT}{F} ln(a_e{}^-) = \frac{RTln(10)}{F} pe \tag{1.18}$$

With pe = 16.9·Eh [V] for T = 25° C

Stability fields for different redox species can be shown in Pourbaix diagrams with the measured Eh (pe) and pH in aqueous solution [54]. Different predominance areas of the different systems are separated by borderlines which reflect a 50:50 % distribution between the given species.

These borderlines can be calculated for the standard state or at a given ionic strength, provided that stability constants and ion interaction coefficients of the aqueous species are known. Fig. 1.5 exemplarily shows the Pourbaix diagram of Pu within 1 ≤ pH ≤ 13 and 25 ≤ pe ≤ –17 in 0.1 M NaCl.

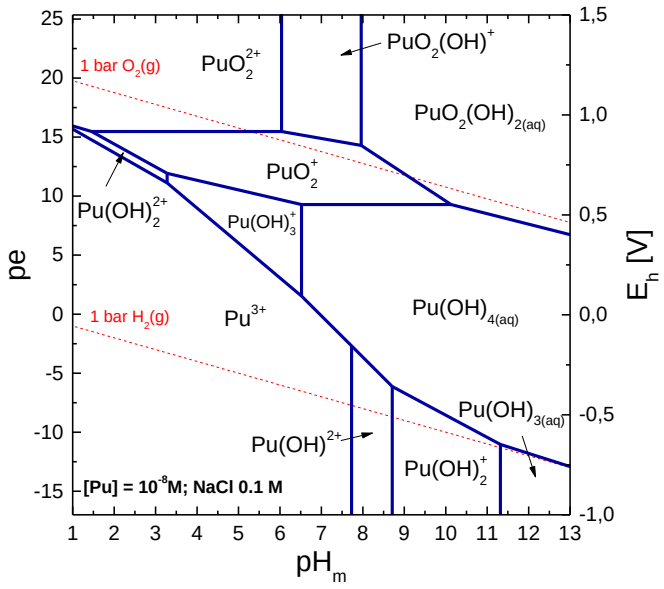

Figure 1.5. *Pourbaix diagram of plutonium. Calculations performed for 10^{-8} M Pu concentration and 0.1 M NaCl at 25°C based on data from NEA TDB[22].*

1.2.2.1 Pu(III/IV) redox chemistry

The redox chemistry of Pu was thoroughly evaluated based on existing literature and own experimental work by Neck et al. under oxidizing, redox neutral and reducing conditions [55-57]. In water, Pu can exist in the oxidation states III to VI.

Neck et al. stated that Pu^{4+} and PuO_2^+ are not directly in equilibrium as the reversible redox couples Pu^{3+}/Pu^{4+} and PuO_2^+/PuO_2^{2+}, but rather in indirect equilibrium via their reactions with Pu(IV) solid, colloids or polymeric species [56].

The kinetics and mechanistic aspects of redox reactions with Pu aquo ions as well as thermodynamic constants are well known in acidic conditions [58]. In the near neutral or alkaline regions only very few systematic or kinetic studies on the redox chemistry of Pu are available. In this pH area, precipitation and hydrolysis must be taken into account. Recently, Fellhauer conducted a very comprehensive work on the redox chemistry of Pu under repository-relevant pH conditions [59]. The author concluded that available thermodynamic data explained well the experimental observations.

Under the reducing conditions expected in a nuclear waste disposal only the oxidation states Pu(III) and Pu(IV) are stable. In near-neutral and slightly alkaline pH conditions, Pu(IV) prevails as the sparingly soluble PuO_2(am,hyd), whereas the solubility of Pu(III) is strongly dependent on the pH and decreases from ~10^{-2} M at pH = 3 to 10^{-8} M at pH = 9 (see also section 1.2.1.1). In general $Pu(OH)_3$(s) could be expected but Neck et al. showed that based on data from the NEA–TDB $Pu(OH)_3$(s) is under all conditions meta stable and slowly transforms into PuO_2(am,hyd). The calculated borderline for this reaction is close to the reductive decomposition of water. Recent work by Fellhauer has provided some hints on the possible overestimation of log $*K°_{s,0}$ selected in the NEA-TDB for $Pu(OH)_3$(s), thus hinting to the clear need of additional experimental studies focusing on this system [59].

$$Pu(OH)_3(s) \rightleftharpoons PuO_2(am,hyd) + e^- + H^+ + H_2O \quad (1.19)$$

with

$$log\ K°_{IIIs\_IVam} = log\ a_w - pH - pe = 0.4 \pm 1.0 \quad (1.19a)$$

The equilibrium between solid PuO_2(am,hyd) and solved Pu^{3+} is very important and controls the total plutonium concentration in aqueous systems under reducing conditions at near neutral and slightly alkaline pH [55, 60]. Rai et al. investigated systematically the reductive dissolution of PuO_2 (am,hyd):

$$PuO_2(am,hyd) + 4\ H^+ + e^- \rightleftharpoons Pu^{3+} + 2\ H_2O \quad (1.20)$$

with

$$log\ K°_{IVam_{IIIaq}} = log\ (Pu^{3+}) + 2\ log\ a_w + \ 4\ pH + pe \quad (1.20a)$$

$$= log\ [Pu^{3+}] + \ log\ \gamma_{Pu^{3+}} + 2\ log\ a_w + \ 4\ pH + pe \quad (1.20b)$$

Redox conditions were kept stable by addition of $FeCl_2$ and 9,10 Anthrahydroquinone-2,6-disulfonate solution. The estimated log $*K°_{IVam\_IIIaq}$ value is 15.6 ± 0.6. In the NEA-TDB a very similar value 15.4 ±0.5 for this reaction is selected under consideration of the work by Rai et al [22]. The reductive dissolution of Pu was also investigated by Fujiwara et al. from pH 3.5 to 9. In this study $Na_2S_2O_4$ was used as reducing agent but the measured redox conditions (pe + pH =10) are too positive, likely hinting to the potential oxidation of the original reducing agent.

The redox equilibria of An^{3+}/An^{4+} and AnO_2^{+}/AnO_2^{2+} are very fast and reversible whereas the redox reaction of An^{4+}/AnO_2^{+} is slower due to the breaking of the metal oxygen bond [22, 61].

$$An^{3+} \rightleftharpoons \ An^{4+} + \ e^- \quad (1.21)$$

with

$$log\ K°_{IIIaq\_IVaq} = \ log(An^{4+}) - log(An^{3+}) - pe \quad (1.21a)$$

$$= log[An^{4+}] + log\ \gamma_{An^{4+}} - log[An^{3+}] - log\ \gamma_{An^{3+}} - pe \quad (1.21b)$$

and

$$An^{4+} + 2H_2O \rightleftharpoons \ AnO_2^{+} + 4H^+ + \ e^- \quad (1.22)$$

with

$$log\ K°_{IVaq\_Vaq} = log\left(AnO_2^{+}\right) - log(An^{4+}) - 2\ log\ a_w - 4\ pH - pe \quad (1.22a)$$

$$= log\left[AnO_2^{+}\right] + log\ \gamma_{AnO_2^{+}} - log[An^{4+}] - log\ \gamma_{An^{4+}} - 2\ log\ a_w - 4\ pH - pe$$

$$AnO_2^{+} \rightleftharpoons \ AnO_2^{2+} + \ e^- \quad (1.23)$$

with

$$log\ K°_{Vaq\_VIaq} = log\left(AnO_2^{2+}\right) - log\left(AnO_2^{+}\right) - pe \quad (1.23a)$$

$$= log\left[AnO_2^{2+}\right] + log\ \gamma_{AnO_2^{2+}} - log\left[AnO_2^{+}\right] - log\ \gamma_{AnO_2^{+}} - pe$$

At pH = 0 the standard potentials of the 3 redox pairs are very similar (~1 V), which allows a coexistence of all four oxidation states at the same time in similar concentrations. At pH > 2 however this is not possible anymore due to the increased stability field of Pu(IV).

1.2.3 Activity models

For the description of real systems with I ≠ 0, the interaction of ions in solutions and the resulting activity coefficients must be accounted for. In systems with $I \geq 0.1$ M, activity coefficients have to be specifically calculated for the corresponding background electrolyte and concentration. In dilute to concentrated saline systems, SIT and PITZER approaches are normally used for the determination of activity coefficients.

1.2.3.1 Specific ion interaction theory (SIT)

The SIT approach is based on the extended Debye-Hückel law (theory) and includes the influence of electrostatic, non-specific long-range, non-binary interactions between charged ions in the calculations of activity coefficients [62]. The validity range of the method is normally considered up to $I \leq 3.5$ M, although recent studies have shown the appropriate performance of this approach up to $I = 13.5$ M [32]. This method is adopted in the NEA-TDB for the correction of ionic strength effects [22]. Note however that the use of Pitzer activity models is normally preferred for the evaluation of concentrated brine solutions.

According with the SIT formalism, the activity coefficient of an ion j is defined as

$$log\gamma_j = z_j{}^2 D + \sum_k \varepsilon(j,k) m_k \quad (1.24)$$

Where z_j is the charge of the ion j, m_k is the molality of the oppositely charged ion k and $\varepsilon(j,k)$ is the specific ion interaction parameter for the given electrolyte, D is the Debye Hückel term defined as:

$$D = \frac{A\sqrt{I_m}}{1 + Ba_j\sqrt{I_m}} \quad (1.25)$$

The constants A and Ba_j are temperature and pressure dependent and equal 0.509 ± 0.001 $kg^{1/2}$ $mol^{-1/2}$ and 1.5 $kg^{1/2} \cdot mol^{-1/2}$, respectively at 25°C and 1 bar.

The activity coefficient of ion j can be thus calculated combining equations 1.24 and 1.25:

$$log\gamma_j = -z_j^2 \frac{0.509\sqrt{I_m}}{1 + 1.5\sqrt{I_m}} + \sum_k \varepsilon(j,k) m_k \quad (1.26)$$

1.2.3.2 Pitzer

Thermodynamic calculations and geochemical modeling in concentrated salt brine solutions with high ionic strength can be performed with the Pitzer approach [63]. The Pitzer formalism describes the effect of ionic strength with short range binary interactions (the second virial coefficient) and additional interactions between ions with the same charge, between neutral species and charged ions and triple interactions. These results in a large number of parameters for a given ion, but the resulting activity coefficients are more accurate especially at high ionic strength.

The semi empirical activity model of Pitzer is based on a virial expansion of the excess Gibbs energy:

$$\frac{G^{ex}}{w_w RT} = f(I) + \sum_i \sum_j m_i m_j \lambda_{ij}(I) + \sum_i \sum_j \sum_k m_i m_j m_k \mu_{ijk}(I) + \cdots \quad (1.27)$$

where w_w is the number of kilograms of water, and $m_i m_j m_k$ are the molalities of all solved species. The first term is a Debye-Hückel term and depends only on the ionic strength, $\lambda_{ij}(I)$ and μ_{ijk}(I) are virial coefficients representing the short-ranged interactions between the solved species.

Activity coefficients for mixed electrolytes in the presence of cations M, c, c' and anions X, a, a' are described by the equations (1.28) and (1.29) for a cation M and an anion X, respectively:

$$ln\gamma_M = z_M^2 F + \sum_a m_a(2B_{Ma} + ZC_{Ma}) + \sum_c m_c(2\phi_{Mc} + \sum_a m_a \psi_{Mca}) \quad (1.28)$$
$$+ \sum_{a<} \sum_{a'} m_a m_{a'} \psi_{Maa'} + z_M \sum_{c<} \sum_a m_c m_a C_{ca} + 2\sum_n m_n \lambda_{nM}$$

$$ln\gamma_X = z_X^2 F + \sum_c m_c(2B_{cX} + ZC_{cX}) + \sum_a m_a(2\phi_{Xa} + \sum_c m_c \psi_{cXa}) \quad (1.29)$$
$$+ \sum_{c<} \sum_{c'} m_c m_{c'} \psi_{Xcc'} + |z_X| \sum_{c<} \sum_a m_c m_a C_{ca} + 2\sum_n m_n \lambda_{nX}$$

with Z=$\sum_i mi|z_i|$ and F representing the Debye-Hückel term and the ionic strength dependence specific to the salt. In the Pitzer model binary parameters $\beta_{ij}^{(o)}$, $\beta_{ij}^{(1)}$, $\beta_{ij}^{(2)}$ and C_{ij}^{φ} specific to the interacting ions are defined. $\beta_{ij}^{(o)}$ describes mainly repulsive forces between similar ions. $\beta_{ij}^{(1)}$represents the attractions between oppositely charged ions and $\beta_{ij}^{(2)}$ corrects deviations caused by electrostatic ion-pair formation and is only considered for 2-2 or higher valence electrolytes. C_{ij}^{φ} becomes only significant at high ionic strength. $\theta_{ii'}$(or $\theta_{jj'}$) and $\Psi_{ii'j}$(or $\Psi_{ijj'}$) are mixing parameters for ternary and higher electrolyte systems. Their contribution is very small except when

non-identical charged species are mixed. λ_{ni} (or λ_{nj}) define interactions between ions and neutral charged species. B_{ca} and C_{ca} can be calculated based on the binary parameters. Φ_{ij} can be calculated based on the electrostatic nonsymmetrical mixing effects, depending on the charged species, ionic strength and solvent properties.

1.3 Aqueous borate speciation and actinide borate chemistry

1.3.1 Boron chemistry and aqueous borate speciation

Boron is a relatively rare element in the earth crust, with a natural occurrence of ~ 10–20 ppm [64]. Large boron resources can be found in Turkey and the West of the USA [65]. More than 150 different boron containing minerals are known. They can be divided in three main groups depending on their origin and geological environment: i. skarn minerals formed within magmatic movements by the intrusion of borate bearing solutions in into carbonate formations, mainly silicates and iron oxides; ii. magnesium oxides related to marine sediments; and iii. sodium and calcium borates formed by volcanic activity [66]. Most common boron minerals found in the environment are Borax ($Na_2B_4O_7{\cdot}10H_2O$), Ulexit ($NaCa[B_5O_6(OH)_6]{\cdot}5H_2O$), Kernit ($Na_2B_4O_7{\cdot}4H_2O$) and Colemanit ($Ca_2B_6O_{11}{\cdot}5H_2O$).

Salts of the boric acid are called borates and consist of trigonal and tetragonal boron-oxygen units BO_3 and BO_4. Borates tend to form polymeric networks containing the polymerized BO_3 and BO_4 units. These are bond together via corner sharing, edge sharing or shared oxygen atoms to form chains, clusters, layers and 3D frameworks [67, 68].

One of the challenges encountered when quantitatively assessing An–borate interaction is the complex and yet relatively unknown aqueous speciation of boron. A number of experimental approaches including potentiometric titrations [69, 70], Raman spectroscopy [71], ^{11}B–NMR [72-75], isopiestic measurements [76, 77] and solubility studies [78-80] have been considered in the literature to assess the speciation of boron in solution. The available thermodynamic data [69, 70, 81] allow the calculation of species distribution for some cases, although the accuracy of these calculations at elevated boron and salt concentration (especially in the case of $MgCl_2$) is importantly hindered.

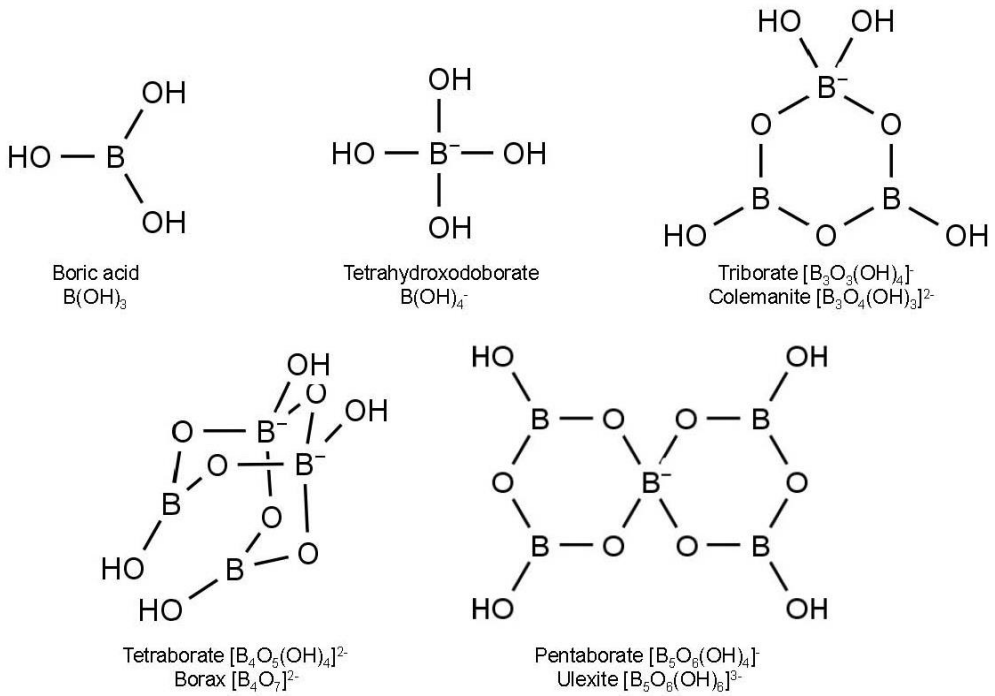

Figure 1.6. *Suggestions for structures of borates in aqueous solution derived from naturally occurring minerals [23].*

Monomeric species $B(OH)_3(aq)$ and $B(OH)_4^-$ prevail at low boron concentration under acidic and alkaline pH conditions, respectively (Fig. 1.6). Due to the neutral character of $B(OH)_3(aq)$ (pKa = 9.25 [82]) and the delocalized charge in $B(OH)_4^-$, these monomeric species have been reported to have a low tendency to complex hard Lewis acids such as actinide cations [15]. Polyborate species (e.g. $B_3O_3(OH)_4^-$, $B_4O_5(OH)_4^{2-}$ and $B_5O_6(OH)_4^-$, among others shown in Fig. 1.6) are known to form with increasing boron concentrations (Fig. 1.7) [69, 70]. These species have been postulated to form stronger complexes with actinides than the corresponding monomeric species [6, 83], although this hypothesis remains open. The main equilibria in aqueous solution are:

$$B(OH)_3 + H_2O \leftrightharpoons B(OH)_4^- + H^+ \quad (1.30)$$

$$2B(OH)_3 + B(OH)_4^- \leftrightharpoons B_3O_3(OH)_4^- + 3H_2O \quad (1.31)$$

$$2B(OH)_3 + 2B(OH)_4^- \leftrightharpoons B_4O_5(OH)_4^{2-} + 5H_2O \quad (1.32)$$

$$4B(OH)_3 + B(OH)_4^- \leftrightharpoons B_5O_6(OH)_4^- + 6H_2O \quad (1.33)$$

Note that analogous oligomeric species have been reported for silicium ($Si_2O_2(OH)_5^-$, $Si_3O_5(OH)_5^{3-}$, $Si_4O_7(OH)_5^{3-}$, among others[22], hence highlighting the similarities existing between B and Si.

The limited experimental data available to assess aqueous boron speciation is especially manifest for elevated ionic strength conditions and $MgCl_2$ and $CaCl_2$ brines. Raman studies conducted by Zhihong and co-workers showed a favored formation of polyborates in the presence of high Mg^{2+} concentrations, although no quantitative thermodynamic description was provided by the authors [84].

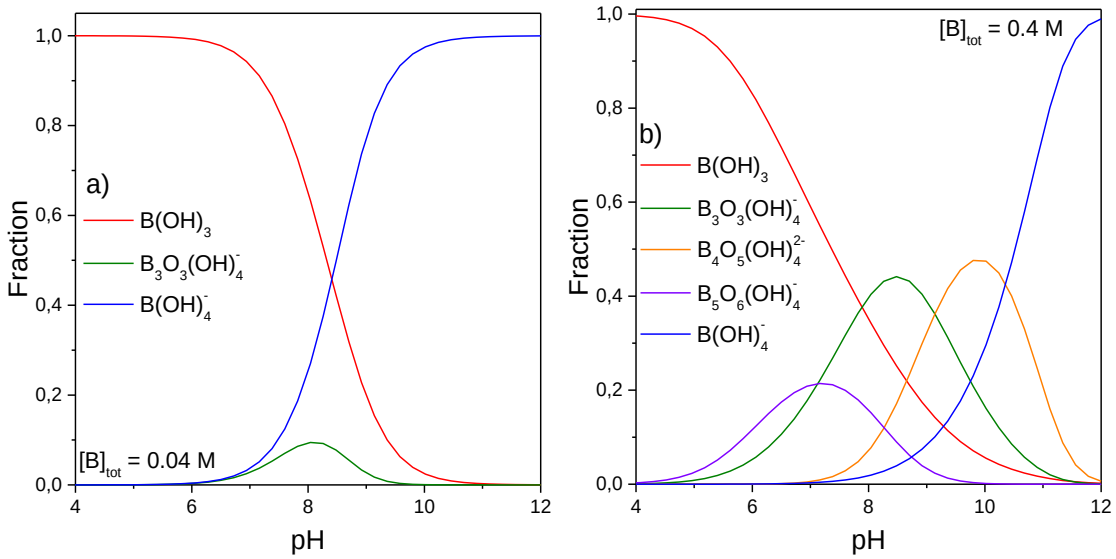

Figure 1.7. *Fraction diagram of aqueous boron species calculated for 4 ≤ pH ≤ 12 at I = 0 for a) $[B]_{tot}$ = 0.04 M, and b) $[B]_{tot}$ = 0.4 M. Thermodynamic data used in the calculations as reported in Ingri et al. (1957) and Ingri (1962) [69, 70].*

The solubility (as equilibrium concentration in saturated solutions) of the systems $CaO–B_2O_3–H_2O$ and $MgO–B_2O_3–H_2O$ was intensively investigated in the 40's to 70's by Soviet scientists, who reported the formation of several mixed solid phases between these alkaline-earth elements and boron (i.e. $2MgO·3B_2O_3·15H_2O$, $2CaO·3B_2O_3·13H_2O$, among others) [79, 80]. Very recently, Wang and co-workers conducted a very comprehensive literature review with the aim of developing a mixed-solvent electrolyte (MSE) thermodynamic model covering the systems $M_nO + B_2O_3 + H_2O$ (with M = Li, Na, Ca, Mg and n = 1, 2). In addition to $B(OH)_3(aq)$, $B(OH)_4^-$, $NaB(OH)_4(aq)$ and $LiB(OH)_4(aq)$ monomeric species, the authors included in their model the polyborate species $B_2O(OH)_5^-$, $B_3O_3(OH)_4^-$, $B_4O_5(OH)_4^{2-}$ and $B_5O_6(OH)_6^{3-}$. No Ca–borate or Mg–borate binary aqueous species were considered by the authors in their thermodynamic model [85]. It should be noted that due to the fact that Wang and co-authors use the thermodynamic MSE approach, the results and data selections cannot be transferred to either the SIT [62] or Pitzer [63] approaches. Felmy et al developed a chemical model to describe the behavior of borates in natural waters using the Pitzer approach [81]. Activity coefficients for the system Na^+-K^+-Ca^{2+}-Mg^{2+}-H^+-Cl^--SO_4^{2-}-CO_3^{2-}-$B(OH)_4^-$-H_2O were reported and allow calculations at high ionic strength and high boron concentrations. The thermodynamic model

by Felmy and co-workers for the interpretation of saline aqueous borate systems has been considered in this work to calculate the speciation of borate in NaCl and $MgCl_2$ systems, and it is discussed in detail in chapter 3 and 9.

1.3.2 Aquatic chemistry of actinide-borate systems

Although the aquatic chemistry of An(III) and An(IV) under repository-relevant conditions is mostly dominated by hydrolysis reactions, the role of other inorganic and organic ligands in complexing (and thus potentially mobilizing) actinides needs to be assessed properly. In contrast to carbonate, phosphate or sulphate, little attention has been dedicated so far to the possible complexation of borate species with actinides [6, 7]. The lack of experimental studies assessing An–borate complexation is well-reflected in the publications of the OECD Nuclear Energy Agency thermodynamic database project (NEA–TDB), where no aqueous borate species or solid compounds are selected for any of the actinides evaluated (U, Np, Pu, Am, Th) [22, 27]. Borkowski and co-workers assessed the effect of borate on Nd(III) solubility in dilute to concentrated NaCl solutions at pH_m = 8.6 and $0 \leq [B]_{tot} \leq 0.16$ M [6]. The authors observed a slight increase in Nd concentration (in the range of $5.0\ 10^{-8}$ M – $2.5 \cdot 10^{-7}$ M) as a function of $[B]_{tot}$, ionic strength and pH which was related to the formation of a $NdHB_4O_7^{2+}$-complex. Note that Borkowski and co-workers derived chemical and thermodynamic models assuming a boron speciation dominated by the species $HB_4O_7^-$ under the particular conditions of their experiments. Recently, Schott et al. investigated the interaction of Eu(III) with borate in aqueous solution [83]. TRLFS experiments confirmed a weak Eu(III)–borate complexation at pH < 6. At pH ~6 and in the presence of high boron concentrations ($0.3\ M \leq [B]_{tot} \leq 0.7$ M), the authors observed the formation of a Eu(III)–borate solid phase. The solid was characterized by XRD, IR and solid-state TRLFS, although these techniques provided inconclusive information on the stoichiometry of the newly formed compound. Kienzler et al. performed leaching experiments with simulated borosilicate glass doped with U(IV), U(VI), Pu(IV), Am(III), Np(IV) and Np(V) in concentrated NaCl solutions. Experiments were performed within $7.5 \leq pH_m \leq 8.5$ at T = 110°C and 190°C [86]. The authors observed no enhanced release of radionuclides in spite of the high borate concentration in solution (~ 10^{-2} mol·kg^{-1}). Chernorukov, Nipruk and co-workers [87-97] conducted a very comprehensive series of thermochemical and solubility experiments with $M^{I,II}$–U(VI)–B solid phases, with M^I = Li, Na, K, Rb, Cs and M^{II} = Mg, Ca, Sr, Ba, Mn, Co, Ni, Zn. The uranoborates were prepared by a combination of hydrothermal and ion-exchange approaches. The authors reported both log K_s and enthalpy data for the synthesized phases. Since all these uranoborates were synthesized at high temperatures (~ 870°C) they are not relevant considering the conditions investigated in this work.

1.3.3 Actinide borate solid phases

No actinide–borate minerals are known to naturally occur in the environment. One of the first reported synthetic crystalline actinide borate compound $K_6[UO_2(B_{16}O_{24}(OH)_8)]\cdot 12H_2O$ was obtained by evaporation of water at room temperature [98]. Gasperin and co-workers synthesized U(VI) and Th(IV) borate compounds such as ThB_2O_5, MgB_2UO_7 and $NaBUO_5$ using molten B_2O_3 at temperatures above 1000°C [99-101]. A variety of borate compounds with lanthanides [102, 103] and, recently, Am(III) and Pu(IV) were prepared by using boric acid flux at moderate temperatures (~200°C) [104-106]. Several uranium borates could be synthesized with this hydrothermal method by the group of Wang et al. In all these compounds, the linear UO_2^{2+} cation is surrounded by nine borate anions. The polymerized BO_3/BO_4 units build layers between the UO_2^{2+} cations. Additional BO_3 groups link the layers together and build a 3D framework. Water or cations like Na^+ are located in large gaps within the structure. The structure of the uranium borate $Na(UO_2)[B_6O_{10}(OH)]\cdot 2H_2O(cr)$ is exemplarily shown in Fig. 1.8.

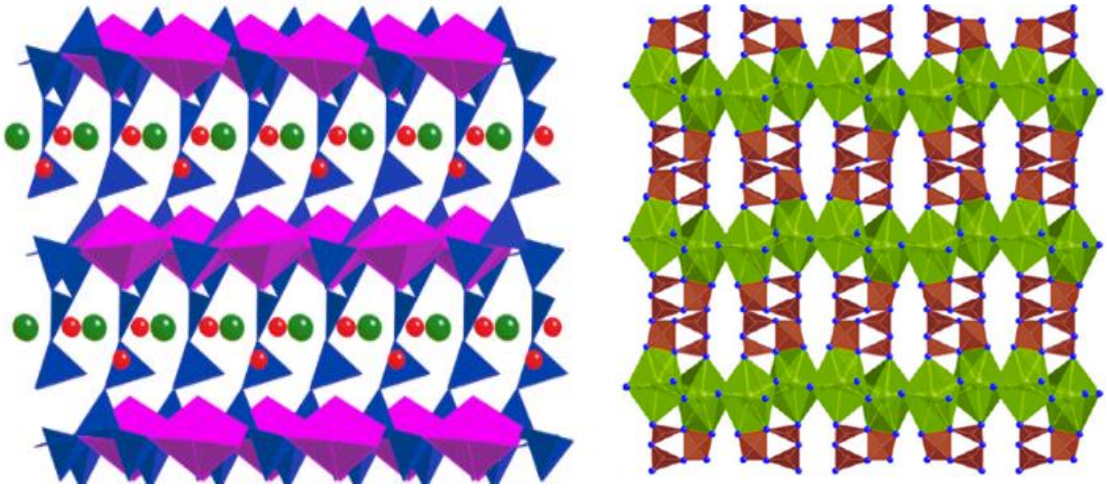

Figure 1.8. *(left) Depiction of $Na[(UO_2)B_6O_{10}(OH)]\cdot 2H_2O(cr)$. UO_8 hexagonal bipyramids are shown in magenta and BO_3/BO_4 units in blue. Green and red circles represent Na^+ and H_2O, respectively (right) Depiction of the structure of $NpO_2[B_3O_4(OH)_2](cr)$. NpO_7 pentagonal bipyramids are shown in green and BO_3/BO_4 units in red [104, 107].*

A few solid neptunium borate compounds have been synthesized with the use of molten boric acid. The melting point for boric acid at 170 °C leads to the disproportionation of Np(V) into Np(IV) and Np(VI). To synthesize a pure Np(V) structure, methyl boric acid was adopted as alternate flux with a lower melting point (89–94°C). The pure $NpO_2[B_3O_4(OH)_2](cr)$ was synthesized without disproportionation (structure shown in Fig. 1.8). In this solid compound, Np forms pentagonal

bipyramids with 7 oxygen atoms where every Np bipyramid is connected via cation cation interactions to four other Np bipyramids. A 3D framework is formed with chains containing of BO_3 and BO_4 units.

In spite of the increasing number of studies reporting the formation of An– and Ln–borate crystalline compounds, only a very few experimental studies are available so far assessing the formation, stability and relevance of these compounds in aqueous systems at lower temperatures (e.g. 25°C). Note also that so far no systematic study on An-borate interactions and their impact on solubility and speciation under a large variation of geochemical boundary conditions (pH, [B], [NaCl], [$MgCl_2$], [$CaCl_2$]) has been performed.

1.4 Time resolved laser fluorescence spectroscopy (TRLFS)

The Time resolved laser fluorescence spectroscopy (TRLFS) is a highly sensitive spectroscopic technique based on the spontaneous emission of light. Spontaneous emission of light also called luminescence is the emitting of electromagnetic radiation by the relaxation of an excited substance. If the relaxation process is between an excited state to the ground state of same spin multiplicities ($\Delta S = 0$) the luminescence is called fluorescence. Intense Luminescence emission by relaxation in aqueous solutions can be observed by some f-elements like Am(III), Cm(III), Bk(III) Cf(III), Pa(IV), U(VI), Eu(III), Gd(III) and Tb(III). F-f transitions between partly filled 4f (lanthanides) and 5f (actinides) energy levels cause characteristic optical spectra for each element. This f-f transitions are sensitive to changes of the ligand field e.g. complexation by ligands and cause visible changes in the spectra. Therefore, it is possible to investigate the complexation of f-elements in aqueous solution even in low concentrations with TRLFS. Several Actinides show, depending on their oxidation state, characteristic fluorescence which can be used for spectroscopic investigations. To this belong UO_2^{2+} [108] Am(III) [109], Cm(III) [110], Pa(IV)[111], Bk(III) [112] and Cf(III)[109].

1.4.1 Fluorescence properties of curium

The ground state of the Cm(III)-ion with the electronic configuration $[Rn]5f^7 6d^1 7s^2$ is $8S_{7/2}$. Excitation via electromagnetic radiation of a certain frequency is moving the Cm(III) ion to a F-, G- or H- state followed by a non-radiative relaxation to the $6D_{7/2}$ state (referred to as A in Fig. 1.9).

Luminescence emission brings the Cm(III) ion back to the ground state. This emission is leading to the characteristic emission spectrum of Cm(III) with a peak maximum at 593.8 nm (see Fig 1.10).

The crystal field splitting of the excited A-state of the Cm(III) ion of about 300 cm^{-1}, occurs with the same magnitude as the thermal energy of electrons at room temperature (kT = 207 cm^{-1}). Hence, not only the lowest crystal field state is occupied at room temperature, leading to a shoulder on the blue side of the emission spectra.

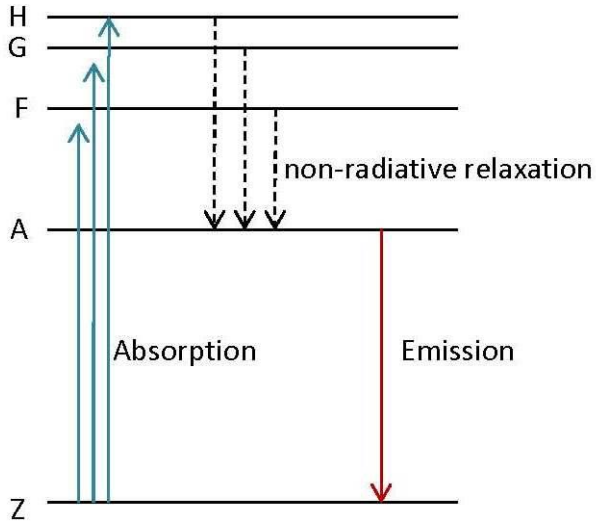

Figure 1.9. *Simplified term diagram for fluorescence processes of the Cm(III) ion.*

Complexation of the Cm(III) ion influences the ligand field experienced by the Cm^{3+} ion. The energy gap between the excited A state and the ground state is minimized, leading to a shift to higher wavelengths in the spectra. The spectral properties such as peak position, peak shape and the fluorescence lifetime give information about the coordination of the Cm(III) ion in the measured environment.

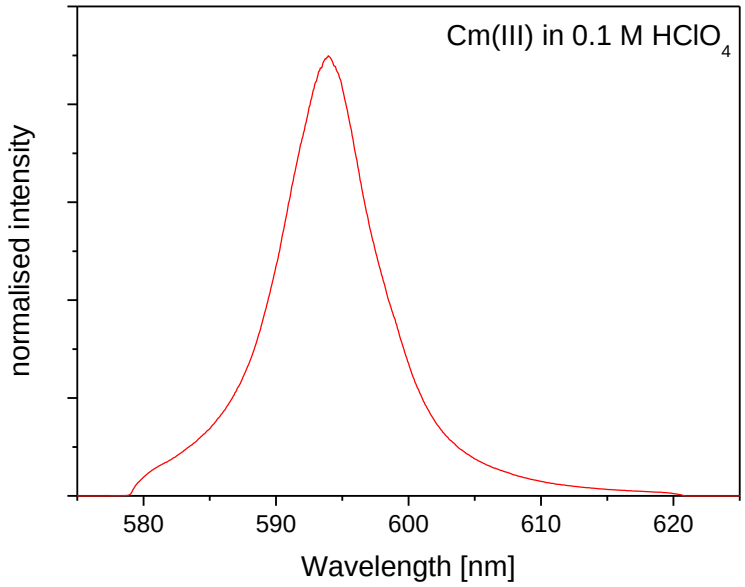

Figure 1.10. *Emission spectrum of Cm(III) in 0.1 M $HClO_4$.*

Investigations of Cm(III) complexation with organic or inorganic ligands in aqueous solution always compete with the hydrolysis of Cm(III). The peak maxima for the different Cm(III) hydrolysis species are shown in Table 1.2. The ternary complexes 1.4 and 1.6 can only be found in alkaline $CaCl_2$ solutions.

Table 1.2. *Peak maxima of Cm(III)-hydroxo complexes.*

Complex	**λ_{max} [nm]**	**Reference**
$Cm(OH)^{2+}$ (1.1)	598.7	[113]
$Cm(OH)_2^{+}$ (1.2)	603.5	[113]
$Cm(OH)_3$ (1.3)	607.5	[25]
$Ca_2[Cm(OH)_4]^{3+}$ (1.4)	609.9	[25]
$Ca_3[Cm(OH)6]^{3+}$ (1.6)	614.7	[25]

More detailed information about the hydration state of the Cm(III) ion can be obtained from the fluorescence lifetime of the excited state. The fluorescence lifetimes of f-elements in aqueous solutions are relatively short due to energy transfer from the excited F-level to vibrational levels of surrounding water molecules in the first coordination sphere of the metal ion. This process is referred to as quenching.

Fluorescence lifetimes can be obtained by measuring the fluorescence emission as function of the delay time (i.e. the time between laser pulse and detection of the camera). A system with n compounds and n lifetimes leads to a n-exponential decay. The Cm aquo ion has a lifetime (τ) of 68 ± 2 µs.

Kimura et al. found a linear correlation between the lifetime and the number of hydration water molecules in the first coordination sphere of Cm(III) [114]:

$$n(H_2O) = 0.65 \cdot k_{obs} - 0.88 \tag{1.34}$$

With the lifetime of 68 µs of the Cm(III) aquo ion a hydration sphere of nine water molecules is obtained. Complexation of the Cm(III) aquo ion leads to a replacement of water molecules with ligands and therefore to a longer lifetime.

1.5 UV-Vis/NIR spectroscopy of neptunium

UV-Vis/NIR spectroscopy is the absorption spectroscopy in the ultraviolet-visible and near infrared region. The absorption spectrum of a solved species in solution correlates with the concentration of the species. Hence, the Beer-Lambert law describes the relationship between the concentration of the species in solution and the extinction $E = -\log\left(\frac{I}{I_0}\right)$

$$E = -log\left(\frac{I}{I_0}\right) = log\left(\frac{I_0}{I}\right) = \varepsilon \cdot c \cdot d \tag{1.35}$$

where I_0 is the intensity of the initial photons, I is the intensity of the transmitted photons, ε is the extinctions coefficient [$L \cdot mol^{-1} \cdot cm^{-1}$], c is the concentration of the absorbed species [$mol \cdot L^{-1}$] and d is the path length [cm] [115].

UV-Vis/NIR spectroscopy can be applied to investigate the different redox states of Np from +III to +VI. Hence, the absorption spectra of the corresponding aquo ions are well known and can be used for their identification and corresponding quantification [116]. The wavelengths of the main absorption bands and extinction factors are listed in Table 1.3. Fig. 1.11 shows the absorption spectra of Np(V) in non-complexing perchloric acid. The use of UV-Vis/NIR spectroscopy is well suited for the investigation of Np under acidic conditions due to the very high solubility of all redox states in these conditions. Nevertheless, the applicability of this technique to the repository-relevant alkaline pH conditions is restricted to Np(V), due to the very low solubility shown by Np(IV) and Np(VI) under these conditions (note that Np(III) is not stable under alkaline conditions).

Table1.3. *Vis-NIR properties for Np(III)- Np(VI) aquo ions in 2 M $HClO_4$.*

Species	**Wavelength [nm]**	**ε [$L \cdot mol^{-1} \cdot cm^{-1}$]**	**Reference**
Np^{3+}	786	44	[116]
Np^{4+}	960	162	[116]
NpO_2^{+}	980	395	[116]
NpO_2^{2+}	1223	22	[116]

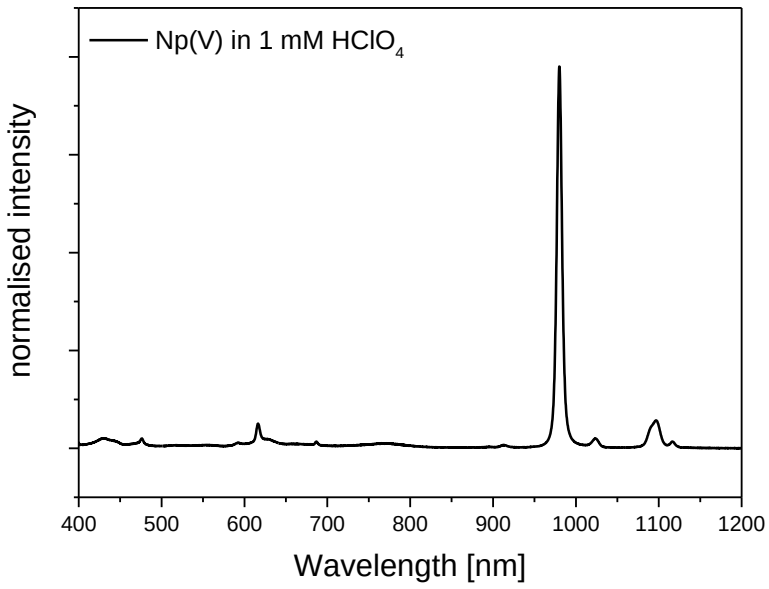

Figure 1.11. *Absorption spectra of Np(V) collected in 1 mM $HClO_4$*

The intensive absorption band at 980 nm of the hydrated NpO_2^+ ion is often used in studies investigating the complexation of Np(V) with different ligands [41, 117]. The position and intensity of the band correlate with the coordination environment of the NpO_2^+ ion. Hence, shifts of the band position are normally related to complex formation, although these can be also induced by changes in the background electrolyte or its concentration. Note that the 980 nm band is usually shifted to higher wavelengths if Np(V) is complexed and water is replaced in the first coordination sphere. Theoretical calculations of Matsika and Pitzer showed that the absorption band of Np(V) is linked to the symmetry of the Np(V) complexes [114, 118].

In the absence of carbonate, chloride is the only possible complexing ligand in NaCl and $MgCl_2$ solutions besides hydroxide. Several studies on the behaviour of Np(V) in the presence of chloride indicate a very weak interaction between NpO_2^+ and Cl^-. Runde et al. found a slight bathochromic peak shift of maximum 0.9 nm in the Vis-NIR absorption spectra of Np(V) in 0-5 M NaCl solution [16]. The peak shift was interpreted to be caused by the formation of inner-sphere $NpO_2Cl(aq)$ and $NpO_2Cl_2^-$ complexes. In 3.5 M $CaCl_2$ solution the formation of a ternary NpO_2-Cl^- complex was recently observed by Fellhauer, and the structure $Ca[NpO_2Cl]^{2+}$ could be identified with EXAFS analysis [41].

1.6 Thermodynamic databases

This section gives insight on some of the thermodynamic databases (TDB) available in the context of radioactive waste disposal, and thus with higher relevance in the framework of this PhD thesis. Furthermore, section 1.6.2 summarizes all equilibrium constants and SIT ion interaction coefficients considered in this work for thermodynamic calculations with Nd(III), Pu(III/IV), Th(IV), Np(V) and U(VI).

1.6.1 NEA–TDB and THEREDA databases

The prediction of the long-term safety of a nuclear waste repository needs a detailed description of the chemistry and migration behavior of radionuclides. To derive this information, geochemical calculations and modeling based on comprehensive and self-consistent thermodynamic databases are required. Databases gathered at national and international level provide the mandatory thermodynamic data such as solubility products, complex formation constants and activity coefficients (based on SIT and PITZER activity models, among others). Thermodynamic data compiled in these databases are normally selected from comprehensive experimental studies after a carefully review process with well-defined guidelines.

The Thermochemical Database (TDB) project of the Nuclear Energy Agency (NEA) provides the most comprehensive thermodynamic data selection currently available for radionuclides, fission products and other elements relevant in the framework of radioactive waste disposal (e.g. Fe). Because of its simplicity and extended applicability (up to I = 3.5 M), the NEA–TDB considers only SIT for ion activity corrections. In the context of this PhD thesis, it is noteworthy that no aqueous borate aqueous species or solid compounds are selected so far in the NEA–TDB for any of the evaluated actinides (U, Np, Pu, Am, Th) [22, 27].

In Germany, the Thermodynamic Reference Database project (THEREDA) is currently under development by several national and international institutions (KIT–INE, GRS, HZDR, TU–BAF and AF Consult). The THEREDA database aims at a comprehensive selection of thermodynamic data for the modeling of geochemical processes occurring in the near and far field of a repository for nuclear waste disposal. THEREDA is compelled to geochemical calculations relevant for radioactive waste disposal in all possible host-rock formations. Because of the need of covering also saline systems and in contrast with NEA–TDB, THEREDA relies mainly in the Pitzer approach to account for ion activity corrections.

1.6.2 Actinide solubility and hydrolysis constants used in this work

Table 1.4 summarizes all solubility and hydrolysis constants used in this work for thermodynamic calculations with Nd(III), Pu(III/IV), Th(IV), Np(V) and U(VI).

Table 1.4. *Solubility and hydrolysis constants used in this work for thermodynamic calculations with Nd(III), Pu(III/IV), Th(IV), Np(V) and U(VI).*

Reaction	**Constant**		**Reference**	
	log *K° ; log *β°			
Redox reactions $Pu^{3+} \rightleftharpoons Pu^{4+} + e^-$	-3.70 ± 0.17		[22]	
Solubility and hydrolysis of An(III)/Nd(III)	Pu(III)	Nd(III)		
$An(OH)_3$ (am) + $3H^+ \leftrightharpoons An^{3+} + 3\ H_2O$	-	17.2 ± 0.4		[24]
$An(OH)_3$ (cr) + $3H^+ \leftrightharpoons An^{3+} + 3\ H_2O$	15.8 ± 1.5	16.0 ± 0.4	[22]	[119]
$An^{3+} + H_2O \leftrightharpoons An(OH)^{2+} + H^+$	-6.9 ± 0.3	-7.4 ± 0.5	[22]	[24]
$An^{3+} + 2\ H_2O \leftrightharpoons An(OH)_2^+ + 2\ H^+$	*-15.1 ± 0.7*[a)]	-15.7 ± 0.70	[22]	[24]
$An^{3+} + 3\ H_2O \leftrightharpoons An(OH)_3 + 3\ H^+$	*-26.2 ± 0.5*[a)]	-26.2 ± 0.5	[22]	[22]
$An^{3+} + 4\ H_2O \leftrightharpoons An(OH)_4^- + 4\ H^+$	*-40.7 ± 0.7*[a)]	-40.7 ± 0.7	[22]	[22]
$An^{3+} + Cl^- \rightleftharpoons AnCl^{2+}$	-	0.24 ± 0.03		[22]
$An^{3+} + 2\ Cl^- \rightleftharpoons AnCl_2^+$	-	-0.74 ± 0.05		[22]
Solubility and hydrolysis of An(IV)	**Pu(IV)**	**Th(IV)**		
$AnO_2\ (am, hyd, fresh) + 4H^+ \leftrightharpoons An^{4+} + 4\ H_2O$	-2.33 ± 0.52	9.3 ± 0.9	[22]	[27]
$AnO_2\ (am, hyd, aged) + 4H^+ \leftrightharpoons An^{4+} + 4\ H_2O$	-8.03 ± 0.51	8.5 ± 0.9	[22]	[27]
$An^{4+} + H_2O \leftrightharpoons An(OH)^{3+} + H^+$	0.6 ± 0.2	-2.5 ± 0.5	[22]	[27]

$An^{4+} + 2\,H_2O \leftrightharpoons An(OH)_2^{2+} + 2\,H^+$	0.6 ± 0.3	-6.2 ± 0.5	[22]	[27]
$An^{4+} + 3\,H_2O \leftrightharpoons An(OH)_3^{+} + 3\,H^+$	-2.3 ± 0.4	-	[22]	-
$An^{4+} + 4\,H_2O \leftrightharpoons An(OH)_4 + 4\,H^+$	-8.5 ± 0.5	-17.4 ± 0.7	[22]	[27]
$2\,An^{4+} + 2\,H_2O \leftrightharpoons An_2(OH)_2^{6+} + 2\,H^+$	-	-5.9 ± 0.2		[27]
$2\,An^{4+} + 3\,H_2O \leftrightharpoons An_2(OH)_3^{5+} + 3\,H^+$	-	-6.8 ±0.2		[27]
$4\,An^{4+} + 8\,H_2O \leftrightharpoons An_4(OH)_8^{8+} + 8\,H^+$	-	-20.4 ± 0.4		[27]
$4\,An^{4+} + 12\,H_2O \leftrightharpoons An_4(OH)_{12}^{4+} + 12\,H^+$	-	-26.6 ± 0.2		[27]
$6\,An^{4+} + 14\,H_2O \leftrightharpoons An_6(OH)_{14}^{10+} + 14\,H^+$	-	-36.8 ± 1.2		[27]
$6\,An^{4+} + 15\,H_2O \leftrightharpoons An_6(OH)_{15}^{9+} + 15\,H^+$	-	-36.8 ± 1.5		[27]
$An^{4+} + Cl^- \leftrightharpoons AnCl^{3+}$	1.8 ± 0.3	1.7 ± 0.1	[22]	[27]
Solubility and hydrolysis of An(V)	**Np(V)**			
$AnO_2\,OH(am, fresh) + H^+ \leftrightharpoons AnO_2^+ + H_2O$	5.3 ± 0.2		[22]	
$AnO_2\,OH(am, aged) + H^+ \leftrightharpoons AnO_2^+ + H_2O$	4.7 ± 0.5		[22]	
$AnO_2^+ + H_2O \leftrightharpoons AnO_2(OH)(aq) + H^+$	-11.3 ± 0.7		[22]	
$AnO_2^+ + 2\,H_2O \leftrightharpoons AnO_2(OH)_2^- + 2\,H^+$	-23.6 ± 0.5		[22]	
Solubility and hydrolysis of An(VI)	**U(VI)**			
$UO_3 \cdot 2H_2O(am) + 2H^+ \leftrightharpoons UO_2^+ + 3H_2O$	5.35 ± 0.13		[53]	
$\frac{1}{2}Na_2U_2O_7 \cdot H_2O(cr) + 3H^+ \leftrightharpoons UO_2^+ + 2\,H_2O + Na^+$	12.2 ± 0.2		[53]	
$UO_2^{2+} + H_2O \leftrightharpoons UO_2(OH)^+ + H^+$	-5.25 ± 0.24		[22]	
$UO_2^{2+} + 2H_2O \leftrightharpoons UO_2(OH)_2 + 2H^+$	-12.15 ± 0.07		[22]	
$UO_2^{2+} + 3H_2O \leftrightharpoons UO_2(OH)_3^- + 3H^+$	-20.25 ± 0.42		[22]	
$UO_2^{2+} + 4H_2O \leftrightharpoons UO_2(OH)_4^{2-} + 4H^+$	-32.4 ± 0.68		[22]	

$2\,UO_2^{2+} + H_2O \leftrightharpoons (UO_2)_2(OH)^{3+} + H^+$	-2.7 ± 1	[22]
$2\,UO_2^{2+} + 2H_2O \leftrightharpoons (UO_2)_2(OH)_2^{2+} + 2H^+$	-5.62 ± 0.04	[22]
$3\,UO_2^{2+} + 4H_2O \leftrightharpoons (UO_2)_3(OH)_4^{2+} + 4H^+$	-11.9 ± 0.3	[22]
$3\,UO_2^{2+} + 5H_2O \leftrightharpoons (UO_2)_3(OH)_5^{+} + 5H^+$	-15.5 ± 0.12	[22]
$3\,UO_2^{2+} + 7H_2O \leftrightharpoons (UO_2)_3(OH)_7^{-} + 7H^+$	-32.2 ± 0.8	[22]
$4\,UO_2^{2+} + 7H_2O \leftrightharpoons (UO_2)_4(OH)_7^{+} + 7H^+$	-21.9 ± 1	[22]
$UO_2^{2+} + Cl^- \leftrightharpoons UO_2Cl^+$	0.17 ± 0.02	[22]
$UO_2^{2+} + 2\,Cl^- \leftrightharpoons UO_2Cl_2$	-1.1 ± 0.4	[22]

a) In analogy with Am(III) [22]

Table 1.5. *Sit parameters used in this work for thermodynamic calculations with Nd(III), Pu(III/IV), Th(IV), Np(V) and U(VI).*

i	j	ε_{ij}	Reference	i	j	ε_{ij}	Reference
H^+	Cl^-	0.12 ± 0.01	[22]				
Na^+	Cl^-	0.03 ± 0.01	[22]	Mg^{2+}	Cl^-	0.19 ± 0.02	[22]
An^{3+}	Cl^-	0.23 ± 0.02	[24]	$An(OH)^{2+}$	Cl^-	-0.04 ± 0.07	[24]
$An(OH)_2^+$	Cl^-	-0.06 ± 0.08	[24]	$An(OH)_3(aq)$	Na^+	-0.17 ± 0.1	[24]
$An(OH)_4^-$	Na^+	-0.03 ± 0.05	[24]				
Pu^{4+}	Cl^-	0.4 ± 0.1	[28]	Th^{4+}	Cl^-	0.25 ± 0.03	[27]
$Pu(OH)_3^+$	Cl^-	0.2 ± 0.1	[28]	$Th(OH)_3^+$	Cl^-	0.19 ± 0.05	[27]
$Pu(OH)_2^{2+}$	Cl^-	0.1 ± 0.1	[28]	$Th(OH)_2^{2+}$	Cl^-	0.13 ± 0.05	[27]
$Pu(OH)_3^+$	Cl^-	0.05 ± 0.1	[28]	$Th(OH)_3^+$	Cl^-	0.06 ± 0.05	[27]
NpO_2^+	Cl^-	0.09 ± 0.05	[22]	$Th_2(OH)_2^{6+}$	Cl^-	0.4 ± 0.16	[27]
$NpO_2(OH)_2^-$	Na^+	-0.01 ± 0.07	[22]	$Th_2(OH)_3^{5+}$	Cl^-	0.29 ± 0.09	[27]
UO_2^{2+}	Cl^-	0.21 ± 0.02	[22]	$Th_3(OH)_5^{7+}$	Cl^-	-	[27]
$UO_2(OH)^+$	Cl^-	0.05 ± 0.1	[59]	$Th_4(OH)_8^{8+}$	Cl^-	0.7 ± 0.2	[27]
$UO_2(OH)_3^-$	Na^+	-0.09 ±0.05	[22]	$Th_4(OH)_{12}^{4+}$	Cl^-	0.25 ± 0.2	[27]
$UO_2(OH)_4^2$-	Na^+	-0.1 ± 0.1	[59]	$Th_6(OH)_{14}^{10+}$	Cl^-	0.83 ± 0.3	[27]
$(UO_2)_2(OH)^{3+}$	Cl^-	0.69 ± 0.07	[22]	$Th_6(OH)_{15}^{9+}$	Cl^-	0.72 ± 0.3	[27]
$(UO_2)_2(OH)_2^{2+}$	Cl^-	0.81 ± 0.17	[22]				

1.7 Aim of the present work

In the present work, the interaction of borate with actinide (III, IV, V, VI) is investigated in diluted to concentrated saline solutions with a combination of solubility experiments, spectroscopic methods (including TRLFS, EXAFS and UV–Vis/NIR) and comprehensive solid phase characterization (accomplished with XRD, XPS, SEM–EDS, XANES/EXAFS). The work comprises experimental conditions relevant for different concepts of radioactive waste disposal, and thus different background electrolytes (NaCl, $MgCl_2$ and $CaCl_2$) as well as a broad pH-range ($6 \leq pH_m \leq 13$) are considered. The main objectives of this work are:

- The solubility of Nd(III) is studied in dilute to concentrated NaCl, $CaCl_2$ and $MgCl_2$ solutions with varying pH and boron concentration. Focus is given to the possible formation of Nd(III)–borate compounds and their eventual role on the immobilization of An(III). Thus a comprehensive solid phase characterization is performed using XRD, XPS and SEM–EDS. Additional TRLFS experiments with Cm(III) give information on the aqueous speciation of An(III)/Ln(III) in the presence of borate. With these data, a first thermodynamic description is proposed for the system Ln(III)/Cm(III)-Na^+-Mg^{2+}-Ca^{2+}-H^+-Cl^--$B(OH)_4^-$ at 25°C.
- The solubility of Np(V) is studied in dilute to concentrated NaCl and $MgCl_2$ solutions with varying pH and boron concentration. As for Ln(III)/An(III), focus is given to the possible formation of Np(V)–borate compounds and their possible impact on the Np source term. Solid phase characterization is accomplished using XRD, SEM–EDS, XPS and EXAFS techniques. The aqueous speciation of Np under increasing concentrations of borate is investigated using UV–Vis/NIR. The combination of solubility data, spectroscopic results and solid phase characterization is aimed at deriving a first thermodynamic description for the system Np(V)-Na^+-Mg^{2+}-H^+-Cl^--$B(OH)_4^-$ at 25°C.
- Because of their stronger hydrolysis and the expectedly weaker interaction with borate, the solubility of Th(IV) and U(VI) is exemplarily investigated in dilute to concentrated NaCl and $MgCl_2$ solutions and at various boron concentrations. Solubility measurements are complemented with solid phase characterization using XRD. The system Pu(III)–Pu(IV) is considered to gain insight on the effect of borate on the chemical behavior of redox sensitive actinides and allow a better assessment of the plutonium source term.

With the focus on practical application, the ultimate goal of this PhD thesis is to assess upper concentration limits of An(III), An(IV), An(V) and An(VI) in the presence of repository-relevant pH, ionic strength and borate concentration, to be used in source term estimations in performance assessment exercises for nuclear waste repositories. For those cases where a relevant impact of borate is observed, this work aims also at providing a quantitative assessment supported by thermodynamic modeling.

2 Experimental

2.1 Chemicals and analytical methods

2.1.1 Chemicals

All chemicals used in the experiments were obtained from Merck or specifically prepared at INE and were not further purified (see Table 2.1). All solutions were prepared with purified water from a Milli-Q-academic apparatus (Millipore, 18.2 MΩ) purged with Argon before use.

Hydrochloric acid and sodium hydroxide were prepared with HCl-Titrisol and carbonate-free NaOH (Merck, Titrisol) standard solutions, respectively. pH buffers used for calibration of the pH electrode were prepared with Titrisol standard buffer solutions by Merck. The pH of the different solutions was adjusted with HCl (Titrisol, Merck), NaOH (Titrisol, Merck), $Ca(OH)_2$ and $Mg(OH)_2$ of appropriate ionic strength. In $MgCl_2$ and $CaCl_2$ solutions, the maximum pH is limited to pH_{max} = 9 and 12 due to the precipitation and consequent pH-buffering of magnesium and calcium hydroxides or hydroxo-chlorides, respectively [5]. Sufficiently long equilibration time (~1 month) was allowed for all borate solutions in dilute to concentrated saline systems before use. This was especially important in the case of Cm(III)–TRLFS, where extensive evolution of the Cm(III) species was observed with time.

Table 2.1. *Chemicals used in the experimental work of this PhD thesis.*

Name	Chem.Formula	Purity	Supplier
sodium chloride	NaCl	p.a.	Merck
calcium chloride	$CaCl_2 \cdot 2H_2O$	p.a	Merck
sodium tetraborate	$Na_2B_4O_7 \cdot 10H_2O$	p.a	Merck
nitric acid	HNO_3	suprapur	Merck
sodium hydroxide	NaOH		Merck/Titrisol
hydrochloric acid	HCl		Merck/Titrisol
neodymium oxide	Nd_2O_3(cr)	a.r.	Merck
neodymium hydroxide	$Nd(OH)_3$(am)	-	INE

neodymium borate	$Nd[B_9O_{13}(OH)_4](cr)$	-	FZJ
thorium nitrate	$Th(NO_3)_4 \cdot 5H_2O(cr)$	p.a.	Merck
thorium hydroxide	$Th(OH)_4(am)$	-	INE
uranium(VI) nitrate	$UO_2(NO_3)_2 \cdot 6H_2O(cr)$	a.r.	Merck
metaschoepite	$UO_3 \cdot 2H_2O(cr)$	-	INE
natrium diuranate	$Na_2U_2O_7 \cdot H_2O(cr)$	-	INE
neptunium hydroxide	$NpO_2OH(am,fresh)$	-	INE
magnesium chloride	$MgCl_2 \cdot 6H_2O$	p.a.	Merck
calcium hydroxide	$Ca(OH)_2$	p.a.	Merck
magnesium hydroxide	$Mg(OH)_2$	p.a.	Merck
sodium dithionate	$Na_2S_2O_4$	(>87%).	Merck
hydroquinone	$C_6H_6O_2$	p.a.	Merck

2.1.2 Transuranium radionuclides used in the experiments

The long-lived curium isotope ^{248}Cm ($t_{1/2}$ = 3.4×10^5 years) was used for the TRLFS measurements. The stock solution used in the experiments (2×10^{-5} M Cm(III) in 0.1 M $HClO_4$) had an isotopic composition of 89.7% ^{248}Cm, 9.4% ^{246}Cm, 0.4% ^{243}Cm, 0.3% ^{244}Cm and 0.1% ^{247}Cm.

A ^{237}Np stock solution was previously prepared with 2.5 g of ^{237}Np ($t_{1/2}$ = 2.14·10^6 years), which was purified from trace impurities of Pu and Am using an ion exchange method [120]. The resulting Np solution (0.32 M ^{237}Np in 0.01 M HCl) was characterized by gamma spectrometry, liquid scintillation counting (LSC), UV–Vis/NIR and alpha spectrometry, which confirmed both the chemical and radiochemical purity of the ^{237}Np stock solution.

Pu solubility experiments were performed with ^{242}Pu with the exact isotopic composition of ^{242}Pu (99.4%), ^{239}Pu (0.58%), ^{238}Pu (0.005%) and ^{241}Pu (0.005%). Since the main isotope is ^{242}Pu ($t_{1/2}$ = 375000 years), no radiolysis effects, occurring by the decay of short lived Pu isotopes in concentrated chloride solutions are expected.

2.1.3 pH measurements in dilute and concentrated saline solutions

2.1.3.1 General

The pH value of a solution is defined as the negative logarithm of the activity of the hydrogen ion (a_{H^+}) [121-123]

$$pH = -\log(a_{H^+}) = -log\ {}^{m}\gamma_{H^+} - log\ m_{H^+} = -log\ {}^{c}\gamma_{H^+} - log\ c_{H^+} \quad (2.1)$$

Where m_{H^+} and c_{H^+} are the molal and molar concentrations of the hydrogen ion, ${}^{m}\gamma_{H^+}$ and ${}^{c}\gamma_{H^+}$ represent the absolute ion activity coefficients of H^+. Since a_{H^+} and the pH of a solution are not directly measurable, an international accepted pH scale was introduced which provides a reproducible method to measure pH and compare the acidity of dilute solutions (I≤ 0.1 m) [123]. The method is based on the measurement of standard buffers of known pH with a H^+ electrode without junction potential (Harned cell)

$$PT/H_2/buffer\ S,\ Cl^-|AgCl|Ag \quad (2.2)$$

The potential difference of this cell is given by

$$E = E^0 - \left(\frac{RT}{F} ln10\right) log[(m_{H^+}\gamma_{H^+})(m_{Cl^-}\gamma_{Cl^-})] \quad (2.3)$$

The reference standard potential E^0 of the Ag|AgCl electrode can be derived with an electrode filling solution of pure 0.01 m HCl. The activity coefficient of Cl^- is not measurable but for low ionic strength (I≤ 0.1 m) it can be calculated using the Bates-Guggenheim convention (based on the Debye-Hückel theory) $\log\gamma_{Cl^-} = -AI^{1/2}/(1+1.5I^{1/2})$. Furthermore operational pH standards (secondary standards) are needed to account for the liquid junction potential. Generally inorganic or organic solutions with well-known pH can be used. They need a small temperature dependence (± 0.01 K^{-1}), low residual liquid junction potential and low ionic strength (I ≤ 0.1 m) to remain valid within the Bates Guggenheim convention.

2.1.3.2 pH measurement with glass electrodes

To measure pH experimentally in a solution, a electrochemical cell consisting of a glass electrode (GE) sensitive to hydrogen ions and a reference electrode (REF) connected with a salt bridge are needed. Both electrodes can be combined in a single glass body. With a sensitive electrometer the potential difference between the electrodes can be measured

$$E = E^0(REF) - E^0(GE) - E_{AS} + \left[\frac{RTln(10)}{F}\right] \cdot log a_{H^+} + E_j \quad (2.4)$$

Where $E^0(REF)$ and $E^0(GE)$ are the temperature-dependent potential of the reference electrode and the glass electrode, respectively. E_{AS} is the asymmetry potential of the glass electrode and Ej the liquid junction potential at the interface between electrolyte in the reference and sample solution. With 25°C the Nernst slope ($\left[\frac{RTln(10)}{F}\right]$) is 59.16 mV.

The unknown pH of a sample solution E(X) can be determined as the voltage difference between *E*(X) and the pH standard buffers E(S) (calibration) [124]

$$pH(X) = pH(S) + [E(S) - E(X)] \cdot \frac{F}{RTln(10)} + [E_j(X) - E_j(S)] \cdot F/RTln(10) \quad (2.5)$$

For low ionic strength (I ≤ 0.1 m) the term $[E_j(X) - E_j(S)] \cdot F/RTln(10)$ can be neglected but for the measurement in high acidity/alkalinity or at elevated ionic strength this term is not negligible anymore and a modified approach is needed [124].

2.1.3.3 pH measurement in saline solutions

In solutions with I ≥ 0.1 m, ion interaction processes affect the activity coefficient of H^+ (γ_{H^+}) and the liquid junction potential. To determine pH in high salinity no longer the activity of H^+ but the concentration of H^+ are used [125]:

$$pH_m = -log(m_{H^+}) \; and \; pH_c = -log(c_{H^+}) \quad (2.6)$$

Where pH_m and pH_c are the negative logarithm of the molal and molar concentration of H^+, respectively.

The values pH_m and pH_c can be calculated from the operationally measured pH_{exp} and an empirical correction factor (A) where liquid junction potential and the activity coefficient of H^+ are included.

$$pH_m = pH_{exp} + A_m \; and \; pH_c = pH_{exp} + A_c \quad (2.7)$$

with

$$A_m = log \; {}^m\gamma_{H^+} + \Delta E_j \frac{F}{RT} ln(10) \quad (2.7a)$$

and

$$A_c = log \; {}^c\gamma_{H^+} + \Delta E_j \frac{F}{RT} ln(10) \quad (2.7b)$$

The correction factor A is experimentally determined for the respective salt system and concentration with a set of reference solutions with known proton concentration.

For pH measurements in this work, a combination glass pH electrode (type ROSS, Orion), freshly calibrated against dilute standard pH buffers (pH 7–13, Merck), was used to determine the molar or molal H^+ concentration, $[H^+]$ and m_{H^+}, respectively. Whenever needed, pH adjustments were performed with HCl-NaCl-NaOH, HCl-$MgCl_2$ and HCl-$CaCl_2$ solutions of proper ionic strength. Alkaline solutions in $MgCl_2$ and $CaCl_2$ were adjusted with $Mg(OH)_2$(s) and $Ca(OH)_2$(s), respectively. All A factors used in this work for NaCl, $CaCl_2$ and $MgCl_2$ solutions were previously reported by Altmaier et al [5, 31] and are summarized in Table 2.2. The pH_m measurements performed following this approach are assigned with an uncertainty of ± 0.04 pH units. Note that the impact of borate on the background electrolyte is not corrected for the determination of pH. Nonetheless, it cannot be excluded that high boron concentrations ($[B]_{tot}$ = 0.4 M) might have impact on pH measurements in this work. The uncertainty of pH measurements in these specific cases is considered ± 0.1 pH units.

Table 2.2. *A_c- and A_m values used in this work for the quantification of pH_c and pH_m, respectively.*

Salt system	**Concentration**	**A_c**	**A_m**
NaCl	0.1 M	-0.08	-0.08
NaCl	1.0 M	0.09	0.08
NaCl	5.0 M	0.95	0.9
$CaCl_2$	0.25 M	0	-0.01
$CaCl_2$	1.0 M	0.34	0.33
$CaCl_2$	3.5 M	1.77	1.71
$MgCl_2$	0.25 M	0.03	0.03
$MgCl_2$	1.0 M	0.4	0.4
$MgCl_2$	3.5 M	1.98	1.93

2.1.4 Eh measurements

The redox potentials in the Pu(III/IV) experiments were measured with Metrohm Pt combination electrodes with an Ag/AgCl reference system. The measured potential was converted to Eh by correction for the potential of the Ag/AgCl reference electrode

$$AgCl(s) + e^- \rightleftharpoons Ag + Cl^- \quad (2.8)$$

with

$$E = E°_{Ag/AgCl} + \frac{RTln(10)}{F} \cdot log\, a_{Cl^-} = 0.208\, V\ (at\ T = 25^\circ\ C\ in\ 3.0\ M\ KCl) \quad (2.9)$$

with $E°_{Ag/AgCl}$ = 0.222 V and (RT/F) = 0.02569 V at T = 25°C. The accuracy of the electrode was checked regularly with a standard redox buffer (+220 mV vs. Ag/AgCl, Schott Instruments).

The measured redox potential of the system can also be used to calculate the pe value in analogy to the pH as negative logarithm of the electron activity.

$$Eh = -\left(\frac{RT}{F}\right) ln\, a_{e^-} \quad (2.10)$$

$$pe = -log\, a_{e^-} = 16.9 \cdot Eh[V]\ at\ T = 25°C \quad (2.11)$$

Eh was measured in the Pu(III/IV) samples until a stable value was reached (~20-30 minutes per sample).

2.1.5 Speciation of boron in aqueous saline solutions

2.1.5.1 ^{11}B-NMR in NaCl, $CaCl_2$ and $MgCl_2$ solutions

^{11}B-NMR spectra were recorded with a Bruker NMR-spectrometer (Avance III, 400 MHz) with a field strength of 9.4 T and a corresponding ^{11}B resonance frequency of 128.4 MHz with a broadband observe probe. The ^{11}B chemical shifts (δ) are referenced externally with respect to BF_3 etherate in $CDCl_3$. All spectra were evaluated with the software Top Spin (Bruker). For all spectra a pulse sequence with a very short delay time (100 µs) was used. The ^{11}B-NMR measurements were performed under atmospheric conditions in teflon liners (Rototec-Spintec, PTFE-FEB-NMR Tube Liner 8'', 5 mm) filled with 400 µL sample solution and mixed with 40 µL D_2O at 25°C. Table 2.3 summaries the samples prepared in dilute and concentrated NaCl, $MgCl_2$ and $CaCl_2$ with 0.04-0.4 M total boron concentration with varying pH_m have been measured as shown in Table 2.3.

Table 2.3. *Experimental conditions in the system investigated by ^{11}B-NMR.*

System	Concentration of background electrolyte	$[B]_{tot}$	pH_m
NaCl	0.1 M	0.04 M, 0.16 M	8; 12
NaCl	5.0 M	0.04 M, 0.16 M	2.6; 8; 12
$CaCl_2$	0.25 M	0.04 M	8; 12
$CaCl_2$	3.5 M	0.04 M	8; 12
$MgCl_2$	0.25 M	0.04 M, 0.16 M, 0.4 M	8
$MgCl_2$	3.5 M	0.04 M, 0.16 M, 0.4 M	8

2.1.6 Determination of total metal concentration and aqueous speciation techniques used for Ln(III) and An(III/IV/V/VI) in solution

2.1.6.1 ICP-MS

The total aqueous concentration of Nd, Th and U was measured by ICP–MS after phase separation by 10 kD ultrafiltration (~1.5 nm, Pall Life Sciences) (Thermo scientific X-Series II for Nd(III) and Perkin Elmer Elan 6100 for Th(IV) and U(VI)). The detection limit of the technique in the investigated systems varied between 10^{-9}–10^{-10} mol·L^{-1}, depending upon the element, the salt concentration in the original sample and the required dilution steps.

2.1.6.2 LSC

The liquid scintillation counting technique is based on the detection of the ionization radiation that is resulting from radioactive decay [126]. The released energy of this process is transformed to photon emission by the photoactive organic molecules (e.g. Naphthalene, terphenyl, 1,4-Bis-(5-phenyloxazol-2-yl)-benzol) in the LSC cocktail. A photocathode is converting the photon emission to electronic emission which is multiplied by a photomultiplier (10^5-10^7) before it can be measured by a detector (e.g. semiconductor detector). The electron emission is proportional to the energy of the radioactive decay of the measured sample.

LSC measurements were performed in PP vials (20 mL, Zinsser Analytic). After 10 kD ultrafiltration (~1.5 nm, Pall Life sciences), a small aliquot of the sample was mixed with 10 mL LSC cocktail

(Ultima Gold XR, Fa. Perkin-Elmer). Samples were measured for 30 minutes with a Perkin Elmer 1220 Quantulus.

The α decay of ^{237}Np (4.79 MeV) and the two β^- decays of the daughter nuclide ^{233} Pa (0.3 and 0.6 keV) are measured by LSC. The resulting spectra of the α decay of ^{237}Np and the high energetic β decay of ^{233}Pa are overlapping. To determine the ^{237}Np concentration in solution it is mandatory to separate the peaks by α/β discrimination. The Quantulus apparatus used in this work provides a pulse shape analyzer (PSA) to perform a simultaneous alpha/beta gross counting, which allows the distinction between alpha and beta pulses.

The Pu stock solution used in this work is composed of α-(^{242}Pu, ^{239}Pu, ^{238}Pu) and β-(^{241}Pu) emitters, as well as traces of the α-emitter ^{241}Am resulting from the decay of ^{241}Pu ($t_{1/2}$ = 14.35 a). The energies of the α-peaks of ^{242}Pu, ^{239}Pu, ^{238}Pu and ^{241}Am are very close to each other and cannot be separated by LSC. In this work the Pu concentration in solution was determined using the low energetic β -emitter ^{241}Pu. To avoid uncertainties by matrix solution effects on the counting efficiency, standard additions with 50 µL of a well-defined $4.36 \cdot 10^{-7}$ M Pu stock solution with the same isotopic composition were used. The detection limits are $5 \cdot 10^{-9}$ M for ^{237}Np (α-radiation measured after α/β-discrimination of the counts from the daughter nuclide ^{233}Pa) and $4 \cdot 10^{-10}$ M for the Pu.

2.1.6.3 Cm(III) TRLFS

A detailed description of the Cm(III) laser fluorescence spectroscopy is given in section 1.4. TRLFS spectra were measured with a Nd:YAG pumped dye laser system (Surelite II Laser, Continuum) at a repetition rate of 10 Hz and a maximum laser energy of 3.5 mJ. Spectra were recorded 1 µs after the exciting laser pulse in a time window of 1 ms at λ_{ex} = 396.6 nm (laser dye: Exalite 398). A Shamrock spectrograph (A-SR-303i-B, Andor Technology) and an ICCD camera (iStar ICCD, Andor Technology) were used for the detection of the fluorescence signal. Both single emission spectra and fluorescence lifetimes were collected.

Time resolved laser fluorescence spectroscopy (TRLFS) experiments were performed with $1 \cdot 10^{-7}$ M Cm(III) per sample in dilute to concentrated NaCl, $CaCl_2$ and $MgCl_2$ solution. Total boron concentrations ranged from 0.004 M to 0.4 M. Spectra in NaCl and $MgCl_2$ systems were collected at pH_m = 8.0 ± 0.1, whereas spectra in $CaCl_2$ were collected at pH_m = 8.0 ± 0.1 and 12.0 ± 0.1. Cm(III)–TRLFS spectra in NaCl an $CaCl_2$ solutions with freshly prepared borate solutions ($[B]_{tot} \geq 0.04$ M) showed very pronounced kinetic effects. Therefore, sufficiently long equilibration times (~ two weeks) were allowed for all matrix solutions used in the TRLFS experiments shown in this work. After this equilibration time, the Cm(III) was spiked to the matrix solutions. The samples were measured within 2 hours after the Cm(III) addition. Measurements with longer equilibration times (up to 2 days) did

not show any relevant kinetic effect on the fluorescence spectra. A detailed list of all investigated samples is given in Table 2.4.

Table 2.4. *Experimental conditions in the TRLFS study with Curium.*

System	Concentration of background electrolyte	$[B]_{tot}$	pH_m
NaCl	0.1 M	0.004 M; 0.04 M; 0.16 M	8; 12
NaCl	5.0 M	0.004 M; 0.04 M; 0.16 M	8; 12
$CaCl_2$	0.25 M	0.004 M; 0.04 M;	8; 12
$CaCl_2$	3.5 M	0.004 M; 0.04 M;	8; 12
$MgCl_2$	0.25 M	0.04 M; 0.16 M; 0.4 M	8; 9
$MgCl_2$	3.5 M	0.04 M; 0.16 M; 0.4 M	8; 9

2.1.6.4 UV-Vis/NIR spectroscopy

A detailed description of the UV-Vis/NIR spectroscopy of neptunium in aqueous solution is provided in section 1.5. Absorption spectra of Np(V) were collected with a Varian UV-Vis spectrometer (Cary 5E) against a reference solution with the same background electrolyte and borate concentration as the measured sample. Spectra were recorded in the range λ = 850 – 1250 nm with a step width of 0.2 nm. All measurements were performed with ~3 mL of sample solution in quartz cuvettes with d = 1 cm.

2.1.7 Solid phase characterization (XRD, XPS, SEM-EDS, EXAFS)

Solid phases from the Nd, Pu, Np and U solubility experiments were characterized by XRD, XPS and SEM-EDS after a given equilibrium time. Selected solid phases from the Np(V) solubility experiments were also investigated by EXAFS.

2.1.7.1 XRD

A small amount (~1 mg) of the solid was separated from the solution by centrifugation (4000 *g*) in the glovebox and washed 3 times with ethanol (2 mL) under an Ar-atmosphere to remove traces of the matrix solution (NaCl, $MgCl_2$ or $CaCl_2$) which would interfere with the XRD analysis. The prepared

solid was measured with a Bruker D8 Advance diffractometer (Cu Kα radiation) equipped with a Sol-X detector. XRD data were collected within $5^{o} \leq 2\Theta \leq 60^{o}$, with a step size of 0.04º and 6 s accumulation time per step to allow for reliable counting statistics.

2.1.7.2 XPS and SEM-EDS

Solid samples for XPS analysis were prepared using the same approach as described for XRD, although the amount of sample was significantly reduced (10–50 µg). After drying, the washed solid phase was pressed on an indium foil and analyzed with an XP spectrometer (ULVAC-PHI, Inc., model PHI 5000 VersaProbe II) equipped with a standard dual anode X-ray source (Mg Kα (1253.6 eV), Al Kα (1486.6 eV)), and with a scanning microprobe X-ray source (monochromatic Al Kα). Calibration of the binding energy scale was performed using well-established binding energies of elemental lines of pure metals (monochromatic Al Kα: Cu $2p_{3/2}$ at 932.62 eV, Au $4f_{7/2}$ at 83.96 eV) [127]. Standard deviations of binding energies of isolating samples were within ±0.2 eV. Survey scans were recorded with a source power of 50 W of the scanning microprobe X-ray source and a pass energy of 187.85 eV of the analyzer, step size 0.8 eV, to identify the elements and to determine their atomic concentrations at the sample surface. Survey scans were recorded to identify the elements and to determine their atomic concentrations. To retrieve information about the chemical state of the elements, narrow scan spectra of elemental lines were recorded at a pass energy of 23.5 eV, step size 0.1 eV. All spectra were charge referenced to the C 1s elemental line of hydrocarbon (C_xH_y) at 284.8 eV.

To gain additional information on the crystallinity, morphology and chemical composition of the solid phase, a second fraction of the washed solid was characterized by scanning electron microscope-energy disperse spectrometry (SEM–EDS), using a FEI Quanta 650 FEG equipped with a Noran EDS unit.

2.1.7.3 EXAFS

EXAFS measurements were performed at the INE-beamline for Actinide Research at the ANKA synchrotron source, Karlsruhe, Germany. The measurements and data evaluation were performed in cooperation with the scientists of the INE-beamline.

Approximately 1 mg of the investigated solid phase in contact with the supernatant solution was directly transferred to a polyethylene vial under Ar atmosphere. The vials were centrifuged at 4000 g for 5 minutes, mounted in a gas-tight cell with windows of Kapton® film (polyimide) inside the Ar-glovebox and transported to the INE-beamline. The samples were measured under continuous Ar-flow within 1 day after preparation for EXAFS measurements.

Bulk XAS data at the Np L_{III}-edge at 17610 eV were collected in fluorescence mode at room temperature using a Ge solid-state detector. The beamline is equipped with a Ge(422) double crystal

monochromator (DCM) coupled with a collimating and a focusing Rh coated mirrors before and after the DCM, respectively. The monochromator was calibrated for the Np-L_{III} edge by assigning the energy of 17,038 eV to the first inflection point of the K-edge absorption spectrum of the Y metal foil. All measurements were recorded at room temperature in fluorescence mode using a multi- element Ge-detector. Multiple scans were run on each sample. All EXAFS spectra were extracted from raw data with the Athena interface of the IFFEFIT software [128]. The Fourier transforms (FTs) were obtained from the k^3-weighted $\chi(k)$ functions using a Kaiser-Bessel window function with an apodization parameter of 1. Multishell fits were performed in real space across the range of the first two shells. Amplitude and phase shifts functions were calculated using the FEFF 8.4 code [129]. The amplitude reduction factor S_0^2 was set to the value of 0.8 [130]. Structural information was obtained by following a multi-shell approach for EXAFS data fitting. The fit was limited to parameters describing the Np coordination to surrounding oxygen and boron atoms (neighbouring atomic distances (R), EXAFS Debye–Waller factors (σ^2), coordination numbers (N) and relative shift in ionization energy E_0 (ΔE_0)).

2.2 Ln(III)/An(III/IV/V/VI) solubility experiments

2.2.1 Nd(III) and An(III/IV/V/VI) solid phase preparation

Amorphous Nd(III) hydroxide used in the solubility experiments was prepared by hydration of crystalline neodymium hydroxide (Nd_2O_3(cr), Merck) in Milli-Q water under an argon atmosphere [24]. The complete transformation of the oxide into the hydroxide phase was confirmed by XRD (JCPDF file No: 70-0214, JCPDS 2001). $Nd[B_9O_{13}(OH)_4]$(cr) was prepared by the group of Dr. Evgeny Alekseev at the research center Jülich (FZJ). For the synthesis of crystalline $Nd[B_9O_{13}(OH)_4]$(cr), Nd_2O_3 and H_3BO_3 were taken as starting materials in a molar ratio 1:15. The mixture was placed in a Teflon liner and sealed in a hydrothermal reactor. The reactor was heated to 220°C for 3 days, and let cool down to room temperature in another 2 days. Excess boric acid (H_3BO_3) was washed out with hot water (90°C). The purity of the material obtained was assessed by XRD.

To prepare $Pu^{IV}O_2$(am,hyd), a purified ^{242}Pu(VI) stock solution was added to a pH-buffered (25 mM MES) and redox-buffered (1.5 mM hydroquinone) solution leading to an immediate formation of aqueous Pu(V) and a slow "reductive precipitation" of $Pu^{IV}O_2$(am, hyd). The mild in situ "reductive precipitation" leads to a microcrystalline $Pu^{IV}O_2$(am,hyd) solid phase which is less affected to aging effects than "fresh" $Pu^{IV}O_2$(am,hyd) prepared by addition of NaOH to an acidic Pu(IV) solution. The washed $Pu^{IV}O_2$(am,hyd) solid was characterized using XRD.

$Th(OH)_4$(am) was prepared under argon atmosphere by titration of thorium chloride stock solution with carbonate-free NaOH up to pH ~10. The precipitate was washed with Milli-Q water several times before further use in the solubility experiments.

NpO_2OH(am,fresh) was prepared under argon atmosphere by titration of a (radiochemically pure) acidic $^{237}Np(V)$ stock solution with carbonate-free NaOH. The resulting precipitate (NpO_2OH(am,fresh)) was separated from the solution by centrifugation and washed several times with water before use in the solubility experiments.

Metaschoepite $UO_3 \cdot 2H_2O$(cr) was prepared under argon atmosphere by a very slow titration of an acidic uranium(VI) chloride stock solution with carbonate-free NaOH. In the precipitation process, the pH was checked regularly and kept always below 5 to avoid the transformation of $UO_3 \cdot 2H_2O$(cr) into sodium uranate or other Na–U(IV)–OH ternary phases. The washed precipitate was characterized by XRD before addition to the solubility experiments.

Sodium uranate, $Na_2UO_2O_7 \cdot H_2O$(cr), was prepared by transformation of initial metaschoepite in 2.5 M NaCl solution at pH_m ~12 for several months. The new formed solid was separated, washed and characterized with XRD before use in the solubility experiments.

2.2.2 Sample preparation

All experiments were prepared and carried out at 22±2 °C in Ar-gloveboxes under exclusion of O_2(g) and CO_2(g). Solubility samples in NaCl, $MgCl_2$ and $CaCl_2$ solutions were prepared from undersaturation conditions in polyethylene vials with 5-20 mL matrix solution and 1-14 mg of the respective Ln/An hydroxide. A detailed list of all prepared samples for $Nd(OH)_3$(am), PuO_2(am,hyd), $Th(OH)_4$(am), NpO_2OH(am,fresh), $UO_3 \cdot 2H_2O$(cr) and $Na_2U_2O_7 \cdot H_2O$(cr) is given in Tables 2.5–2.10. Boron concentrations ($[B]_{tot}$) in $MgCl_2$, NaCl and $CaCl_2$ solutions were restricted to 0.4 M, 0.16 M and 0.04 M, respectively. The limitations in solubility observed for these systems are likely related with the formation of stable Mg-, Na- and Ca-borate solid phases [85]. Preliminary spectroscopic experiments (Cm(III)–TRLFS) conducted with freshly prepared borate solutions showed Cm(III)-borate complex formation with pronounced kinetic effects, which decreased notably with the pre-equilibration of borate in the corresponding saline solution. Consequently, the boron containing saline solutions were equilibrated for at least 2 weeks before the addition of the Ln/An hydroxide phase. Solubility experiments with PuO_2(am,hyd) were performed in 0.1 M NaCl solution and $[B]_{tot}$ = 0.16 M in the present of 2 mM $Na_2S_2O_4$ and hydroquinone as reducing system. Ln/An concentrations, pH and Eh (Pu experiments) were determined at regular time intervals for up to 860 days. The concentration of Ln/An(III) was quantified after phase separation by 10 kD ultrafiltration (~ 1.5 nm, Pall Life Sciences) by ICP-MS and LSC (see section 2.16). Selected

equilibrated alteration phases from solubility experiments were characterized using several techniques as described in section 2.1.7.

Table 2.5. *Experimental conditions in the solubility study with $Nd(OH)_3(am)$.*

System	Concentration of background electrolyte	$[B]_{tot}$	pH_m	Equilibration time
NaCl	0.1 M	0.004 M; 0.04 M; 0.16 M	7-13	7-142 days
NaCl	5.0 M	0.004 M; 0.04 M; 0.16 M	8-13	7-142 days
$CaCl_2$	0.25 M	0.004 M; 0.04 M	8-12	7-142 days
$CaCl_2$	3.5 M	0.004 M; 0.04 M	8-12	7-142 days
$MgCl_2$	0.25 M	0.004 M; 0.04 M 0.16 M; 0,4 M	8-12	7-72 days
$MgCl_2$	3.5 M	0.004 M; 0.04 M; 0.16 M; 0.4 M	8-12	7-72 days

Table 2.6. *Experimental conditions in the solubility study with $Nd[B_9O_{13}(OH)_4](cr)$.*

System	Concentration of background electrolyte	$[B]_{tot}$	pH_m	Equilibration time
NaCl	0.1 M; 5.0 M	0.16 M	6-9	7-48 days
$MgCl_2$	0.25 M; 3.5 M	0.16 M	6-9	7-48 days

Table 2.7. *Experimental conditions in the solubility study with PuO_2(am,hyd).*

System	Concentration of background electrolyte	$[B]_{tot}$	Reducing chemical	pH_m	Equilibration time
NaCl	0.1 M	0.16 M	$Na_2S_2O_4$	7.5; 9	14-300 days
NaCl	0.1 M	0.16 M	Hydroquinone	7.5; 9	14-300 days

Table 2.8. *Experimental conditions in the solubility study with $Th(OH)_4$(am).*

System	Concentration of background electrolyte	$[B]_{tot}$	pH_m	Equilibration time
NaCl	0.1 M	0 M; 0.16 M	7; 9; 11	14-860 days
NaCl	5.0 M	0 M; 0.16 M	8; 9; 11	14-860 days
$MgCl_2$	0.25 M	0 M; 0.16 M	7.5; 9	14-860 days
$MgCl_2$	3.5 M	0 M; 0.16 M	7.5; 9	14-860 days

Table 2.9. *Experimental conditions in the solubility study with NpO_2OH(am,fresh).*

System	Concentration of background electrolyte	$[B]_{tot}$	pH_m	Equilibration time
NaCl	0.1 M	0.04 M; 0.16 M	8-9	14-300 days
NaCl	5.0 M	0.04 M; 0.16 M	8-9	14-300 days
$MgCl_2$	0.25 M	0.04 M; 0.16 M	8-9	14-300 days
$MgCl_2$	3.5 M	0.04 M; 0.16 M	8-9	14-300 days

Table 2.10. *Experimental conditions in the solubility study with $UO_3 \cdot 2\ H_2O$(cr) and $Na_2U_2O_7 \cdot H_2O$(cr).*

System	Concentration of background electrolyte	$[B]_{tot}$	pH_m	Equilibration time
NaCl	0.1 M	0 M; 0.04 M;0.16 M	*7*; 9; 11	14-138 days
NaCl	5.0 M	0 M; 0.04 M;0.16 M	*8;* 9; 11	14-138 days
$MgCl_2$	0.25 M	0 M; 0.04 M; 0.16 M	*7.5; 9*	14-138 days
$MgCl_2$	3.5 M	0 M; 0.04 M; 0.16 M	*7.5; 9*	14 138 days

3 ^{11}B-NMR in NaCl, $CaCl_2$ and $MgCl_2$ solutions

The speciation of boron in aqueous solutions is very complex and strongly dependent on $[B]_{tot}$, pH and ionic strength. Because of their different symmetry with respect to the boron atom, boron species can be investigated and determined by ^{11}B-NMR spectroscopy. Many studies, mostly all at low ionic strength conditions have previously investigated boron speciation and the characteristic chemical shift of boron species forming under a wide pH range [72, 73, 75, 131, 132]. At low boron concentration ($[B]_{tot} < 0.025$ M) and low background electrolyte concentrations, only one ^{11}B resonance signal corresponding to the monomeric species $B(OH)_4^-$ and $B(OH)_3(aq)$ is observed. The chemical shift correlates to a mean of those of boric acid $B(OH)_3(aq)$ and $B(OH)_4^-$ weighted according to their relative concentrations at a given pH [133]. In strongly acidic pH conditions ($pH \leq 2$) only $B(OH)_3(aq)$ is present with a chemical shift of 18-20 ppm [133]. Under strongly alkaline pH conditions ($pH > 11$), $B(OH)_4^-$ is the dominant boron species with a chemical shift in the ^{11}B-NMR spectra of 0–2 ppm [134]. Polyborates species such as triborate $[B_3O_3(OH)_4]^-$, tetraborate $[B_4O_5(OH)_4]^{2-}$ and pentaborate $[B_5O_6(OH)_4]^-$ have been reported to form at high boron concentrations [69, 70, 81]. The presence of these species in solution can be followed as multiple peaks in the ^{11}B-NMR spectra [72]. In contrast to dilute systems, the influence of high ionic strength on the speciation of boron in aqueous salt solution and the effect on ^{11}B-NMR spectra is not sufficiently investigated. Recent studies by Hertam in LiCl and $MgCl_2$ solutions indicate no or only slight influence by monovalent cations like Li^+ but a strong influence and peak broadening on the measured ^{11}B-NMR spectra in the presence of Mg^{2+} [135]. Raman spectroscopy studies by Zhihong et al. observed a favoured formation of polyborates in presence of divalent cations like Ca^{2+} and Mg^{2+} [84].

In this work, ^{11}B-NMR spectra were collected in dilute to concentrated NaCl and $MgCl_2$ solutions within $2.6 \leq pH_m \leq 12$ and $0.04\ M \leq [B]_{tot} \leq 0.4\ M$ with the aim of gaining further insight on the speciation of boron, especially under the poorly investigated highly saline conditions.

3.1 ^{11}B-NMR studies in NaCl solutions

^{11}B-NMR spectra collected for 0.1 M and 5.0 M NaCl solutions with $0.04\ M \leq [B]_{tot} \leq 0.16\ M$ at $pH_m = 2.6$, 8 and 12 are shown in Fig. 3.1. A single reference signal corresponding to the exchange peak of the monomeric species ($B(OH)_3(aq)$–$B(OH)_4^-$) is observed in all systems with $[B]_{tot} \leq 0.04$ M. At this $[B]_{tot}$ no (or very few) polyborates are present in solution. In the NaCl system at $pH_m = 2.6$, the peak at ~ 20 ppm can be unequivocally assigned to $B(OH)_3(aq)$. In dilute and concentrated NaCl systems and $pH_m = 8$, the peak observed 17-18 ppm indicates the predominance of $B(OH)_3(aq)$ in the solution. For the same pH a broad second peak can be observed at $[B]_{tot} = 0.16$ M. According to studies in KCl, NaCl and LiCl solutions this broad peak at ~12–14 ppm can be assigned to the triborate species

$B_3O_3(OH)_4^-$ [72, 135]. At pH_m = 12, the chemical shift observed at 0–3 ppm agrees very well with the expected predominance of $B(OH)_4^-$ in the solution at high pH_m. The results in NaCl solutions are in good agreement with data from Borkowski and co-workers measured in water at comparable $[B]_{tot}$ [136].

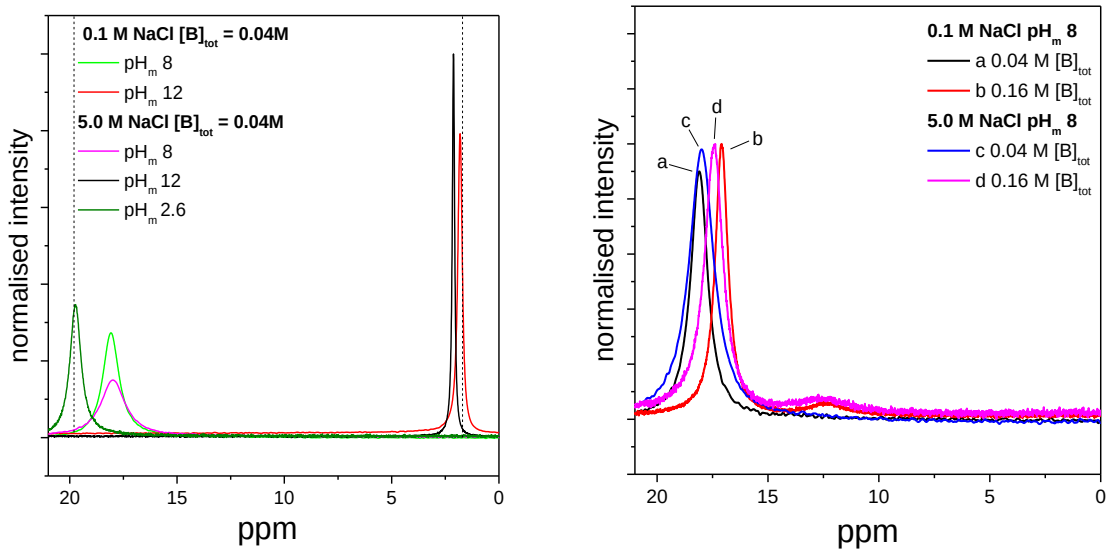

Figure 3.1: *^{11}B-NMR spectra collected in 0.1 M and 5.0 M NaCl solutions: (left) spectra with 2.6 ≤ pH_m ≤ 12 and $[B]_{tot}$ = 0.04 M, (right) spectra with pH_m = 8 and a) 0.04 M $[B]_{tot}$ b) 0.16 M $[B]_{tot}$ in 0.1 M NaCl and c) 0.04 M $[B]_{tot}$ d) 0.16 M $[B]_{tot}$ in 5.0 M NaCl.*

3.2 ^{11}B-NMR studies in $CaCl_2$ and $MgCl_2$ solutions

^{11}B-NMR spectra collected for 0.25 M and 3.5 M $CaCl_2$ with $[B]_{tot}$ = 0.4 M at pH_m = 8 and 12, and collected for 0.25 M and 3.5 M $MgCl_2$ with 0.04 M ≤ $[B]_{tot}$ ≤ 0.4 M at pH_m = 8 are shown in Fig. 3.2. For comparison purposes, peak positions for $B(OH)_3$(aq) and $B(OH)_4^-$ in NaCl solutions are shown as dashed lines. Analogously to the NaCl system (Fig. 3.1), a single resonance peak is visible in the spectra collected for samples in $CaCl_2$ and $MgCl_2$ solutions with $[B]_{tot}$ = 0.04 M. Nevertheless, significantly broader peaks are detected in these salt solutions compared to the NaCl system. At pH_m = 8, the peak at ~17–18 ppm observed in the NaCl system and indicating the predominance of $B(OH)_3$(aq) is shifted to lower ppm in $CaCl_2$ and $MgCl_2$ solution. Note further that the peak broadening and peak shift are more pronounced in concentrated $MgCl_2$ and $CaCl_2$ solutions for the same pH (pH_m = 8) and boron concentration ($[B]_{tot}$ = 0.04 M). This observation can be likely explained by the complexation of Mg/Ca with B, as presented in the thermodynamic calculations shown in Fig. 3.3 conducted using the thermodynamic and activity models reported by Felmy and co-workers on the system Mg^{2+}–$B(OH)_4^-$-Cl^-–H_2O [81].

In 0.25 M $MgCl_2$ solutions with pH_m = 8, the peak position is shifted from ~ 16 ppm to ~13 ppm when increasing $[B]_{tot}$ from 0.04 M to 0.4 M. The observed peak at $[B]_{tot}$ = 0.4 M is very broad and shows a pronounced shoulder at ~12 ppm and a second small peak at 0.7 ppm. The shoulder and the additional peak indicate the presence of more than one boron species present in the investigated solution. A significant peak broadening is also observed in 3.5 M $MgCl_2$ solutions. The fraction diagram shown in Fig. 3.3 shows the predominance of $B(OH)_3$(aq) and $MgB(OH)_4^+$ species, and thus the observed peak broadening cannot be attributed to the presence of polyborate species. In contrast to the NaCl system, no peak assignment is possible in $CaCl_2$ and $MgCl_2$ systems at pH_m 8 due to the lack of literature data.

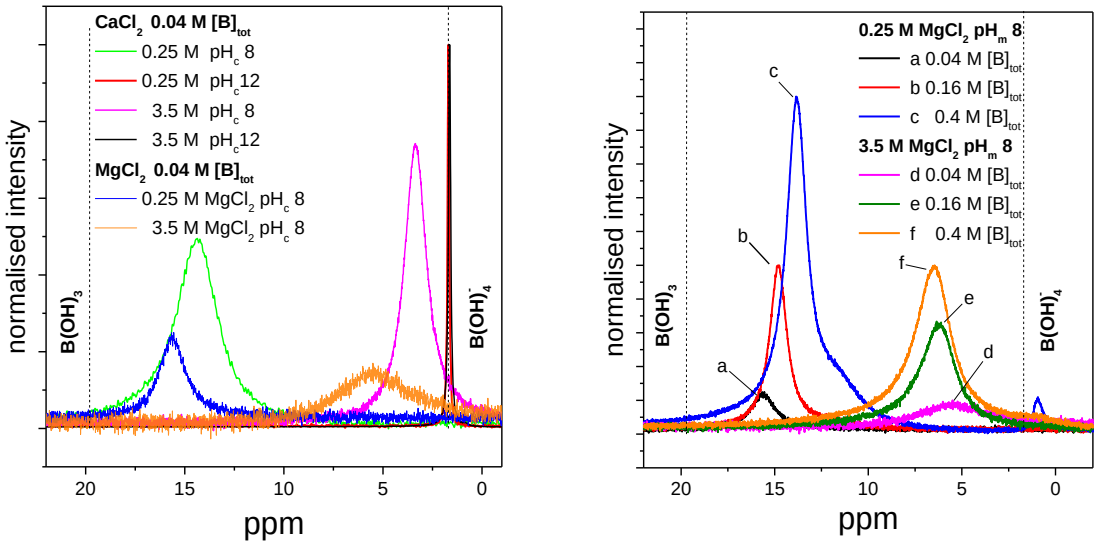

Figure 3.2. *^{11}B-NMR spectra collected in 0.25 M and 3.5 M $CaCl_2$ and $MgCl_2$ solutions: (left) spectra with 8 ≤ pH_m ≤ 12 and $[B]_{tot}$ = 0.04 M, (right) spectra with pH_m = 8 and a) 0.04 M $[B]_{tot}$ b) 0.16 M c) 0.4 M $[B]_{tot}$ in 0.25 M $MgCl_2$ and d) 0.04 M $[B]_{tot}$ e) 0.16 M $[B]_{tot}$ f) 0.4 M $[B]_{tot}$ in 3.5 M $MgCl_2$.*

At pH_m = 12 in $CaCl_2$ systems the peak position at ~ 2 ppm indicates $B(OH)_4^-$ as main borate species similar to observations made in NaCl systems. In contrast to systems at lower pH values, no broadening of this peak is observed at increased $CaCl_2$ concentration. No further information on aqueous boron speciation in saline solution can be drawn from the measured NMR spectra.

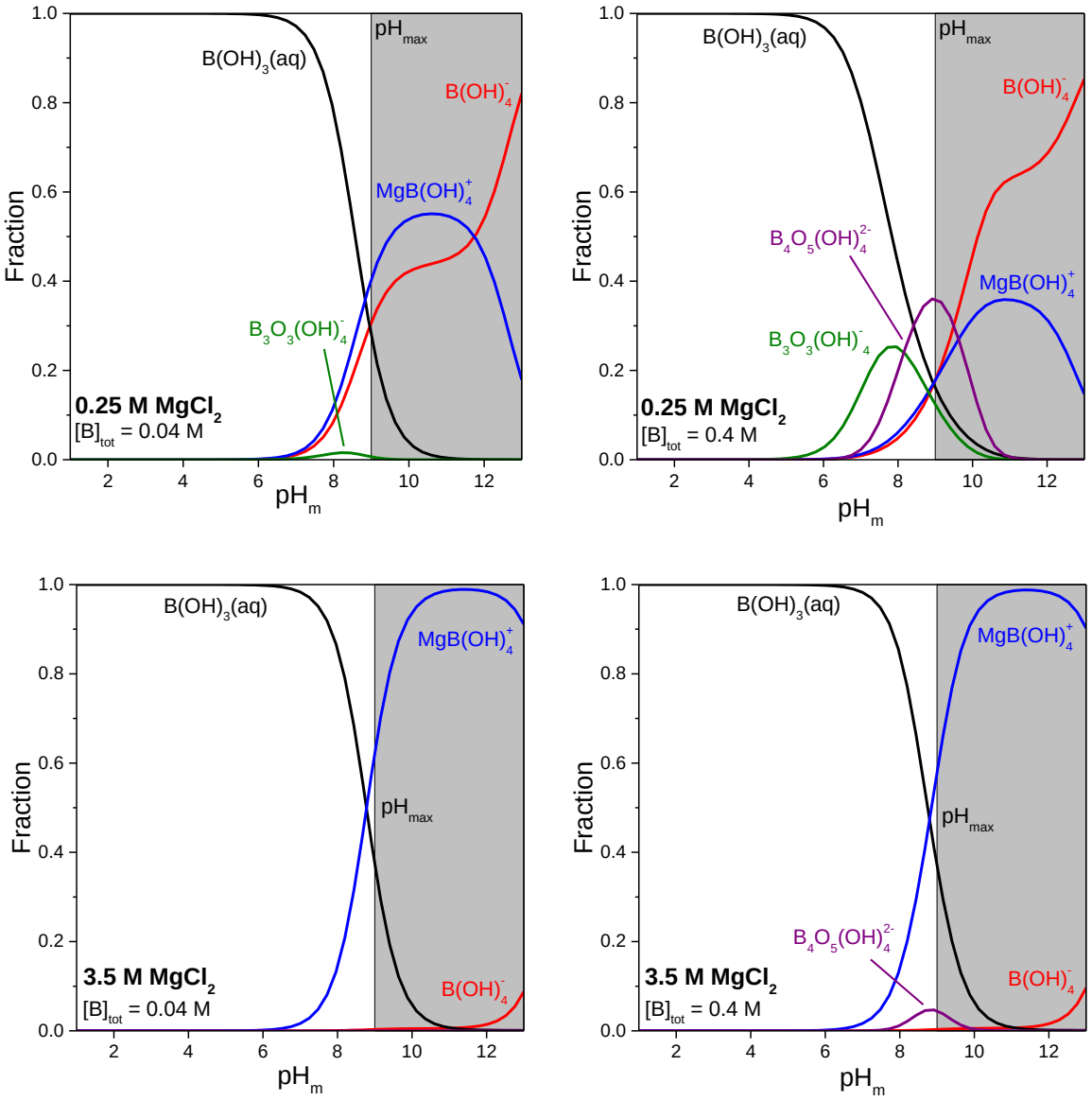

Figure 3.3. *Fraction diagram of aqueous borate species in 0.25 M and 3.5 M $MgCl_2$ as calculated with the thermodynamic and activity models reported in Felmy et al. [81]. The highest pH in dilute to concentrated $MgCl_2$ solutions is limited to pH_{max} ≈9 by the precipitation of $Mg(OH)_2$(s) or Mg–OH–Cl phases, and thus calculations above this pH represent only a modelling exercise giving insight on the possible interaction Ca–borate in $CaCl_2$ systems (where pH_{max} ≈12) under the assumption of a comparable complexation behavior of Ca^{2+} and Mg^{2+}.*

3.3 Conclusions

[11]B-NMR studies conducted in NaCl, $CaCl_2$ and $MgCl_2$ solutions at pH_m = 2.6, 8 and 12 give insight in the complex borate speciation in saline solutions. Spectra measured in NaCl solutions are similar to spectra collected in water with the same pH_m and comparable $[B]_{tot}$. According to the collected spectra and consistently with literature data, the speciation of boron is only weakly influenced by the

presence of monovalent cations like Na^+ , K^+ and Li^+ [72, 135]. Based on the reported literature data, the detected peaks can be correctly assigned to the expected boron species, although no quantitative analysis of the spectra is possible.

In contrast to the NaCl systems, very broad peaks are observed in $CaCl_2$ and $MgCl_2$ solutions. At $pH_m = 8$ the peak position in both $CaCl_2$ and $MgCl_2$ systems is significantly shifted compared to peaks at same pH_m and $[B]_{tot}$ measured in NaCl solutions, indicating the formation of Ca/Mg–borate complex. This is in good agreement with thermodynamic calculations indicating the formation of the complex $MgB(OH)_4^+$. For more specific information on the boron speciation in presence of high NaCl, $CaCl_2$ and $MgCl_2$ concentrations, additional comprehensive experiments are needed.

4 Interaction of Ln(III)/An(III) with borate

The interaction of Ln(III)/An(III) with borate was investigated from undersaturation conditions with $Nd(OH)_3$(am) in dilute to concentrated NaCl, $CaCl_2$ and $MgCl_2$ solutions with 0.04 M ≤ $[B]_{tot}$ ≤ 0.4 M at 6 ≤ pH_m ≤ 13. Samples were equilibrated for up to 142 days, and pH_m and [Nd(III)] were monitored at regular time intervals. After attaining equilibrium conditions, selected solid phases were characterized by XPS, SEM-EDS and XRD. For comparison purposes, additional solubility experiments with a well-defined Nd(III) borate solid phase, $Nd[B_9O_{13}(OH)_4](cr)$, were performed in NaCl and $MgCl_2$ solutions with $[B]_{tot}$ = 0.16 M. The aqueous phase was further investigated by TRLFS with 10^{-7} M Cm(III) in 0.1 – 5.0 M NaCl, 0.25 – 3.5 M $MgCl_2$ and 0.25 – 3.5 M $CaCl_2$ with 0.004 M ≤ $[B]_{tot}$ ≤ 0.4 M and pH_m = 8. Additional Cm(III) TRLFS spectra were collected at pH_m = 12 for $CaCl_2$ systems. Chemical and thermodynamic models based on the experimentally obtained solubility data, TRLFS and solid phase analysis were derived for the Nd^{3+}-Na^+-Mg^{2+}-Ca^{2+}-H^+-Cl^--$B(OH)_4^-$-OH^--H_2O using the SIT approach. These are separately discussed in chapter 9.

4.1 Solubility of Nd(III) in NaCl, $CaCl_2$ and $MgCl_2$ solutions

The experimental solubility data of Nd(III) determined in 0.1 M – 5.0 M NaCl and 0.25 M – 3.5 M $MgCl_2$ and $CaCl_2$ solutions in the presence of 0.004 M ≤ $[B]_{tot}$ ≤ 0.4 M are shown in Fig. 4.1-Fig. 4.6. Note that only data corresponding to thermodynamic equilibrium (constant pH_m and [Nd(III)]) are presented in the figures. For comparison purposes, Fig. 4.1 – 4.6 also show the experimental solubility data and calculated solubility curves for $Nd(OH)_3$(am) as reported by Neck et al. in the absence of borate under analogous pH_m and ionic strength conditions [24]. In 0.1 M, 5.0 M NaCl and 0.25 M, 3.5 M $MgCl_2$ systems (Fig. 4.1, Fig. 4.3, Fig. 4.4 and Fig. 4.6), undersaturation solubility data obtained with $Nd[B_9O_{13}(OH)_4](cr)$ and $[B]_{tot}$ = 0.16 M are also provided.

No significant effect of borate on Nd(III) solubility is observed in near neutral to slightly alkaline pH_m values (7 ≤ pH_m ≤ 9) and $[B]_{tot}$ ≤ 0.04 M (dilute salt systems: 0.1 and 1.0 M NaCl; 0.25 M $MgCl_2$) or $[B]_{tot}$ ≤ 0.004 M (concentrated salt systems: 5.0 M NaCl; 1.0 and 3.5 M $MgCl_2$). Under these conditions, the concentration of Nd(III) is in good agreement with borate-free solubility data obtained under analogous pH_m and ionic strength conditions [24].

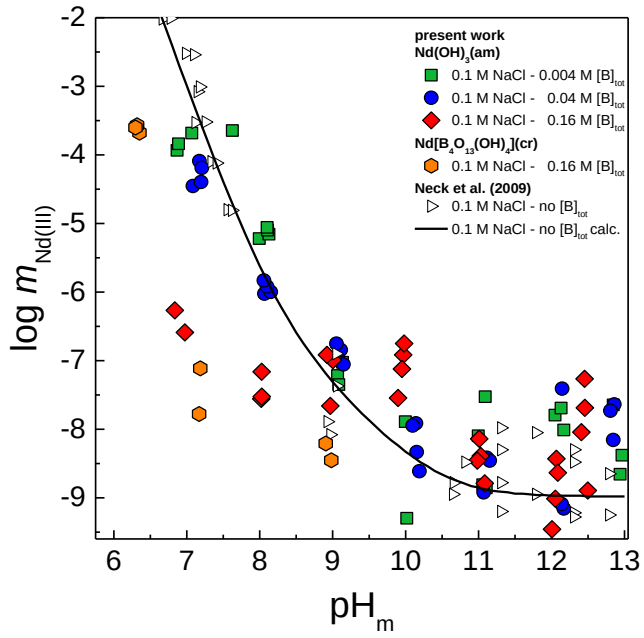

Figure 4.1. *Solubility of $Nd(OH)_3(am)$ and $Nd[B_9O_{13}(OH)_4](cr)$ in the presence of $0.004\ M \leq [B]_{tot} \leq 0.16\ M$ in 0.1 M NaCl solutions. Comparison with experimental (open symbols, black) and calculated (solid line) solubility data in the absence of borate as reported in Neck et al. (2009) [24].*

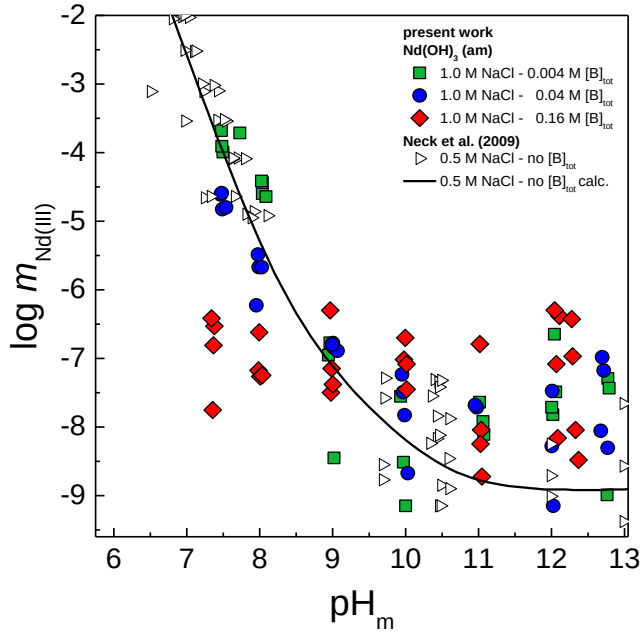

Figure 4.2. *Solubility of $Nd(OH)_3(am)$ in the presence of $0.004\ M \leq [B]_{tot} \leq 0.16\ M$ in 1.0 M NaCl solutions. Comparison with experimental (open symbols, black) and calculated (solid line) solubility data in the absence of borate as reported in Neck et al. (2009) [24].*

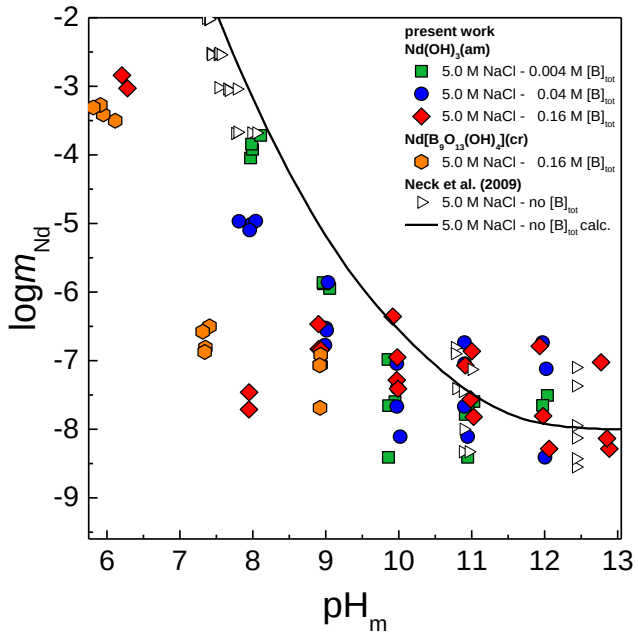

Figure 4.3. *Solubility of $Nd(OH)_3(am)$ and $Nd[B_9O_{13}(OH)_4](cr)$ in the presence of $0.004\ M \leq [B]_{tot} \leq 0.16\ M$ in 5.0 M NaCl solutions. Comparison with experimental (open symbols, black) and calculated (solid line) solubility data in the absence of borate as reported in Neck et al. (2009) [24].*

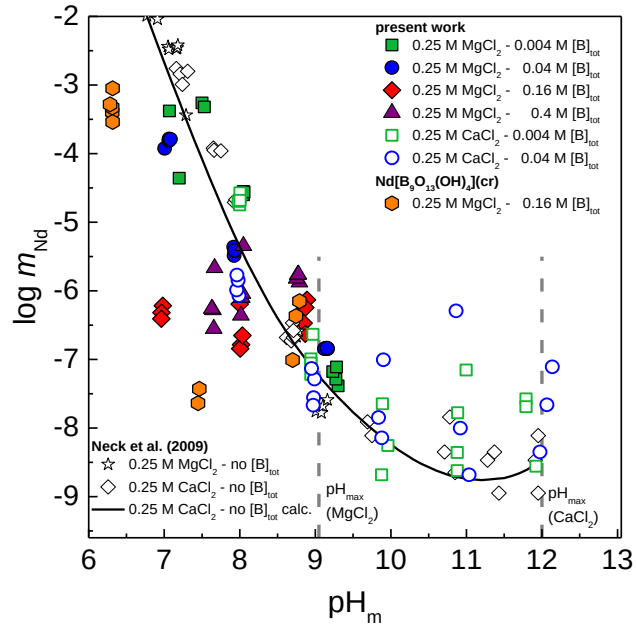

Figure 4.4. *Solubility of $Nd(OH)_3(am)$ and $Nd[B_9O_{13}(OH)_4](cr)$ in the presence of $0.004\ M \leq [B]_{tot} \leq 0.4\ M$ in 0.25 M $MgCl_2$ and $CaCl_2$ solutions. Comparison with experimental (open symbols, black) and calculated (solid line) solubility data in the absence of borate as reported in Neck et al. (2009) [24].*

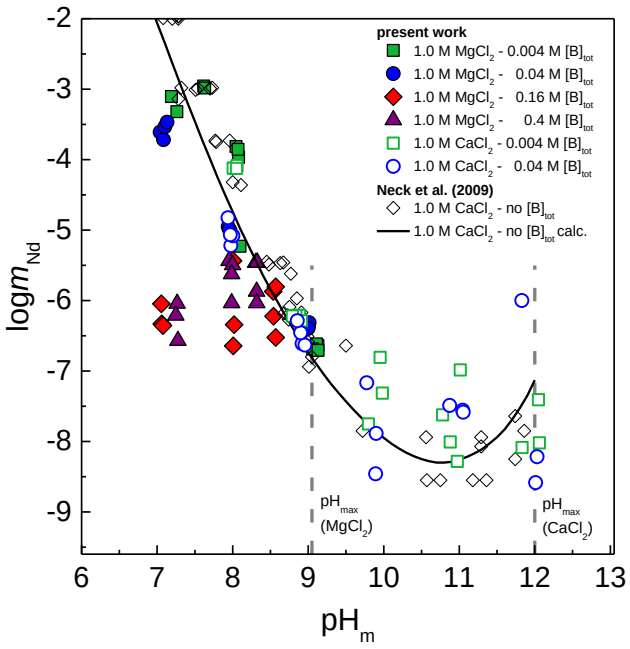

Figure 4.5. *Solubility of $Nd(OH)_3(am)$ in the presence of $0.004\ M \leq [B]_{tot} \leq 0.4\ M$ in 1.0 M $MgCl_2$ and $CaCl_2$ solutions. Comparison with experimental (open symbols, black) and calculated (solid line) solubility data in the absence of borate as reported in Neck et al. (2009) [24].*

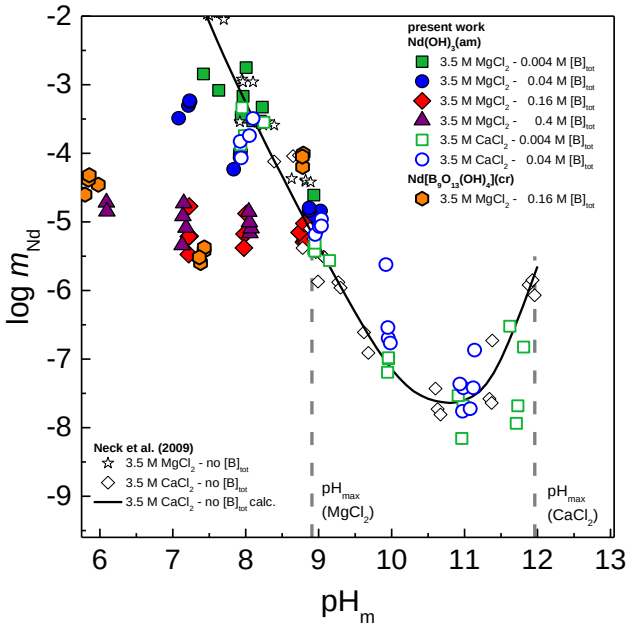

Figure 4.6. *Solubility of $Nd(OH)_3(am)$ and $Nd[B_9O_{13}(OH)_4](cr)$ in the presence of $0.004\ M \leq [B]_{tot} \leq 0.4\ M$ in 3.5 M $MgCl_2$ and $CaCl_2$ solutions. Comparison with experimental (open symbols, black) and calculated (solid line) solubility data in the absence of borate as reported in Neck et al. (2009) [24].*

At enhanced $[B]_{tot} \geq 0.16$ M, a significant decrease in the Nd(III) concentration occurs for all NaCl and $MgCl_2$ systems evaluated. The drop in solubility at $[B]_{tot}$ ~0.16–0.4 M is accompanied with a changed slope of the solubility curve from –2 to approximately 0. This observation clearly indicates the transformation of $Nd(OH)_3$(am) into a new solubility controlling borate-bearing solid phase. After an equilibration time of 72 to 142 days (depending upon salt system), the measured Nd(III) concentrations remain constant at ~$10^{-6.5}$ M (in 0.25 M $MgCl_2$) to 10^{-5} M (in 3.5 M $MgCl_2$). These solubility limits are more than three orders of magnitude lower than those observed in the absence of borate, as summarized in Table 4.1. The decrease in Nd(III) solubility in NaCl solutions is similar, although the overall solubility is slightly lower indicating that increasing $MgCl_2$ concentrations and resulting high ionic strength enhances significantly the solubility of Nd(III) in the presence of borate as it is also the case in borate-free systems. No (or very limited) effect of borate on Nd(III) solubility is observed in $CaCl_2$ solutions in contrast to NaCl and $MgCl_2$ systems, very likely due to the lower boron solubility in this background electrolyte ($[B]_{tot} \leq 0.04$ M).

Table 4.1. *Comparison of experimental Nd(III) concentrations at $[B]_{tot} \geq 0.16$ M and calculated Nd(III) concentrations in borate-free NaCl and $MgCl_2$ solutions.*

Matrix	**pH_m**	**log [Nd] borate free [24]**	**log [Nd] $[B]_{tot} \geq 0.16$ M**	**Δ log [Nd]**
0.1 M NaCl	7.1	–3.0	–6.6	3.3
1.0 M NaCl	7.3	–3.4	–7.7	3.3
5.0 M NaCl	8.0	–3.2	–7.8	4.6
0.25 M $MgCl_2$	7.0	–2.7	–6.4	3.7
1.0 M $MgCl_2$	7.3	–2.9	–6.6	3.7
3.5 M $MgCl_2$	7.2	–1.3	–5.5	4.2

Additional Nd(III) solubility experiments from undersaturation conditions were performed in NaCl and $MgCl_2$ systems using a well-defined Nd–borate solid phase $Nd[B_9O_{13}(OH)_4](cr)$. The measured solubility of this Nd-borate phase agrees well with the data measured for $Nd(OH)_3$(am) in comparable $[B]_{tot}$ = 0.16 M, suggesting that similar processes or solid phases are controlling the solubility in both systems. Note that $Nd[B_9O_{13}(OH)_4](cr)$ was prepared with very high $[B]_{tot}$ at elevated temperatures and high pressure. The formation of this crystalline Nd(III)–borate solid phase appears unlikely under the conditions of the present study (T = 25°C, P = 1 bar) or in repository systems.

Under hyperalkaline conditions ($pH_m \geq 10$) very scattered solubility data are obtained. Similar observations have been reported previously for Nd(III) and Th(IV) in the absence of boron [24, 29] (see chapter 7), and are likely correlated to a combination of factors such as very low concentrations of Nd(III) and Th(IV) in solution (often close to the detection limit of ICP–MS), tendency of neutral species to sorb (i.e. $Nd(OH)_3(aq)$, $Th(OH)_4(aq)$), and presence of colloidal nanoparticles not retained in the 10 kD filtration step. A slight increase in Nd(III) solubility compared to the borate free data could be claimed for some of the samples with $[B]_{tot} \geq 0.16$ M in this pH_m region, especially in the case of 0.1 M and 1.0 M NaCl systems (Fig. 4.1 and Fig. 4.2). A similar effect at $pH_m = 9$ is observed for Pu(III/IV) solubility data in the presence of comparable $[B]_{tot}$ (see chapter 6). Despite the very large scattering in the measured concentration of Nd(III), the absence of a relevant borate effect on Nd(III) solubility above $pH_m = 9$ is proposed for both NaCl and $CaCl_2$ solutions. This observation can be interpreted by a decreased interaction between Nd(III) and borate due to the enhanced hydrolysis of Nd(III) with increasing pH_m.

4.2 Solid phase characterization

Solid phases of selected solubility experiments were investigated after attaining equilibrium conditions by XRD, SEM–EDS and XPS. Fig. 4.7 a to d show the XRD diffractograms obtained for selected solid phases of the Nd(III) solubility experiments together with the initial $Nd(OH)_3(am)$. In all cases the characteristic pattern of $Nd(OH)_3(am)$ (JCPDF file No: 70-0215, JCPDS 2001[137]) is observed, indicating that the initial solid phase has been (at least partially) retained throughout the equilibration process in borate-bearing solutions. Note however that XRD is a bulk-sensitive technique which cannot detect surface coatings or the presence of amorphous phases. Fig. 4.7 also shows the diffractogram of the crystalline $Nd[B_9O_{13}(OH)_4](cr)$, synthesized at high $[B]_{tot}$, and elevated temperatures and pressures (see section 2.2.1). Very distinct XRD pattern are observed for this solid phase, confirming that none of the solubility experiments initiated with $Nd(OH)_3(am)$ led to the formation of this solid phase (above the detection limit of XRD, ~5%).

In contrast to XRD, XPS analyses of the solid phases from solubility samples with $[B]_{tot} \geq 0.16$ M confirm the presence of a newly formed borate-bearing secondary phase on the surface of $Nd(OH)_3(am)$ (Fig. 4.8). The combination of these observations with solubility and XRD data strongly hints towards the formation of a borate-bearing Nd(III) surface coating, which is responsible of controlling the solubility of Nd(III) under these conditions. Note that similar XPS spectra were also obtained in the case of $Nd[B_9O_{13}(OH)_4](cr)$, thus hinting that a similar coating formed on the surface of both solid phases in boron-bearing saline solutions.

The different outcome obtained by XRD and XPS basically reflects the different properties of these techniques: XRD is a bulk method insensitive to amorphous materials, whereas XPS is a surface-sensitive technique that provides accurate information of the chemical composition of both amorphous

and crystalline materials within a depth of ~0.9 to ~2.7 nm (in the configuration considered in this study, see section 2.1.7.2).

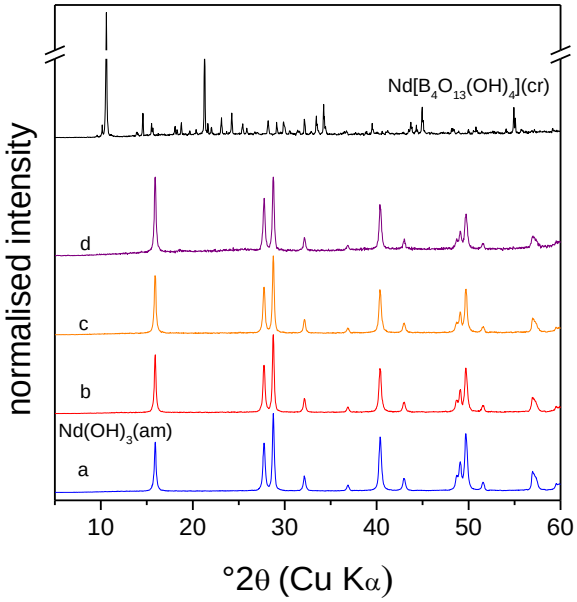

Figure 4.7. *XRD pattern of initial $Nd(OH)_3$(am) (a) and $Nd(OH)_3$(am) alteration phases collected from solubility experiments in 0.1 M NaCl at pH_m = 7(b), 5.0 M NaCl at pH_m = 8 (c) and 3.5 M $MgCl_2$ at pH_m = 7.5 (d) in the presence of $[B]_{tot}$ = 0.04 M. Upper diffractogram corresponds to $Nd[B_9O_{13}(OH)_4](cr)$ after equilibrating for 100 days in a 3.5 M $MgCl_2$ solution with $[B]_{tot}$ = 0.16 M and pH_m = 7.3.*

Table 4.2. *Composition of the newly formed Nd(III)-borate coating (in at. %) based on XPS analyses(analytical uncertainties lie within 10-20 %).*

Sample	B	O	Na	Mg	Cl	Nd(III)
0.1 M NaCl / 0.16M $[B]_{tot}$	27.1	62.8	3.1	-	-	6.0
5.0 M NaCl / 0.16M $[B]_{tot}$	19.2	59.9	5.0	-	1.4	9.1
3.5 M $MgCl_2$ / 0.004M $[B]_{tot}$		56.7	-	0.3	2.5	22.3
3.5 M $MgCl_2$ / 0.4 M $[B]_{tot}$	15.0	63.4	-	4.6	1.5	10.1

XPS analyses of the Nd(III) secondary phases formed as a coating in NaCl and concentrated $MgCl_2$ solutions confirm the stoichiometric presence of boron and Na^+/Mg^{2+}. The composition of these newly

formed solid phases (in at. %) are listed in Table 4.2. For dilute NaCl solution the formation of a solid phase with the stoichiometry $NaNd[B_3O_4(OH)_3]_2(am)$ can be proposed.

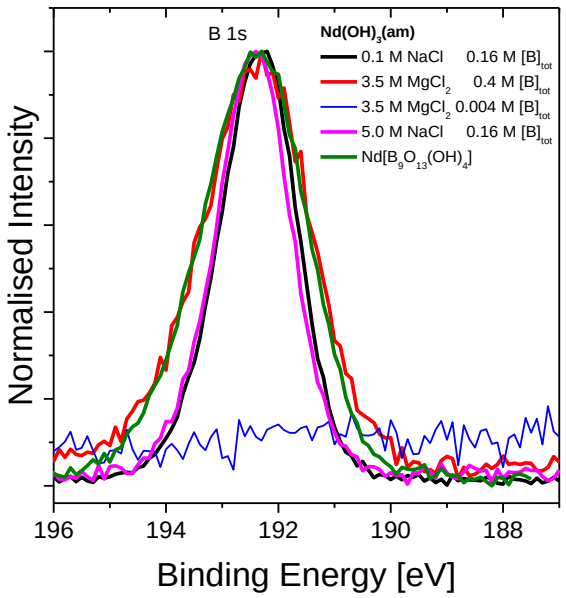

Figure 4.8. *Narrow scan of the B 1s spectra for Nd(III) solid phases in NaCl and $MgCl_2$ solutions at pH_m = 7–8 with various $[B]_{tot}$ obtained by XPS.*

SEM images of the surface of selected Nd(III) alteration phases are shown in Fig. 4.9, Fig. 4.10 and Fig. 4.11. A clear change of the surface of Nd(III) solid phases equilibrated in the presence of $[B]_{tot} \geq 0.16$ M can be observed in the SEM images indicating the formation of a secondary phase on the surface of the original solid. SEM images also show different surface transformations in the presence of borate depending on the salt system and salt concentration. The SEM image of the solid found in 0.1 M NaCl solution and at $[B]_{tot}$ = 0.16 M (Fig. 4.10 a) shows sharp crystalline platelets, whereas less ordered and smaller platelets can be observed in 3.5 M $MgCl_2$ solution (Fig. 4.11 b). These findings are in good agreement with solid phase analysis of Np(V) borate solids (see chapter 7), where the most crystalline structure was also formed in 0.1 M NaCl. The surface structure of the crystalline $Nd[B_9O_{13}(OH)_4](cr)$ (Fig. 4.9 b, initial material before equilibration with borate-bearing solutions) shows significant differences with the Nd(III) borate surface coatings found in the solubility experiments. As already hinted by the combination of XRD and XPS analysis, SEM indicates that the transformation of the original $Nd(OH)_3(am)$ in the presence of borate under the experimental conditions of this study lead to the formation of a new Nd(III)–borate solid phase but does not reach the very crystalline structure of $Nd[B_9O_{13}(OH)_4](cr)$, which was prepared under increased temperatures and pressure with very high $[B]_{tot}$.

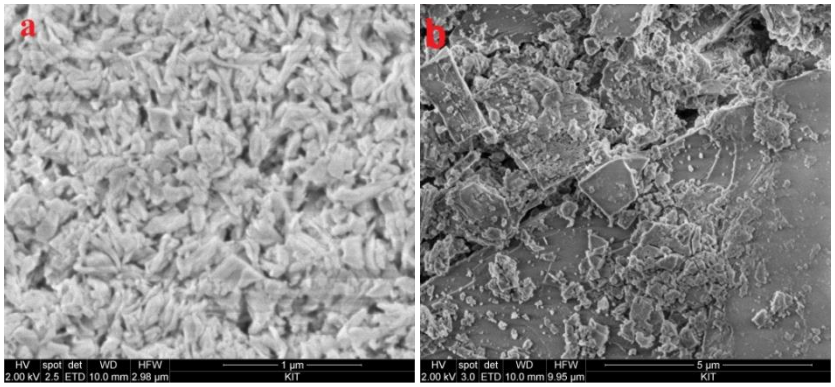

Figure 4.9. *SEM images of the original $Nd(OH)_3(am)$ (a) and $Nd[B_9O_{13}(OH)_4](cr)$ (b) material before equilibrating with borate-bearing solutions.*

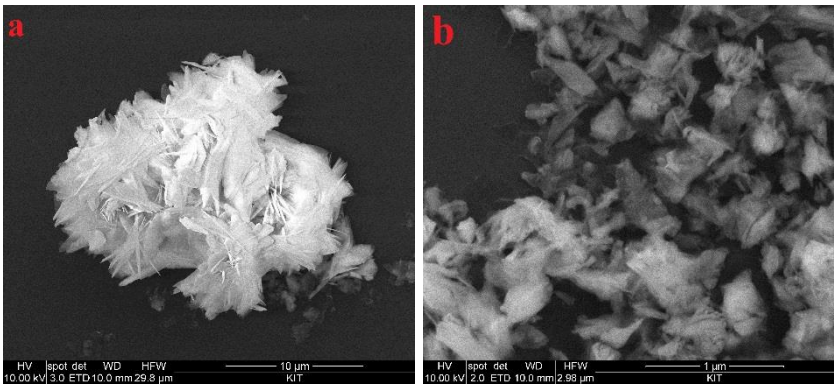

Figure 4.10. *SEM images of alteration phases from Nd(III) solubility experiments in 0.1 M NaCl with $[B]_{tot}$ = 0.16 M at pH_m = 7 (a) and in 5.0 M NaCl with $[B]_{tot}$ = 0.16 M at pH_m = 8 (b).*

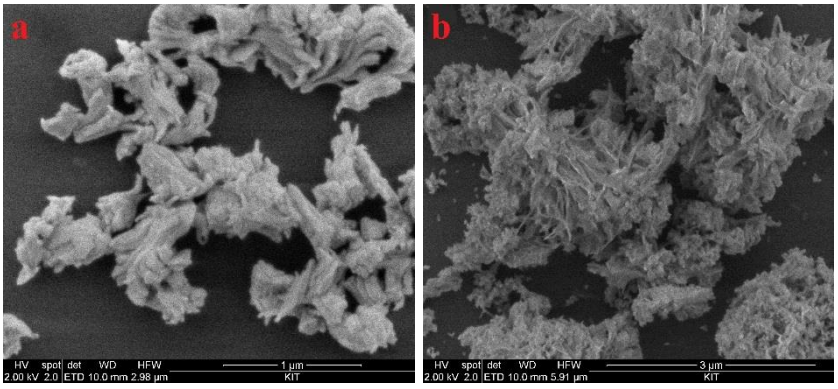

Figure 4.11. *SEM images of alteration phases from Nd(III) solubility experiments in 3.5 M $MgCl_2$ with $[B]_{tot}$ = 0.004 M at pH_m = 8 (a) and in 3.5 M $MgCl_2$ with $[B]_{tot}$ = 0.4 M at pH_m = 7.5 (b).*

Under similar conditions as those investigated in the present study (pH_m = 6, $[B]_{tot} \geq 0.3$ M), the formation of a Eu(III) borate solid phase was recently reported by Schott et al. [83]. The authors provided evidence (solid-phase TRLFS, IR) of the formation of a distinct Eu(III)–borate solid phase, whose amorphous character was also highlighted by the absence of relevant XRD reflections.

4.3 Cm(III) aqueous speciation in the presence of borate: TRLFS

Fluorescence emission spectra of Cm(III) were measured with $0.004 \text{ M} \leq [B]_{tot} \leq 0.4$ in 0.1 M–5.0 M NaCl and 0.25 M–3.5 M $CaCl_2$ and $MgCl_2$ solutions at pH_m = 8. The normalised spectra in 0.1 M and 5.0 M NaCl solution are presented in Fig. 4.7 and Fig. 4.8. Spectra at pH_m = 8 in 0.25 M and 3.5 M $MgCl_2$ solutions are presented in Fig. 4.12 and Fig. 4.13. In $CaCl_2$ solutions additional spectra with $0.004 \leq [B]_{tot} \leq 0.04$ M at pH_{max} ~12 were taken and are shown in Fig. 4.14. Furthermore, fluorescence decay measurements were performed for Cm(III) in NaCl, $CaCl_2$ and $MgCl_2$ solutions with $0.004 \text{ M} \leq [B]_{tot} \leq 0.4$ at pH_m = 8. Note that boron concentrations in NaCl and $CaCl_2$ solutions were restricted due to the precipitation of Na- and Ca-borate solid phases, to 0.16 M and 0.04 M, respectively. The resulting fluorescence lifetimes are presented in Table 4.3.

4.3.1 Cm(III) TRLFS studies in NaCl solutions

In the near neutral pH_m region (pH_m = 8) in the absence of borate, several Cm(III) species are expected to be present in solution simultaneously. Their relative contribution depends on the ionic strength and electrolyte composition of the respective solution. Besides the free Cm^{3+} aquo ion, also Cm(III) complexes such as $CmCl^{2+}$, $CmCl_2^+$, $Cm(OH)^{2+}$ and $Cm(OH)_2^+$ can be present in different proportions. At very low $[B]_{tot}$ = 0.004 M no significant influence of borate on Cm(III) aqueous speciation can be observed in all investigated samples (Fig. 4.12 and Fig. 4.13). The peak maximum, located at ~603 nm of the scattered spectra in 0.1 M NaCl solution can be associated mainly with the $Cm(OH)_2^+$ complex as reported by Fanghänel et al. [113]. In the absence of complexing ligands other than hydroxide, generally a strong decrease in aqueous Cm(III) concentration at higher pH_m ($pH_m \geq 8$) is observed due to sorption on surfaces and precipitation as hydroxide. This explains the low intensities and spectral scattering observed for these measured spectra at very low $[B]_{tot}$.

In 5.0 M NaCl and $[B]_{tot}$ = 0.004 M two peaks with maxima at 594 nm and 604 nm can be found. The first peak can be attributed to the Cm(III) aquo ion (with small contributions of chloro complexes very likely present in higher NaCl concentrations), the second peak can be assigned to the second hydrolysis species $Cm(OH)_2^+$, as expected at pH_m = 8 [113]. The measured spectra with low $[B]_{tot}$ in NaCl solutions are in good agreement with the corresponding solubility data (Fig. 4.1 and Fig. 4.3).

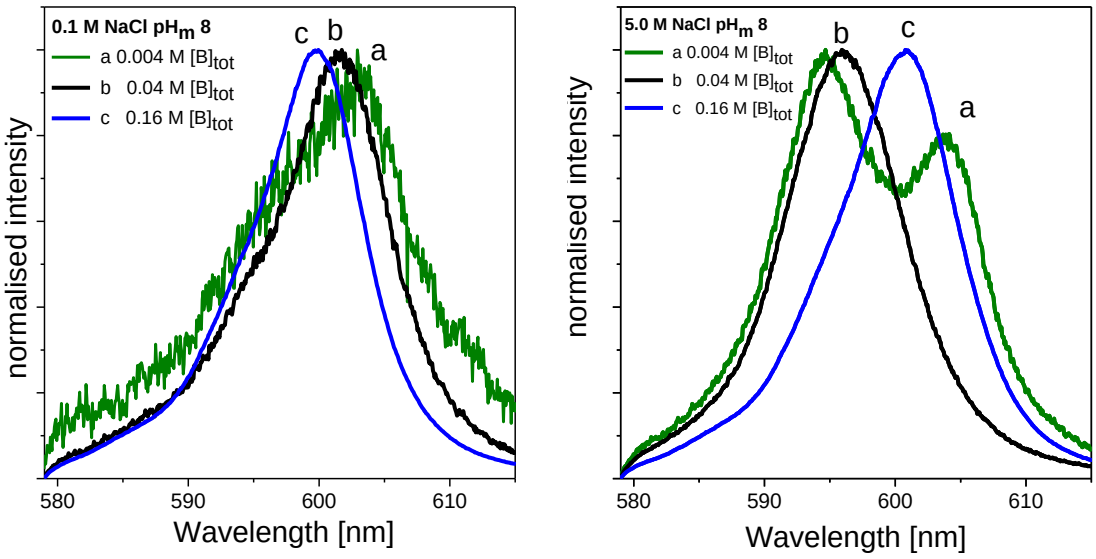

Figure 4.12. *TRLFS emission spectra of Cm(III) in 0.1 M and 5.0 M NaCl solutions at pH_m = 8 and various borate concentrations.*

With increasing $[B]_{tot}$ ($[B]_{tot}$ > 0.004M), an effect of borate on the Cm(III) speciation is observed in 0.1 M NaCl solutions with a peak shift to shorter wavelengths in combination with an increased fluorescence intensity of the spectra. Such a hypsochromic peak shift appears when complexes with weaker ligands are formed as a consequence of their lower ligand field splitting. In the presence of more than one complexing ligand, weaker complexes will only form if the weak ligand concentration considerably exceeds the concentration of the stronger ligand (i.e. hydroxide anion) as it is the case at pH_m = 8 for $[B]_{tot}$ > 0.004 M. At $[B]_{tot}$ = 0.16 M the competition between borate complexation and hydrolysis leads to a suppression of the Cm(III) hydrolysis species and the formation of a borate containing Cm(III) complex with a peak maximum at ~ 600 nm. A very short fluorescence lifetime (τ = 59 µs) at $[B]_{tot}$ = 0.16 M is observed in 0.1 M NaCl solutions. This decrease in the fluorescence lifetime together with a clear shift in the emission spectra in comparison to the Cm(III) aquo ion cannot be explained at the moment. The presence of Cm(III) containing colloids by precipitation of a Cm(III) borate solid, in accordance to the analogue Nd(III)-solubility experiments (Fig. 4.1), could lead to a decrease in the fluorescence lifetime.

The double peak observed in 5.0 M NaCl solution and at $[B]_{tot}$ = 0.004 M indicates that the Cm(III) hydrolysis at pH_m = 8 is less pronounced compared to 0.1 M NaCl and considerable amounts of uncomplexed Cm^{3+} are still present. By increase of $[B]_{tot}$ to 0.04 M, the peak maximum assigned to the second hydrolysis species at ~ 604 nm disappears due to competition with borate and a broad peak with a peak maximum at ~ 596 nm can be detected consisting of contributions of Cm^{3+} and a new formed Cm(III) borate component. Further increase of $[B]_{tot}$ up to 0.16 M leads to a decrease of the

Cm(III) aquo ion contribution, the fluorescence peak is shifted to ~ 601 nm which can be explained only by the formation of a Cm(III)–borate complex. At the same time an increase of the corresponding fluorescence lifetime from 77 µs at $[B]_{tot}$ = 0.04 M to 108 µs at $[B]_{tot}$ = 0.16 M is measured. The fluorescence decay curves in all investigated systems show a single averaged exponential decay for all spectra, caused by a faster ligand exchange than the lifetime of the excited state. Kimura et al. found a linear relation between the number of H_2O entities in the first hydration sphere of the curium ion and the fluorescence decay constant [138]. According to this relation 4 H_2O molecules are removed from the first hydration sphere of the Cm(III) complex at $[B]_{tot}$ = 0.16 M. Note that no influence of high ionic strength on this linear relation is considered. The peak positions (~ 600-601 nm) at $[B]_{tot}$ = 0.16 M for both 0.1 M and 5.0 M NaCl solutions are very similar implying that similar Cm–borate species are formed. TRLFS investigations of Cm(III) with inorganic ligands such as Cl^-, CO_3^{2-} and SO_4^{2-} show that peak positions of $\lambda \geq 600$ nm for the most part indicate the coordination of the Cm(III) ion with more than one ligand [139, 140]. The presence of hydrolysis species under the investigated conditions together with the limitation of the boron concentrations to 0.16 M allows no systematic investigations of the Cm(III) borate complexation in NaCl systems.

Table 4.3. *Fluorescence lifetimes (τ) and peak maxima (λ_{max}) in NaCl, $CaCl_2$ and $MgCl_2$ solutions at pH_m = 8 and various $[B]_{tot}$.*

Background electrolyte	0.004 M $[B]_{tot}$		0.04 M $[B]_{tot}$		0.16 M $[B]_{tot}$		0.4 M $[B]_{tot}$	
	τ [µs]	λ_{max} [nm]	τ [µs]	λ_{max} [nm]	τ [µs]	λ_{max} [nm]	τ [µs]	λ_{max} [nm]
0.1 M NaCl	–	603	77 ± 5	601	59 ± 5	600	–	–
5.0 M NaCl	85 ± 5	604	77 ± 5	596	108 ± 5	601	–	–
0.25 M $CaCl_2$	72 ± 5	594	78 ± 5	597	–		–	–
3.5 M $CaCl_2$	73 ± 5	595	77 ± 5	596	–		–	–
0.25 M $MgCl_2$	–	–	85 ± 5	597	96 ± 5	600	114 ± 7	603
3.5 M $MgCl_2$	–	–	87 ± 5	597	95 ± 5	600	121 ± 7	602

4.3.1 Cm(III) TRLFS studies in $CaCl_2$ and $MgCl_2$ solutions

In contrast to NaCl systems, no Cm(III) hydroxide species are found in dilute to concentrated $MgCl_2$ solutions under near neutral pH_m conditions (pH_m = 8) and absence of borate [141]. Note that these findings are in contrast to studies with $Nd(OH)_3(am)$ in $MgCl_2$ solutions, where hydrolysis species of Nd(III) species are prevailing at this pH [24]. In $MgCl_2$ solutions spectra with high boron concentrations up to 0.4 M $[B]_{tot}$ could be measured and allow a systematic investigation of the Cm(III) borate complexation.A broad emission peak at ~597 nm at $[B]_{tot}$ = 0.04 M can be observed for both investigated $MgCl_2$ concentrations. The shift of the peak maximum compared to the borate-free system indicates the complexation of Cm(III) with borate. The corresponding fluorescence lifetimes (77 µs – 87 µs, depending upon salt system and ionic strength) are significantly increased compared to the fluorescence lifetime of the Cm(III) aquo ion with 64 µs± 3 µs [142].

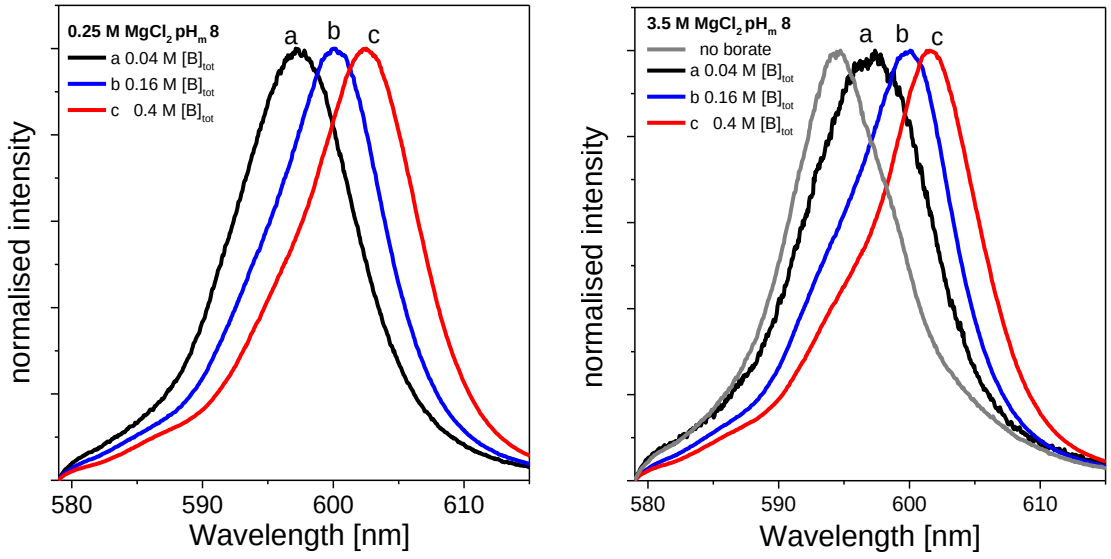

Figure 4.13. *TRLFS emission spectra of Cm(III) in 0.25 M and 3.5 M $MgCl_2$ solutions at pH_m = 8 and various $[B]_{tot}$. Comparison with a spectrum in the absence of borate as reported in Herm [141].*

In contrast to NaCl systems, Cm(III)–borate complexation results in a bathochromic peak shift (shift to longer wavelengths). The different behavior observed in NaCl and $MgCl_2$ systems (hypsochromic *vs.* bathochromic peak shift) is likely due to the absence of hydrolysis species forming in the latter system. With increasing $[B]_{tot}$, the peak maxima of the fluorescence emission bands are further shifted to higher wavelengths, clearly indicating the formation of Cm(III) complexes with borate. These pronounced bathochromic peak shifts support the assumption that more than one Cm(III)–borate complexes exist under these conditions, as also proposed for the NaCl system. The bathochromic peak shift of the Cm(III) emission with increasing $[B]_{tot}$ is accompanied with an increase of the fluorescence lifetimes up to 121 µs for 3.5 M $MgCl_2$ and $[B]_{tot}$ = 0.4 M (see Table 4.3). According to the Kimura

equation [138], 3 H_2O molecules are removed in the Cm(III) complexes found in 0.25 M and 3.5 M $MgCl_2$ with $[B]_{tot}$ = 0.16 M, and 4 to 4.5 H_2O molecules for 0.25 M $MgCl_2$ and 3.5 M $MgCl_2$ with $[B]_{tot}$ = 0.4 M, respectively. The formation of Cm(III)–borate species in weakly alkaline $MgCl_2$ solutions shows no clear dependence on ionic strength of the solution within the uncertainty limits of the technique, as already observed in NaCl systems.

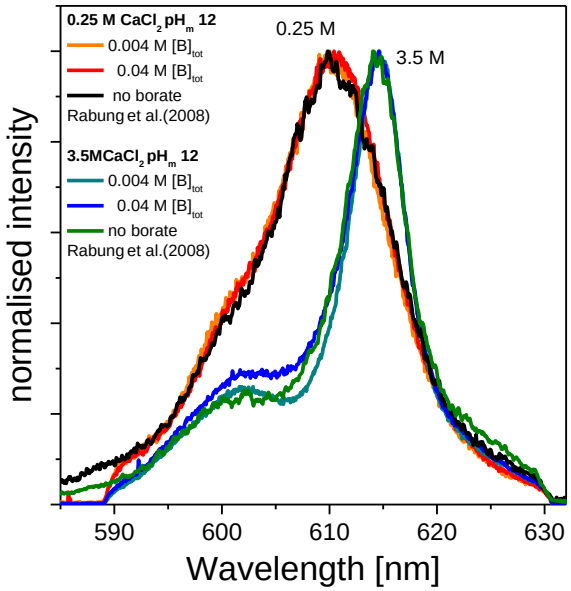

Figure 4.14. *TRLFS emission spectra of Cm(III) in 0.25 M and 3.5 M $CaCl_2$ at pH_m = 12 and various borate concentrations in comparison with borate-free literature data [25].*

Under highly alkaline conditions (pH_m = 12), no influence of borate on the emission spectra can be observed in $CaCl_2$ solutions and $[B]_{tot} \leq 0.04$ M (Fig. 4.11). The measured spectra and corresponding fluorescence lifetimes in presence of borate in both 0.25 M and 3.5 M $CaCl_2$ solutions are in good agreement with the borate-free system [25]. As already discussed for the Nd(III) solubility data, borate is a weak ligand that can only compete with hydrolysis under near-neutral pH conditions and relatively high $[B]_{tot}$, but cannot outcompete hydrolysis under hyperalkaline conditions.

4.4 Conclusions

Solubility studies with $Nd(OH)_3$(am) and TRLFS investigations with Cm(III) confirm the formation of aqueous complexes of Ln(III) and An(III) with borate in dilute to concentrated NaCl, $MgCl_2$ and $CaCl_2$ solutions under near-neutral pH_m conditions and $[B]_{tot} \geq 0.04$ M. At $[B]_{tot} \geq 0.16$ M and near-neutral pH_m (pH_m = 8), Cm(III)–borate aqueous species outcompete hydrolysis and become predominant. TRLFS indicates that (at least) two Cm(III)–borate species (maybe 1:1 and 1:2) form in NaCl and $MgCl_2$ solutions, although the exact stoichiometry of the complexation reaction remains

unknown. A similar trend can be found in UV-Vis studies with Np(V) (see chapter 7) in $MgCl_2$ solutions with comparable $[B]_{tot}$. Despite the clear formation of Ln^{III}/An^{III}–borate aqueous species in near neutral pH_m conditions, no significant increase in solubility is observed for $Nd(OH)_3$(am) in the presence of $[B]_{tot} \leq 0.4$ M in all investigated systems. Conversely, a clear drop in the Nd(III) solubility of 2–3 orders of magnitude occurs at $6 \leq pH_m \leq 9$, indicating the formation of a new solubility controlling borate-bearing solid phase. This mechanism is confirmed by XPS and SEM–EDS technique, which suggest that the formation of a Nd(III)-borate solid phase takes place as a coating on an unreacted $Nd(OH)_3$(am) core. Unlike solubility studies with $NpO_2(OH)$(am) (chapter 7), no complete transformation of the initial Nd(III) solid occurred in samples with $[B]_{tot} \geq 0.16$ M. The significant decrease observed in the Ln(III)/An(III) solubility at $pH_m < 9$ related to the formation of secondary An(III)–borate alteration phases represents a hitherto unknown actinide retention mechanism in repository systems. A thermodynamic evaluation and model of the Ln(III)/An(III) interactions in the presence of borate in NaCl, $CaCl_2$ and $MgCl_2$ systems is proposed in chapter 9.

5 Solubility of Th(IV) in the presence of borate

The solubility of Th(IV) was studied from undersaturation conditions in the presence of $[B]_{tot}$ = 0.16 M within $6.5 \leq pH_m \leq 11$ in dilute to concentrated NaCl and $MgCl_2$ solutions. For comparison purposes, samples with Th(IV) in the same pH_m and ionic strength conditions but absence of borate were prepared and measured following the same experimental approach as for the borate-bearing samples. The Th(IV) concentration was regularly quantified in combination with pH_m measurements for up to 860 days.

5.1 Solubility data of Th(IV) in dilute to concentrated NaCl and $MgCl_2$ solutions

Fig. 5.1 and Fig. 5.2 show the solubility of $Th(OH)_4(am)$ determined in 0.1 M – 5.0 M NaCl and 0.25 M – 3.5 M $MgCl_2$ solutions with $[B]_{tot}$ = 0 and 0.16 M and varying pH_m. Data points below the detection limit were set to log m_{Th} = –10 for dilute (0.1 M NaCl and 0.25 M $MgCl_2$) and -9 and -8.5 for concentrated (5.0 M NaCl and 3.5 M $MgCl_2$) solutions, respectively, due to the different dilution steps needed in each case for ICP–MS measurements. For comparison purposes, Fig. 5.1 and Fig. 5.2 also show the calculated solubility of $Th(OH)_4(am)$ (both for fresh and aged phases) in dilute NaCl and $MgCl_2$ systems in the absence of borate [27]. Under these boundary conditions and provided the predominance of the neutral species $Th(OH)_4(aq)$ over the complete pH-range investigated in this work, no significant effect of ionic strength is foreseen according with thermodynamic calculations.

Fig. 5.1 and Fig. 5.2 show that the solubility of $Th(OH)_4(am)$ remains largely unaffected by borate in dilute NaCl and $MgCl_2$ solutions over the entire pH_m range considered in this work. However, a slight increase in the solubility of Th(IV) compared to borate-free systems can be claimed for samples with $[B]_{tot}$ = 0.16 M, both in concentrated NaCl and $MgCl_2$ solutions at $pH_m \approx 8–9$. Although Th(IV)–borate complexation appears unlikely considering the strong tendency of Th(IV) towards hydrolysis, this hypothesis cannot be completely ruled out in view of the experimental data gained in this work. Large scattering of the measured data is observed in all samples. A similar behavior in this pH_m region ($pH_m > 6$) has been reported for Nd(III) and Th(IV) in the absence of boron. This observation can be likely explained by the tendency of neutral aqueous species to sorb (*i.e* $Th(OH)_4(aq)$), the presence of colloidal nanoparticles not removed from the solution by ultrafiltration and the very low concentrations of Th(IV) in solution (close to the detection limit of ICP–MS) [24, 29]. Note further that especially tetravalent actinides tend to form stable colloids in saline solution. In the case of thorium, these have been reported to increase the total concentration in solution 2–3 orders of magnitude [29].

The difficulties in evaluating the aquatic chemistry of Th(IV) within this pH region are also reflected on the quality (i.e. associated uncertainty) of the thermodynamic data available for this system in the

absence of borate. The solubility reaction controlling the aqueous chemistry of Th(IV) within the pH-range 6–14 is provided in equations (5.1) and (5.2) for the two different Th(IV) oxy-hydroxides selected in the NEA–TDB, namely $Th(OH)_4$(am,fresh) and $Th(OH)_4$(am,aged). The equilibrium constants selected for both solubility reactions have a very large associated uncertainty (± 0.9 log-units), accordingly supporting the very large dispersion obtained in the present work for the solubility of Th(IV) in the absence and presence of borate

$$Th(OH)_4(am,fresh) \rightleftharpoons Th(OH)_4(aq) \qquad log\ {}^*K^\circ_{s,0} = -8.1 \pm 0.9 \tag{5.1}$$

$$Th(OH)_4(am,aged) \rightleftharpoons Th(OH)_4(aq) \qquad log\ {}^*K^\circ_{s,0} = -8.9 \pm 0.9 \tag{5.2}$$

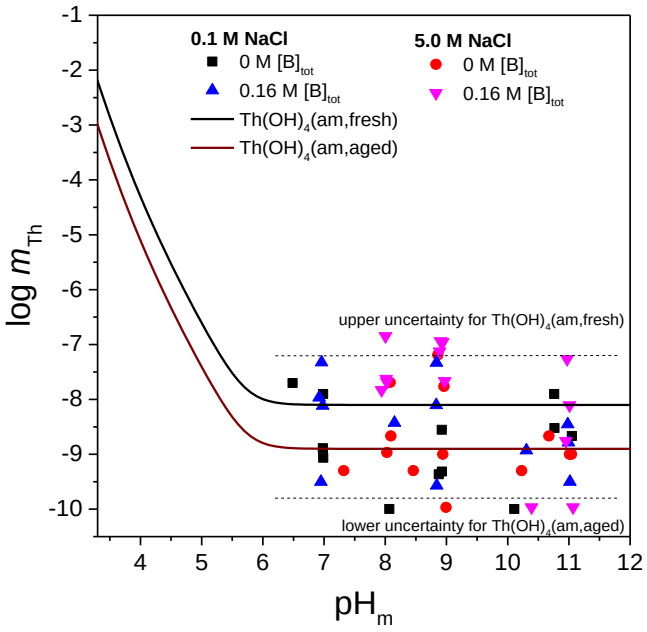

Figure 5.1. *Solubility of $Th(OH)_4$(am), experimentally determined in the presence of $0\ M \leq [B]_{tot} \leq 0.16\ M$ in 0.1 M and 5.0 M NaCl solutions. Comparison with solubility of $Th(OH)_4$(am,fresh) and $Th(OH)_4$(am,aged), as calculated for 0.1 M NaCl using the NEA-TDB thermodynamic selection [27].*

In contrast to observations made for Nd(III) (see chapter 4) and Np(V) (see chapter 7), no evident decrease in solubility is observed for $Th(OH)_4$(am) in NaCl and $MgCl_2$ systems with $[B]_{tot}$ = 0.16 M and $6.5 \leq pH_m \leq 9$, hence disregarding a possible transformation of the initial oxy-hydroxide solid phase. This observation is related with the significantly lower solubility of $Th(OH)_4$(am) compared to $Nd(OH)_3$(am) and NpO_2OH(am), as well as with the much stronger hydrolysis of An(IV), which is expected to outcompete any possible complexation with borate. Based on the lower Th(IV)

concentrations measured after longer equilibration times (t > 100 days, both in the absence and presence of borate), and in agreement with previous observations reported in the literature, $Th(OH)_4$(am,fresh) slowly transforms into a more stable $Th(OH)_4$(am,aged) phase with lower solubility [27, 33].

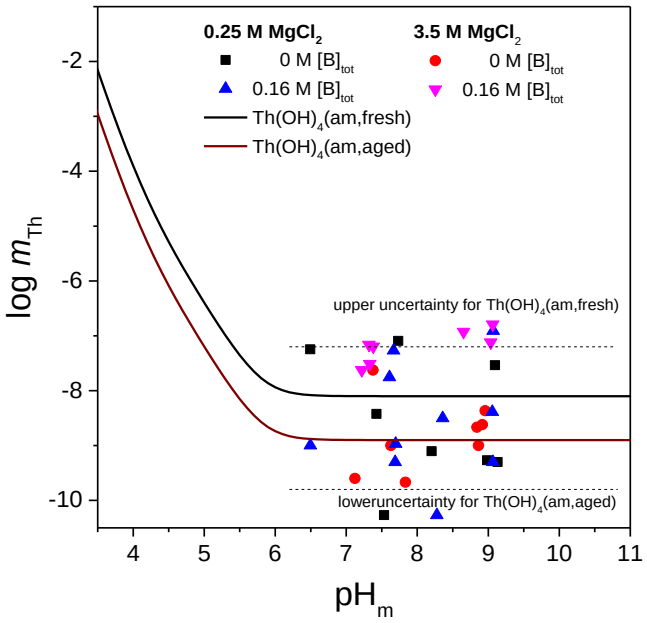

Figure 5.2. *Solubility of $Th(OH)_4$(am) experimentally determined in the presence of $0\ M \leq [B]_{tot} \leq 0.16\ M$ in 0.25 M and 3.5 M $MgCl_2$ solutions. Comparison with solubility of $Th(OH)_4$(am,fresh) and $Th(OH)_4$(am,aged), as calculated for 0.25 M $MgCl_2$ using the NEA-TDB thermodynamic selection [27].*

5.2 Conclusions

In contrast to Ln(III)/An(III), An(V) and An(VI) systems investigated in this work, no significant effect of borate on the Th(IV) solubility was observed in dilute NaCl and $MgCl_2$ systems within $6.5 \leq pH_m \leq 11$ and $[B]_{tot} = 0.16$ M. A slight increase in the solubility of Th(IV) could be claimed for both concentrated NaCl and $MgCl_2$ systems at $pH_m = 7.5–9$, which may hint towards a weak Th(IV)–borate complexation in this pH_m region under these experimental conditions. Further experimental evidences would be needed to confirm this possibility. The weaker Th(IV)–borate interaction compared to Ln(III)/An(III), An(V) and An(VI) is in good agreement with the strong hydrolysis tendency of tetravalent actinides, which significantly outcompetes the formation of weaker complexes. The sparingly soluble Th(IV) oxy-hydroxide phase controlling the solubility in the conditions of this experiment retains very low Th(IV) concentrations in solution, and thus prevents the formation of any secondary phase in the presence of borate. Note that, under alkaline to hyperalkaline pH conditions,

only strong ligands (hard Lewis bases) such as carbonate or certain organic molecules (among others) are able to outcompete hydrolysis and enhance the solubility of Th(IV) [143-146].

The large scattering in the solubility data observed both in the absence and presence of borate is attributed to the predominance of the neutral aqueous species $Th(OH)_4(aq)$ and the possible formation of polymeric/colloidal Th(IV) species [29], and reflects also the large uncertainty associated to the thermodynamic data available for Th(IV) aqueous species and solid compounds forming in these conditions.

6 Interaction of Pu(III/IV) with borate

The solubility of Pu(III/IV) was studied from undersaturation conditions with freshly prepared $Pu^{IV}O_2$(am,hyd) in the presence of $[B]_{tot}$ = 0.16 M within $7.5 \leq pH_m \leq 9.0$ in 0.1 M NaCl solutions. Reducing conditions were set by addition of ~0.03 M $Na_2S_2O_4$ and 0.01 M hydroquinone, respectively. In all samples $[Pu]_{tot}$, pH_m and Eh were regularly measured for up to 300 days. At the end of the solubility experiments, Pu solid phases contacted with the borate-bearing solution were characterized by XPS.

6.1 Solubility of Pu(III/IV) in NaCl solutions

The solubility of $Pu^{IV}O_2$(am,hyd) in 0.1 M NaCl solution with $[B]_{tot}$ = 0.16 M in the presence of $Na_2S_2O_4$ and hydroquinone at pH_m = 7.5 and 9.0 is presented in Fig. 6.1. Experimental Eh and pH values of the samples are displayed in the Pu Pourbaix diagram (Fig. 6.2). XPS spectra are shown in Fig. 6.3.

Measured Eh values for the two samples with hydroquinone are in the stability field of $Pu^{IV}O_2$(am,hyd). The experimental Pu(IV) solubility at pH_m ~7.5 is at the detection limit for LSC, i.e. $1 \cdot 10^{-9}$ M. This upper limit value is consistent with the expected $Pu^{IV}O_2$(am,hyd) solubility. XPS analysis confirm $Pu^{IV}O_2$(am,hyd) as solubility controlling phase (Fig. 6.3). In conclusion, no significant effect of borate on the Pu(IV) aqueous and solid phase speciation is observed at pH_m = 7.5 in slightly reducing solutions which is consistent with the results obtained for Th(IV) (chapter 5). At pH_m = 9.0 the experimental $Pu^{IV}O_2$ (am,hyd) solubility is significantly enhanced compared to the Pu solubility expected for the measured (pe + pH) conditions (log [Pu(IV)] = -10.8) (Fig. 6.1). In the first two measurements ($t \leq 14$ d), [Pu] was at ~10^{-7} M and slowly decreased to ~10^{-8} M within 300 days. Thus, no stable conditions were reached indicating that strong kinetics affect the equilibration process. Note that no change in the oxidation state of Pu in the solid phase was detected by XPS (Fig 6.1), although the low concentrations in solution prevent the accurate characterization of the redox state in the aqueous phase. Although the complexation of Pu(IV) with borate was considered unlikely due to the very strong tendency of An(IV) towards hydrolysis in alkaline solutions [147, 148], the experimental observations gained in this work could be explained properly on the basis of this hypothesis. Note that a similar increase in solubility is found for $Th(OH)_4$(am) in concentrated NaCl and $MgCl_2$ solutions at pH_m = 9, thus indicating that the complexation of Pu(IV) and Th(IV) with borate cannot be completely ruled out (chapter 5). Note however that no Th(IV) solubility increase in these conditions was found for dilute NaCl solutions. The enhanced [Pu] can hardly be attributed to the initial presence of Pu(III) as the redox conditions (pe + pH) are clearly in the stability field of Pu(IV) (the hydroquinone sample at pH_m = 7.5 is even closer to the stability field of Pu(III), but does

not show any indication for the presence of Pu(III)). More experimental data in the investigated conditions with longer equilibration times are needed to completely understand the observed processes.

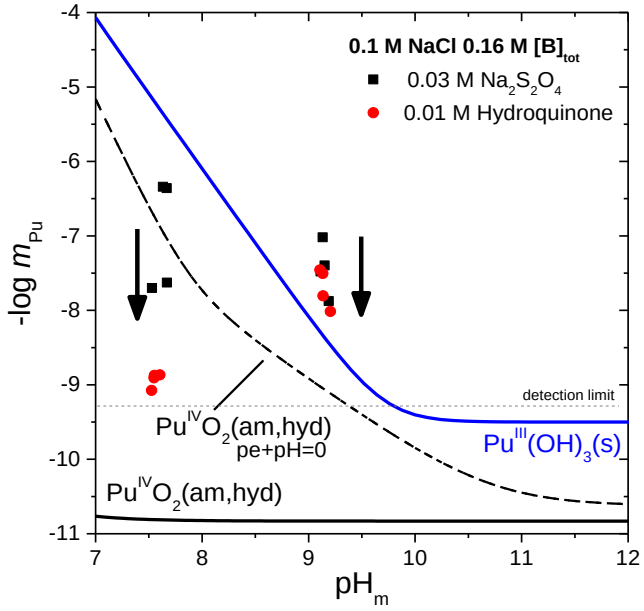

Figure 6.1. *Solubility of $Pu^{IV}O_2$(am,hyd) in the presence of $[B]_{tot}$ = 0.16 M with 0.03 M $Na_2S_2O_4$ and 0.01 M hydroquinone in 0.1 M NaCl solutions. Comparison with calculated solubility data for $Pu^{IV}O_2$(am,hyd) (black solid line) and $Pu(OH)_3$(s) (blue solid line) and the calculated equilibrium of Pu(III)(aq) with $Pu^{IV}O_2$(am,hyd) with pe + pH = 0 (dashed line) in the absence of borate as reported in NEA-TDB [22].*

Redox conditions in the two samples with $Na_2S_2O_4$ are very close to the borderline of $Pu^{IV}O_2$(am,hyd)/$Pu(OH)_3$(s). At pH_m = 7.5, fast transformation of the initial $Pu^{IV}O_2$ (am,hyd) into a dark solid phase occurred within one week. The main oxidation state of the latter is Pu(III) as confirmed by XPS analysis after 300 days. The peak shape and position of the $4f_{3/2}$ and $4f_{7/2}$ transitions are in agreement with Pu(III) reference spectra [149, 150]. The experimental Pu solubility within the first two measurements (~ $5 \cdot 10^{-7}$ M) is clearly above the Pu(IV) solubility curve, but slightly lower than expected for $Pu(OH)_3$(s) according to the data from NEA. The solubility constant log $*K°_{s,0}\{Pu(OH)_3(s)\}$ = 15.8 ± 1.5 is reported with a large uncertainty of 1.5 log-units which can explain the deviations [22]. Recent results from Fellhauer further suggest a lower value for the solubility constant of ~ log $*K°_{s,0}\{Pu(OH)_3(s)\}$ = 14.35 [59]. Therefore it is likely that the solubility for t ≤ 14 d is controlled by $Pu(OH)_3$(s). For t > 14 d (i.e. in the last two measurements) pe-values are slightly increasing, and $[Pu]_{tot}$ decreasing to ~2 10^{-8} M. Note that $Na_2S_2O_4$ is only metastable in neutral pH conditions [151, 152]. The slightly increasing pe values for the sample at pH_m = 7.5 points to slow

decomposition of $Na_2S_2O_4$. While the measured (pe + pH) values suggest a solubility control by the reductive dissolution equilibrium (equation 6.1; implying a quantitative re-oxidation of $Pu(OH)_3(s)$ to $PuO_2(am,hyd)$), XPS clearly revealed the presence of a rather oxidation state pure Pu(III) solid phase. Therefore, the decrease in $[Pu]_{tot}$ for t > 14 d is likely caused by the formation of a Pu(III) borate coating or borate containing Pu(III) solid phase similar to the findings in Nd(III) solubility studies (chapter 4).

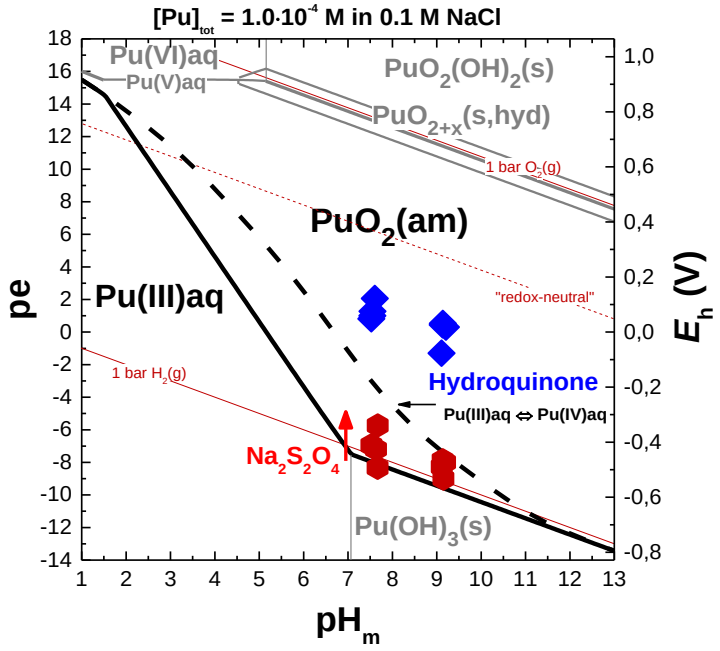

Figure 6.2. *Pourbaix diagram calculated for* $[Pu]_{tot} = 10^{-4}$ *M in 0.1 M NaCl and absence of borate. Dashed and solid lines represent the calculated borderlines for the individual Pu redox species [22, 55]. pe and* pH_m *values are shown for the solubility samples in the presence of hydroquinone (blue) and* $Na_2S_2O_4$ *(red).*

For the sample at $pH_m = 9$ ($Na_2S_2O_4$), XPS analysis indicates the presence of both Pu(III) and Pu(IV) in the solid phase after t = 300 d (Fig 6.3). The measured $[Pu]_{tot}$ at $pH_m = 9$ after short equilibration time is enhanced compared to the solubility expected under these pe + pH conditions, i.e. the reductive dissolution equilibrium (equation 6.1).

$$PuO_2(am,hyd) + 4\,H^+ + e^- \rightleftharpoons Pu^{3+} + 2\,H_2O \qquad (6.1)$$

As the experimental [Pu] is even higher than that of $Pu(OH)_3(s)$ in borate-free systems, the formation of Pu(III) borate complexes has to be considered, analogously to the Cm(III) borate complexes observed under comparable experimental conditions. In solubility studies with $Nd(OH)_3(am)$, the

increase in [Nd(III)] in 0.1 M and 1.0 M NaCl at pH_m = 9 and 10 in presence of $[B]_{tot} \geq 0.16$ M is attributed to Nd(III)-borate complexes (see chapter 4). The initial [Pu] decreased with time (by ~ 1 order of magnitude after t = 300 d) indicates that no equilibrium has been attained. As for the sample at pH_m = 7.5 ($Na_2S_2O_4$), the decrease of initial [Pu] (i.e. [Pu(III)]) is consistent with the formation of a Pu(III) borate coating or borate containing Pu(III) solid phase as reported for Nd(III) in chapter 4.

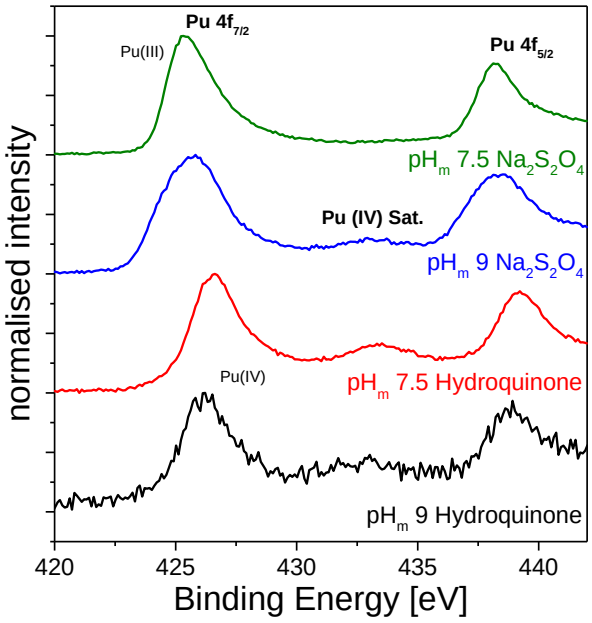

Figure 6.3. *Narrow scan of the $4f_{5/2}$ and $4f_{7/2}$ spectra of Pu of solid phases from 0.1 M NaCl with $[B]_{tot}$ = 0.16 M in the presence of $Na_2S_2O_4$ and hydroquinone, respectively.*

6.2 Conclusions

Solubility studies with $Pu^{IV}O_2$(am,hyd) under mildly reducing conditions controlled by hydroquinone and with $[B]_{tot}$ = 0.16 M show a differential behavior at pH_m = 7.5 and pH_m = 9.0. Hence, the very low solubility determined at pH_m = 7.5 is in good agreement with the reported solubility of Pu(IV) in equilibrium with $Pu^{IV}O_2$(am,hyd) in the absence of borate. The solubility increase observed at pH_m = 9 could be explained by a possible Pu(IV)-borate interaction, similar to observations made with Th(IV) in concentrated NaCl and $MgCl_2$ solutions at same pH. Note however that a Pu(IV)-borate complexation leading to an increased Pu(IV) solubility was considered unlikely on the basis of the strong tendency of Pu(IV) towards hydrolysis, and thus additional experiments evidences are needed to clarify the influence of borate on the Pu(IV) solubility and speciation in this pH_m region. The slow decrease of the measured Pu concentration at this pH_m with time clearly indicates that no equilibrium conditions are reached after 300 days. XPS analysis of the alteration phases in the presence of

hydroquinone and $[B]_{tot}$ = 0.16 M showed no reduction of the initial Pu(IV) solid, as expected under the measured pe + pH conditions.

In the presence of $Na_2S_2O_4$, a complete (pH_m = 7.5) and partial (pH_m = 9) reduction of the initial $Pu^{IV}O_2$(am,hyd) to a Pu(III) solid phase occurs according to XPS analyses. At pH_m = 7.5, the measured Pu solubility at short equilibration times ($t \leq 14$ d) are in agreement with a solubility control by $Pu(OH)_3$(s). The continuous decrease in $[Pu]_{tot}$ (i.e. [Pu(III)]) with time and the XPS results at the end of the solubility experiments are consistent with the formation of a Pu(III) borate coating or formation of a Pu(III)-borate solid phase similar to observations gained for Nd(III) under analogues experimental conditions. At pH_m = 9, the formation of Pu(III)-complexes likely occurs slightly enhancing the Pu(III) solubility compared to the borate-free system. The latter agrees with the findings for Cm(III) and Np(V) at this pH_m with comparable $[B]_{tot}$ in NaCl media. In most samples, no stable Pu(III/IV) concentrations are measured clearly indicating that longer equilibration times than 300 days are needed. Additional experimental efforts are needed to gain a conclusive insight on the impact of borate on the Pu solubility and redox chemistry under weakly alkaline reducing conditions.

7 Solubility of Np(V) and UV-Vis in the presence of borate

The solubility of Np(V) with borate was investigated from undersaturation conditions using $NpO_2OH(am)$ as starting material. Experiments were performed in NaCl and $MgCl_2$ solutions with $0.04\ M \leq [B]_{tot} \leq 0.16\ M$ at $6 \leq pH_m \leq 9$. [Np(V)] and pH_m were monitored at regular time intervals for up to 270 days. After reaching equilibrium conditions, solid phases from selected samples were characterized by XPS, SEM–EDS, XRD, XANES and EXAFS. The interaction of Np(V) with borate in the aqueous phase was further investigated in an independent batch series with ~10^{-4} M Np(V) in 0.25 M and 3.5 M $MgCl_2$ with $0.04\ M \leq [B]_{tot} \leq 0.16\ M$ and $pH_m = 8$ and 9 by UV-VIS/NIR spectroscopy. Based on the comprehensive experimental data chemical and thermodynamic models were proposed for the system NpO_2^+-Na^+-Mg^{2+}-H^+-Cl^--$B(OH)_4^-$-OH^--H_2O using the SIT approach. These are separately discussed in chapter 9.

7.1 Solubility of Np(V) in NaCl and $MgCl_2$ solutions

The experimental solubility data of Np(V) in 0.1 M NaCl, 5.0 M NaCl, 0.25 M $MgCl_2$ and 3.5 M $MgCl_2$ solutions in the presence of $0.04\ M \leq [B]_{tot} \leq 0.16\ M$ are shown in Figs. 7.1- 7.4. The figures also show experimental and calculated solubility of Np(V) in the absence of borate as reported by Petrov et al., Neck et al. and the NEA-TDB [22, 36, 40].

Within the timeframe of this study, low boron concentrations ($[B]_{tot} = 0.04$ M) show no significant effect on the solubility of Np(V) in 5.0 M NaCl and 0.25 M and 3.5 M $MgCl_2$ solutions with $8 \leq pH_m \leq 9$.The experimentally measured Np(V) solubility in these systems is in good agreement with Np(V) solubility data in the absence of borate [36, 40, 153]. A slight increase in the Np(V) solubility is observed in 0.1 M NaCl solutions with $pH_m = 9$ and $[B]_{tot} \geq 0.04$ M, indicating the possible formation of Np(V)–borate complexes in solution (Fig. 7.1). Similar to observations made for Nd(III) (see chapter 4), a distinct decrease in solubility occurs in 0.1 M and 5.0 M NaCl solutions with higher boron concentration ($[B]_{tot} = 0.16$ M) and $pH_m \leq 9$ (Fig. 7.1 and Fig. 7.2). The drop in the solubility is accompanied by a transformation of the initial greenish NpO_2OH (am) into a white-grayish solid phase. The solid phase transformation was fast in 5.0 M NaCl (≈ 2 weeks), but slower in 0.1 M NaCl where it occurred only for $pH_m \leq 8.5$. Note that samples prepared from oversaturation conditions in 0.1 M NaCl and $[B]_{tot} = 0.16$ M result in very similar experimental observations than samples prepared from undersaturation conditions: a slight increase of Np(V) concentration at pH_m ~ 8.8 and a drop in the Np(V) solubility at $pH_m \leq 8.5$ together with a slow transformation of the solid phase. In both cases, the concentration of Np(V) in equilibrium with the newly formed solid phase is approximately three orders of magnitude lower than the solubility of $NpO_2OH(am,fresh)$.

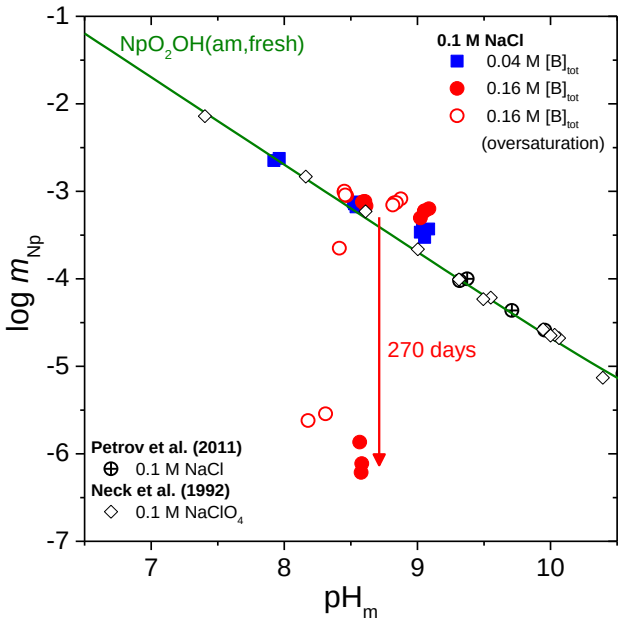

Figure 7.1. *Solubility of Np(V) in the presence of 0.04 M ≤ [B]$_{tot}$ ≤ 0.16 M in 0.1 M NaCl solutions (blue and red symbols). Comparison with experimental (open symbols, black) solubility data in the absence of borate as reported by Neck et al. (1992) and Petrov et al. (2011) [36, 40]. Solid line corresponding to the solubility of NpO$_2$OH(am,fresh) in 0.1 M NaCl calculated according to the NEA–TDB selection [22].*

The transformation is tentatively faster at lower pH$_m$ values, see Figs. 7.1 – 7.4. It is therefore likely that the non-occurrence of a solid phase transformation in 0.1 M NaCl and pH$_m$ > 8.5 is due to insufficient equilibration time.

A comparable decrease in Np(V) solubility accompanied by a transformation of the initial greenish NpO$_2$OH(am) into a newly formed white–gray solid phase occurs in dilute MgCl$_2$ systems at pH$_m$ < 9 and [B]$_{tot}$ = 0.16 M (Fig. 7.3). Similarly to the dilute NaCl system the solubility of Np(V) decreased slowly and attained a constant value (~$10^{-6.5}$ M) only after 270 days. In 3.5 M MgCl$_2$ solutions with [B]$_{tot}$ = 0.16 M only a minor decrease in Np(V) solubility is observed after 270 days. As observed in Nd(III), Cm(III) and U(VI) solubility studies (see chapters 4 and 8) actinide borate interactions in MgCl$_2$ solutions are less pronounced than in NaCl solutions at comparable pH$_m$ and ionic strength conditions. As discussed in chapter 3 based on the ^{11}B-NMR data gained in this work in combination with the thermodynamic model reported by Felmy and co-workers [81], the formation of Mg–borate complexes decreases the concentration of free borate and outcompetes the formation of An–borate aqueous complexes and solid phases.

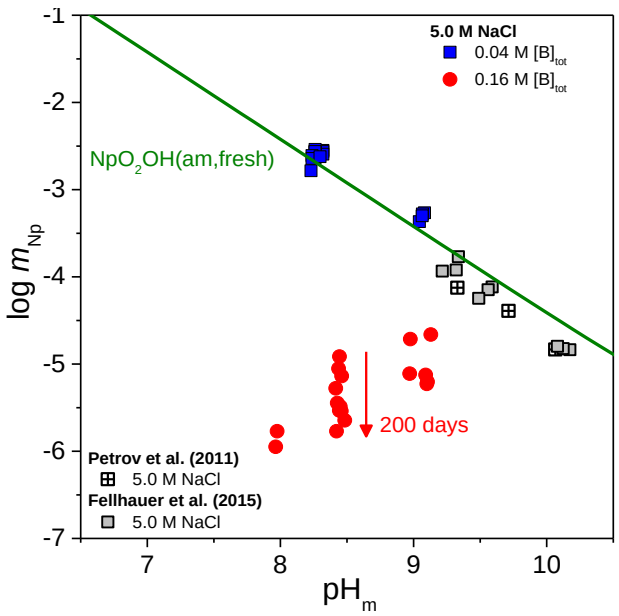

Figure 7.2. *Solubility of Np(V) in the presence of 0.04 M ≤ [B]$_{tot}$ ≤ 0.16 M in 5.0 M NaCl solutions (blue and red symbols). Comparison with experimental (open symbols, black) solubility data in the absence of borate as Fellhauer et al (2015) and Petrov et al. (2011) [40, 153]. Solid line corresponding to the solubility of NpO$_2$OH(am, fresh) in 5.0 M NaCl calculated according to the NEA–TDB selection [22]. Arrow indicates that the decrease in the concentration of Np for the same solubility sample was only completed after 270 days.*

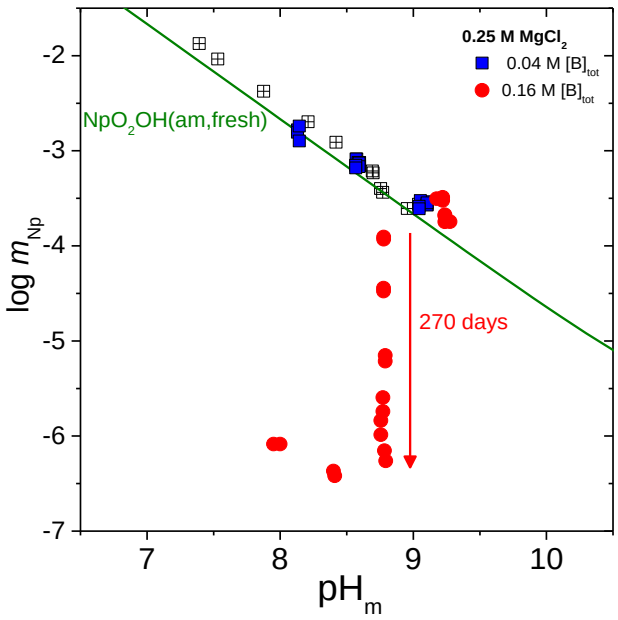

Figure 7.3. *Solubility of Np(V) in the presence of 0.04 M ≤ [B]$_{tot}$ ≤ 0.16 M in 0.25 M MgCl$_2$ solutions (blue and red symbols). Comparison with experimental (open symbols, black) solubility data in the absence of borate as reported by Petrov et al. (2011) [40]. Solid line corresponding to the solubility of NpO$_2$OH(am,fresh) in 0.25 M MgCl$_2$ calculated according to the NEA–TDB selection [22].*

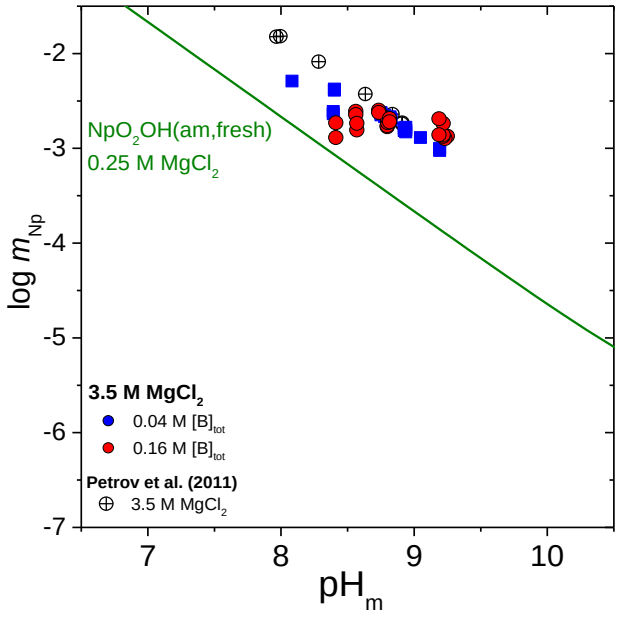

Figure 7.4. *Solubility of Np(V) in the presence of 0.04 M ≤ [B]$_{tot}$ ≤ 0.16 M in 3.5 M $MgCl_2$ solutions (blue and red symbols). Comparison with experimental (open symbols, black) solubility data in the absence of borate as reported by Petrov et al. (2011) [40]. Solid line corresponding to the solubility of NpO_2OH(am, fresh) in 0.25 M $MgCl_2$ calculated according to the NEA–TDB selection [22]. Calculations were restricted to 0.25 M $MgCl_2$ due to a lack of ion interaction parameters for high concentrated $MgCl_2$ systems.*

7.1.1 Solid phase characterization

Solid phases of selected solubility experiments in 0.1 M, 5.0 M NaCl and 0.25 M $MgCl_2$ with $[B]_{tot}$ = 0.16 M were investigated after attaining equilibrium conditions by XRD, SEM–EDS and XPS. Np-L_{III} XANES and EXAFS spectra were also acquired for the alteration phases formed in 0.25 M $MgCl_2$, 0.1 M NaCl and 5.0 M NaCl, all of them with $[B]_{tot}$ = 0.16 M and pH_m ~ 8.5. Spectra were collected at the INE-Beamline for Actinide Research at ANKA [154], and were evaluated by Dr. Kathy Dardenne and Dr. Marika Vespa (KIT-INE).

7.1.1.1 XRD, XPS and SEM–EDS measurements

In contrast to the initial X-ray amorphous NpO_2OH(am,fresh), XRD diffractograms of the transformed solid phases show a series of sharp peaks, indicating the crystalline character of the newly formed solid phase (Fig. 7.5). Although with certain similarities, the diffractograms obtained for the solid phases formed in NaCl and $MgCl_2$ solutions are markedly different, indicating that the cation of the background electrolyte participates (or at least influences) in the formation of the secondary solid phase. Note that the collected diffractograms gave no positive match with any of the existing borate

entries in the JCPDS database. Note further that, in spite of the several washing steps with ethanol, all diffractograms collected for Np(V) secondary phases formed in 5.0 M NaCl solutions showed only very strong reflexes corresponding to NaCl (data not shown in Fig. 7.5).

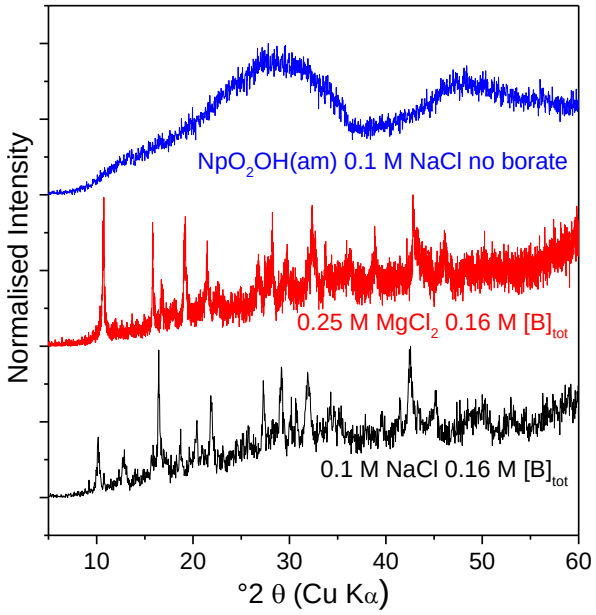

Figure 7.5. *Diffractograms of the solubility-controlling Np(V) solid phases in the absence and presence of borate ($[B]_{tot}$ = 0.16 M) in 0.1 M NaCl and 0.25 M $MgCl_2$ solutions at pH_m ~8.5.*

XPS analyses of the Np(V) secondary phases formed in dilute NaCl and $MgCl_2$ solutions confirm the stoichiometric presence of boron and Na^+/Mg^{2+}. The composition of the newly formed solid phases (in at. %) are listed in Table 7.1, and hint towards the formation of solid phases with stoichiometry $NpO_2[B_5O_6(OH)_4]\cdot 2NaOH$ and $(NpO_2)_2[B_5O_6(OH)_4]_2\cdot 3Mg(OH)_2$(cr), respectively.

Table 7.1. *Composition of the newly formed Np(V)-borate solids (in at. %) based on XPS and EDS analyses (analytical uncertainties lie within 10-20 %).*

Sample	B	O	Na	Mg	Cl	Np(V)
0.1 M NaCl 0.16M $[B]_{tot}$	24.4	62.0	9.4	-		4.2
0.25 M $MgCl_2$ 0.16M $[B]_{tot}$	21.1	68.2	-	6.3		4.5
5.0 M NaCl phase I	2.1	21.2	40.5	-	32.5	1.3
5.0 M NaCl phase II*	23.6	57.4	13.6	-	2.0	4.5

*based on EDS analysis

SEM images of the surface of the Np(V)–borate solid phases formed in NaCl and $MgCl_2$ solutions are shown in Fig. 7.6. Solid phases collected from samples in 0.1 M NaCl (Fig. 7.6 a) and 0.25 M $MgCl_2$ solutions (Fig. 7.6 b) show a homogeneous transformation and distribution of Np(V) in the entire investigated area. The sample equilibrated in 0.1 M NaCl contains very thin (~20 nm) hexagonal platelets with a diameter of ~ 500 nm. The structure of the sample equilibrated in 0.25 M $MgCl_2$ looks similar in shape but appears more amorphous. The investigation of the Np(V)–borate solid phase formed in 5.0 M NaCl (Fig. 7.6 c and d) clearly shows the co-existence of two phases. Hence, massive, crystalline hexagonal blocks appear surrounded by an amorphous phase. EDS analyses indicated the predominance of Na and Cl in the block structures, whereas the amorphous phase (phase II in Table 7.1) would correspond to the newly formed Np(V)–borate phase. The identification of NaCl and presence of an amorphous Np(V) phase is consistent with the observations collected by XRD, where only the pattern of NaCl could be identified and no additional peaks of a newly formed Np(V)–borate solid phase were observed.

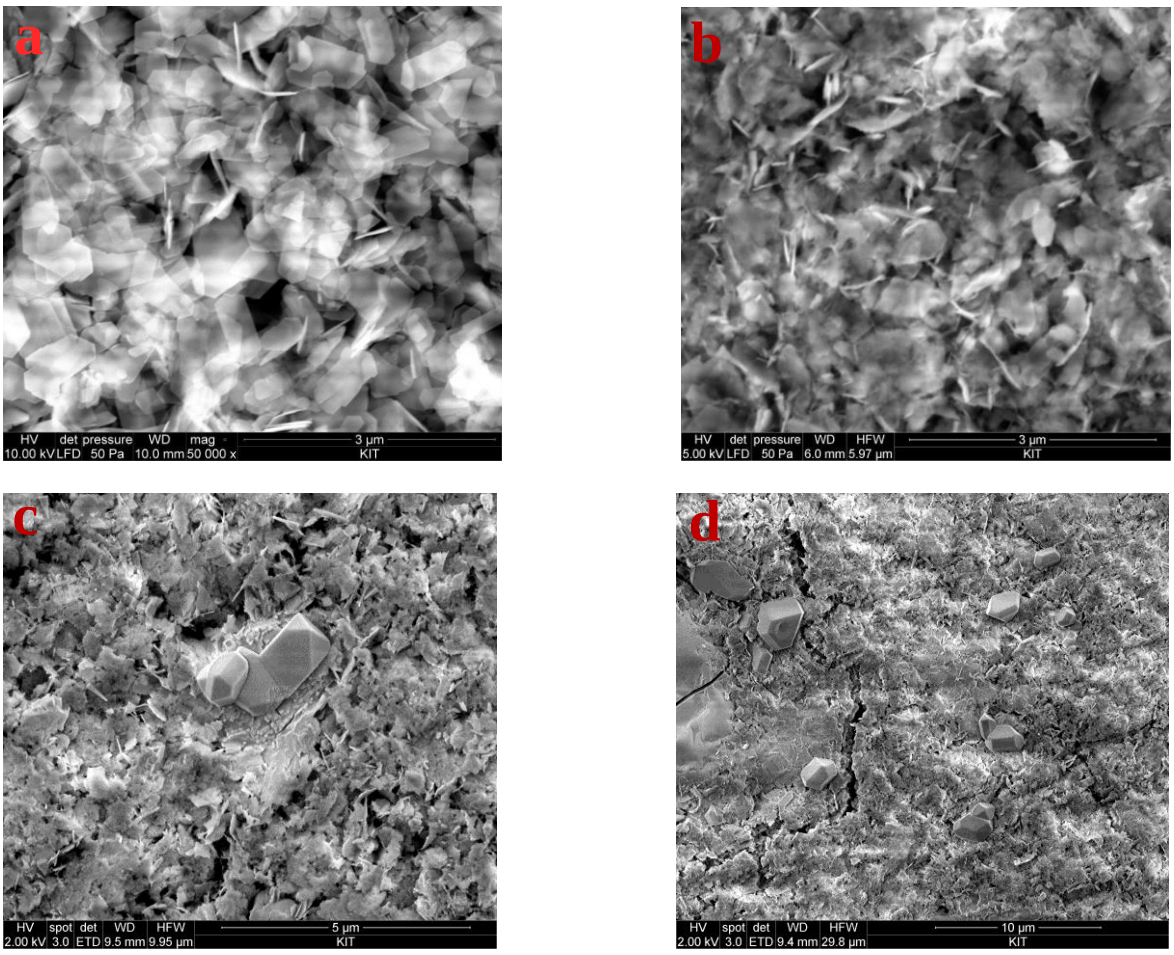

Figure 7.6. *SEM-images of the new formed solubility-controlling Np(V) solid phases in the presence of borate ($[B]_{tot}$ = 0.16 M) in 0.1 M NaCl (a) and 0.25 M $MgCl_2$(b) and 5.0 M NaCl (c, d).*

7.1.1.2 XANES and EXAFS measurements

XANES and EXAFS spectra of the newly formed Np(V)-borate compounds were collected for the solid phases equilibrated in 0.1 M and 5.0 M NaCl and 0.25 M $MgCl_2$ with $[B]_{tot}$ = 0.16 M and pH_m ~8.5. XANES spectra of these three samples are shown in Fig. 7.7, together with the reference spectra of Np(V) (solid phase) as previously reported in the literature [42]. The shape and energy position of the inflection point of the XANES spectra unequivocally confirm the predominance of Np(V) in all measured samples, and disregards any (unlikely) reduction or oxidation process occurring in the course of the experiment.

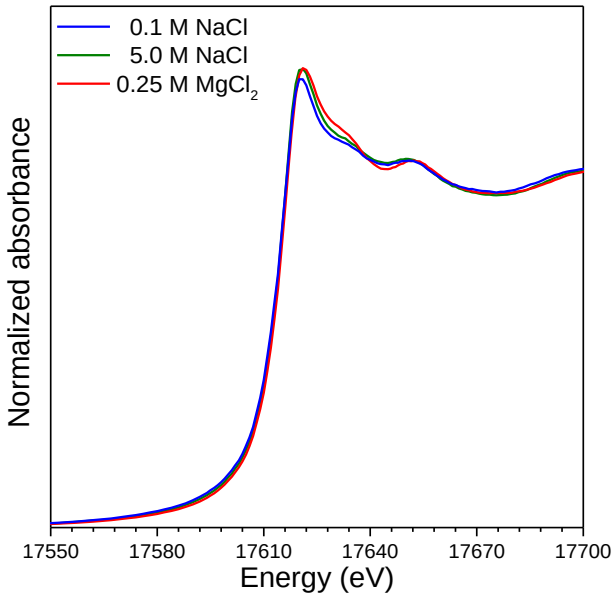

Figure 7.7. *Np-L_{III} edge XANES spectra of solid phases collected from solubility experiments in 0.1 M NaCl, 5.0 M NaCl and 0.25 M $MgCl_2$ with $[B]_{tot}$ = 0.16 M and pH_m = ~8.5.*

Fourier Transforms and the k^3-weighted EXAFS spectra for the Np(V)–borate phases are shown in Fig. 7.8 together with the corresponding best fit models. The k^3-weighted χ(k) spectra of samples from 0.1 M NaCl, 5.0 M NaCl and 0.25 M $MgCl_2$ solutions are very similar. The greatest differences are observed in the *k*-space ~6-8 $Å^{-1}$, where the oscillation splits showing a beat pattern between 6-7 and a maxima at ~7.7 $Å^{-1}$ for the NaCl samples, whereas in the $MgCl_2$ sample this oscillation is dampened with a maxima at ~ 7.4 $Å^{-1}$. This difference can be explained with the presence of the different cations (Na^+ and Mg^{2+}) in the Np(V)–borate structure.

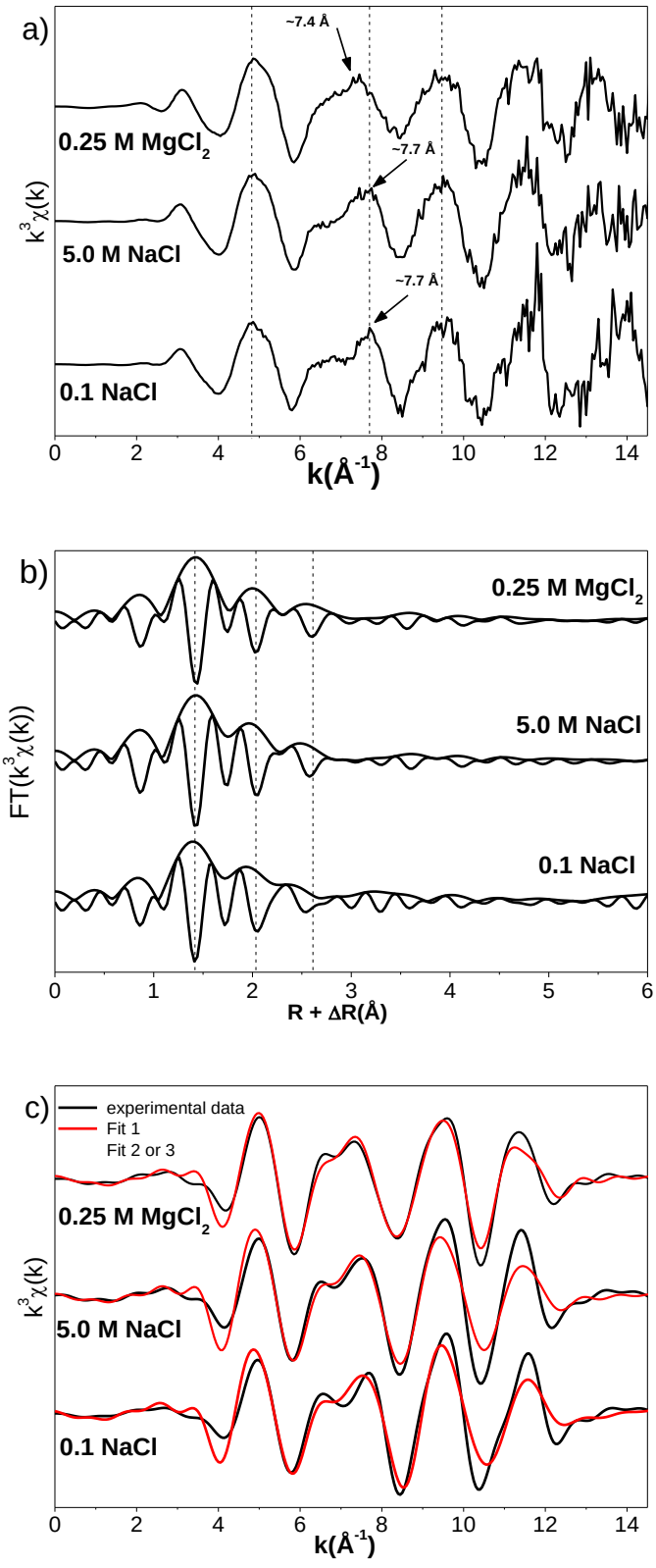

Figure 7.8. *Np L_{III}-edge experimental spectra a) k^3-weighted EXAFS spectra; b) corresponding Fourier transform of the EXAFS spectra and c) experimental (black solid line) and fitted (red line) k^3-weighted EXAFS function of the Fourier-back transform spectra (range: ca. R+ΔR = 1.1-3.7 Å).*

The spectral features observed in the k^3-weighted $\chi(k)$ spectra are intensified in the k^3-weighted EXAFS function of the Fourier-backtransform spectra (Fig. 7.8 c), especially for the $MgCl_2$ sample.

The first two shells of the Radial Structure Functions (RSF) (modulus, |FT|, and imaginary parts, ImFT) described at R+Δ ~1.4 and ~1.9 Å represent the axial (O_{ax}) and equatorial oxygen atoms (O_{eq}) (Fig. 7.8 b). The distances to the axial oxygen atoms are very similar in all measured samples, whereas distances from Np(V) to the equatorial oxygen atoms of the sample from $MgCl_2$ solution are slightly longer, although they lay within the error of the fit.

A very small shift to longer distances is observed for the third shell (corresponding to B) depending upon concentration and type of background electrolyte. The structural parameters resulting from the EXAFS fit, using FEFF 8.4 calculated paths of an atomic cluster based on a starting structure of a Neptunyl-borate ($Ba_2(NpO_2)_{6.59}[B_{20}O_{36}(OH)_2]H_2O$) are shown in Table 7.2 [155]. For the fit, the data was transformed in the *k*-space between ~ 4.3–11.9 $Å^{-1}$ and in the R-space between ~ 1.1-3.7 Å. The fit was performed in the FT^{-1} space.

To model the experimental obtained spectra, a step-by-step approach was used. First O_{ax} were fitted, followed by O_{eq} and at last boron (B) was added to the structure. The best results are given by two model fits. In the first model (fit 1) all coordination numbers (CN) were fixed to the following values: O_{ax} = 2, O_{eq} = 5, B = 2; in the second model (fit 2) the coordination numbers were fixed to: O_{ax} = 2, O_{eq} = 6 and B = 3. These coordination numbers are consistent with previously published Np(V)–borate compounds [104, 155].

As already observed in the Radial Structure Functions (RSF) (Fig. 7.8 b), the Np–O_{ax} distances are similar for all samples, and the Np–O_{eq} distances are comparable for all samples within error. The fit of the Np–B shell shows different Np–B distances depending on the type and concentration of background electrolyte. The shortest Np–B distance of ~ 3.02 Å is found in the sample from 0.1 M NaCl and the longest Np–B distance of 3.13 Å is observed in the sample from dilute $MgCl_2$ solution. The sample from concentrated NaCl shows a distance of 3.09 Å. The relatively short Np–B distances found in the structures are comparable to the Np–B distance in the starting structure indicating a bicoordination of the boron atoms to two equatorial oxygens.

Debye Waller (DW) values fitting O_{ax} are relatively small and were fixed for the solids from 0.25 M $MgCl_2$ and 5.0 M NaCl to the value resulted from the fits using only O_{ax}. Debye Waller values of O_{eq} are generally higher (~ 0.01) in all fits of all three samples indicating a less stable structure.

Table 7.2. *Structural parameters obtained from the EXAFS evaluation of Np(V) solid phases formed in borate-bearing NaCl and $MgCl_2$ solutions.*

Sample	Path	CN	R [Å]	σ^2[Å^2]	ΔE_0 [eV]	R-factor
0.1 M NaCl / 0.16 M $[B]_{tot}$ / FIT 1	Np-O_{ax}	2	1.82	0.001	9.56	0.166
	Np-O_{eq}	5	2.50	0.009		
	Np-B	2	3.02	0.004		
	Np-O_{ax1}-Np-O_{ax1}	2	3.64	0.003		
	Np-O_{ax1}-Np-O_{ax2}	2	3.71	0.002		
0.1 M NaCl 0.16 M $[B]_{tot}$ / FIT 2	Np-O_{ax}	2	1.82	0.001	9.14	0.168
	Np-O_{eq}	6	2.50	0.011		
	Np-B	3	3.02	0.005		
	Np-O_{ax1}-Np-O_{ax1}	2	3.63	0.003		
	Np-O_{ax1}-Np-O_{ax2}	2	3.71	0.002		
5.0 M NaCl 0.16 M $[B]_{tot}$ / FIT 1	Np-O_{ax}	2	1.84	0.001	13.56	0.096
	Np-O_{eq}	5	2.52	0.010		
	Np-B	2	3.09	0.002		
	Np-O_{ax1}-Np-O_{ax1}	2	3.68	0.004		
	Np-O_{ax1}-Np-O_{ax2}	2	3.75	0.002		
5.0 M NaCl 0.16 M $[B]_{tot}$ / FIT 2	Np-O_{ax}	2	1.84	0.001	13.6	0.099
	Np-O_{eq}	6	2.53	0.013		
	Np-B	3	3.09	0.004		
	Np-O_{ax1}-Np-O_{ax1}	2	3.68	0.004		
	Np-O_{ax1}-Np-O_{ax2}	2	3.75	0.002		
0.25 M $MgCl_2$ 0.16 M $[B]_{tot}$ / FIT 1	**Not possible**	-	-	-	-	-
0.25 M $MgCl_2$ 0.16 M $[B]_{tot}$ / FIT 2	Np-O_{ax}	2	1.85	0.001	15.17	0.065
	Np-O_{eq}	6	2.51	0.017		
	Np-B	3	3.13	0.001		
	Np-O_{ax1}-Np-O_{ax1}	2	3.70	0.004		
	Np-O_{ax1}-Np-O_{ax2}	2	3.78	0.002		
0.25 M $MgCl_2$ 0.16 M $[B]_{tot}$ / FIT 3	Np-O_{ax}	2.1	1.85	0.001	14.72	0.047
	Np-O_{eq}	2.8	2.50	0.007		
	Np-B	3.1	3.13	0.001		
	Np-O_{ax1}-Np-O_{ax1}	2	3.70	0.004		
	Np-O_{ax1}-Np-O_{ax2}	2	3.78	0.002		

The Debye Waller (DW) values fitting the Np–B distances lie within the range of 0.005- 0.002 for both solids from NaCl solutions. For the solid from $MgCl_2$ solution the Debye Waller values behave slightly different. The structure could not be fitted with fit 1 due to negative Debye Waller values, whereas fit 2 provides good results. A third fit (fit 3) was performed in which the coordination numbers were left free and the Debye Waller factors were fixed to 0.005 – 0.002. The resulting CN for O_{ax} remain 2, whereas O_{eq} have a CN = 2.8 with a relatively high error of 1.6. The CN for boron is 3.1 with a relatively high error of 1.3. The results of the third fit suggest a CN for the equatorial oxygens between 1 -5 and for boron a CN between 2- 4.

All fits confirmed the Np(V)–borate compound formed in 0.1 M NaCl as the most stable and well crystallized structure, whereas the structures formed in 5 M NaCl and in 0.25 M $MgCl_2$ are less stable and undefined probably consisting of a mixture of different phases. Note that EXAFS analyses are in good agreement with the findings obtained by XRD and SEM–EDS techniques.

7.1.2 Np(V)–borate interactions in $MgCl_2$ solutions: aqueous speciation by UV–Vis/NIR spectroscopy

Absorption spectra of Np(V) measured with 0 M $\leq [B]_{tot} \leq$ 0.16 M in 0.25 M and 3.5 M $MgCl_2$ solutions at pH_m = 8 and 9 are presented in Figs. 7.9 and 7.10, respectively. Np(V) absorption spectra measured for the same background solutions but in the absence of borate show the characteristic NpO_2^+ absorption band with a peak maximum at $\lambda \sim 980$ nm [156]. In 3.5 M $MgCl_2$ a peak shift to higher wavelengths and peak broadening can be observed indicating the formation of Np(V)-chloro complexes, in good agreement to previous investigations in $CaCl_2$ media [59]. At very low $[B]_{tot}$ ($[B]_{tot}$ = 0.004 M), only a minor decrease in the absorbance of the main band can be observed, indicating that uncomplexed NpO_2^+ predominates in solution. In 0.25 M $MgCl_2$ systems and for $[B]_{tot} \geq$ 0.04 M the intensities of the absorption band decrease, the widths increase, and peak maxima are shifted to higher wavelengths by ~ 2 nm at pH_m = 8 and ~ 5 nm at pH_m = 9, respectively. The results clearly indicate the formation of a Np(V)–borate complex in dilute $MgCl_2$ systems. The more pronounced shift and broadening of the peak observed at pH_m = 9 indicate stronger influence of borate on the Np(V) speciation at higher pH_m and the possible formation of more than one Np(V) borate species.

In 3.5 M $MgCl_2$ solutions at pH_m 8, an increase of the intensity of the main absorption band at ~980.5 nm can be observed in the presence of 0.004 M $[B]_{tot}$. The unexpected increase in the intensity is probably caused by an analytical or experimental error and cannot be explained at the moment. As already observed in dilute $MgCl_2$ solutions, further increase of $[B]_{tot}$ leads to a peak shift of the main absorption band to higher wavelengths and a pronounced increase of the FWHM (full width at half

maximum). In contrast to the findings in 0.25 M $MgCl_2$ solutions, no significant pH_m dependence is observed in 3.5 M $MgCl_2$ solution.

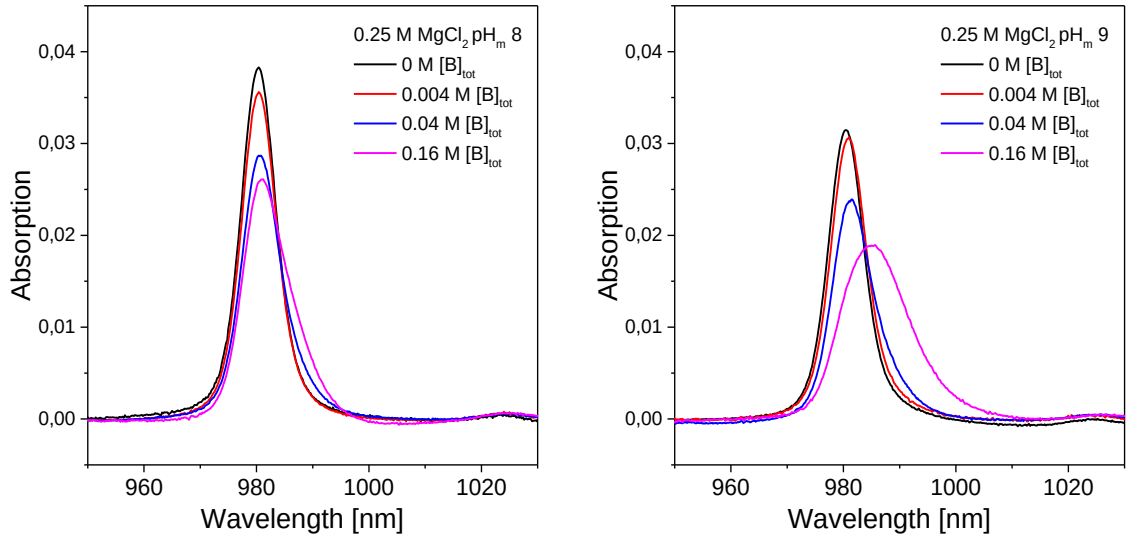

Figure 7.9. *UV-Vis/NIR absorption spectra of Np(V) in 0.25 M $MgCl_2$ solutions at pH_m 8 -9 in the presence of borate (0 M ≤ $[B]_{tot}$ ≤ 0.16 M).*

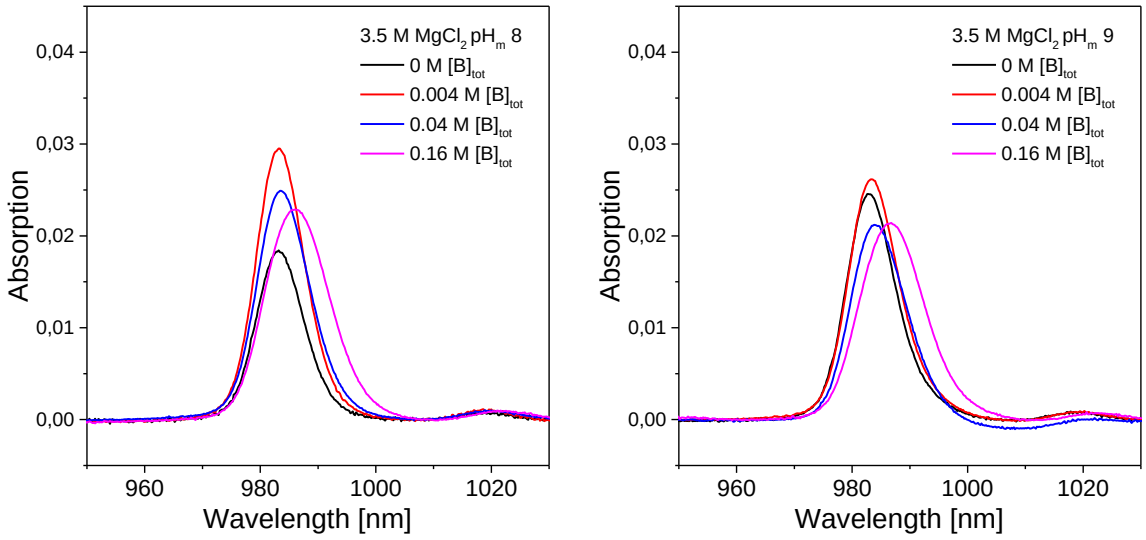

Figure 7.10 *.UV-Vis/NIR absorption spectra of Np(V) in 3.5 M $MgCl_2$ solutions at pH_m 8-9 in the presence of borate (0 M ≤ $[B]_{tot}$ ≤ 0.16 M).*

Based on the UV-Vis/NIR results, the formation of at least one Np(V)–borate complex has to be considered for $MgCl_2$ solutions with $[B]_{tot} \geq 0.04$ M and $pH_m = 8 - 9$. In order to quantify the concentration / fraction of the Np(V)–borate aqueous species, the NpO_2^+ absorption band was

subtracted from the spectra measured in the presence of borate. The deconvoluted spectra of the samples at pH_m = 8 with $[B]_{tot}$ = 0.04 M and 0.16 M are shown in Fig. 7.11. The figure clearly shows the contributions of NpO_2^+ and Np(V)–borate complex at λ = 980 nm and ~ 985 nm, respectively.

Based on the known Np(V) concentrations, the extinction coefficient (ε) of the Np(V)–borate species was quantified as ~ 400 L mol^{-1} cm^{-1}, and the ratio NpO_2^+:Np(V)–borate was calculated as summarized in Table 7.3. As discussed above, the formation of a second Np(V)–borate species takes place at pH_m = 9 and high $[B]_{tot}$. The quantitative determination of the concentration of this second species was not possible due its minor contribution to the overall signal and to the limited number of spectra available at high $[B]_{tot}$.

Note that no quantitative data was obtained in 3.5 M $MgCl_2$ solutions due to the unknown amount of additional Np(V)–Cl complexes present in solution. Experimental solubility studies with Np(V) in concentrated $MgCl_2$ solutions are currently on-going at KIT–INE with the aim of deriving the corresponding thermodynamic and activity models. Although the formation of binary Np(V)–Cl species have been already reported in the literature, the possible formation of ternary Mg–Np(V)–Cl species analogous to those described for Np(V) in concentrated $CaCl_2$ systems (Fellhauer, 2013) needs to be evaluated [59].

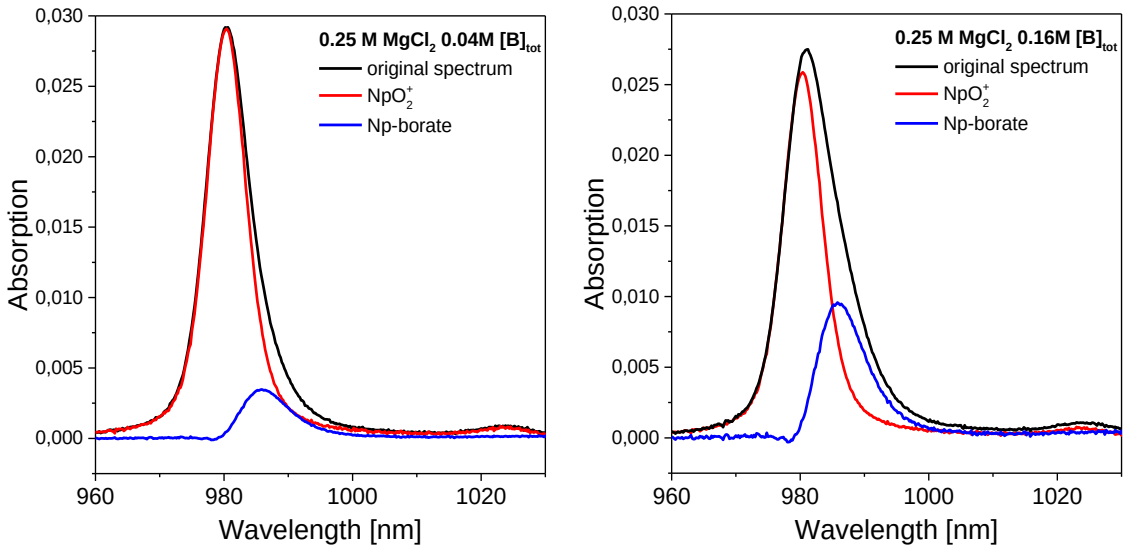

Figure 7.11. *Peak deconvolution of a Np(V) spectrum in 0.25 M $MgCl_2$ at pH_m = 8 with $[B]_{tot}$ = 0.04 M (left) and $[B]_{tot}$ = 0.16 M (right) showing the absorption band of the Np(V)–borate complex at λ ~985 nm separated from the absorption band of NpO_2^+ at 980 nm.*

Table 7.3. *Fraction of NpO_2^+ and Np(V)–borate complex as calculated based on the peak deconvolution of UV–Vis/NIR spectra collected in 0.25 M $MgCl_2$ solutions at pH_m = 8 and 9 with 0.004 M ≤ $[B]_{tot}$ ≤ 0.16 M.*

Matrix	$[B]_{tot}$	pH_m	NpO_2^+	Np(V)–borate
0.25 M $MgCl_2$	0.004 M	8	99 %	1 %
0.25 M $MgCl_2$	0.04 M	8	88 %	12 %
0.25 M $MgCl_2$	0.16 M	8	69 %	31 %
0.25 M $MgCl_2$	0.004 M	9	84 %	16 %
0.25 M $MgCl_2$	0.04 M	9	73 %	27 %
0.25 M $MgCl_2$	0.16 M	9	36 %	64 %

As already discussed in previous sections of this PhD thesis, the speciation of boron is highly complex. Several borate species, whose concentration is strongly dependent on pH_m, $[B]_{tot}$, type and concentration of background electrolyte, could behave as possible complexing ligands. In order to determine the most likely borate ligand in the Np(V)–borate system, the estimated [Np-borate]/[NpO_2^+] ratio was plotted against the concentrations of the different possible borate species $B(OH)_4^-$, $B_3O_3(OH)_4^-$ and $B_4O_5(OH)_4^-$, as calculated with the Pitzer model reported by Felmy et al. [81] and described in chapter 3 and 9. As suggested by Schott and co-workers [83] for the systems Eu(III)-borate, a correlation with the contributions of all polyborate species was also evaluated. Only considering $B(OH)_4^-$ as complexing ligand a linear correlation with a suitable slope (slope ~1) could be achieved (see Fig. 7.12). Although the complex formation between actinides and polyborates has been suggested previously [83], the monomer $B(OH)_4^-$ has the highest Lewis base character compared to the bigger polyborate anions (with larger delocalization of the charge) and therefore appears as reasonable candidate for the complexation with Np(V). Based on this hypothesis, the complexation of Np(V) with borate can be described as:

$$NpO_2^+ + B(OH)_4^- \rightleftharpoons NpO_2[B(OH)_4](aq) \quad (7.1)$$

with

$$\log {}^*\beta_{(1,1)} = \log [NpO_2[B(OH)_4](aq)] - \log [NpO_2^+] - \log [B(OH)_4] \quad (7.2)$$

With equation 7.2 a correlation between the logarithmic concentration ratios of the Np(V) species and the concentration of $B(OH)_4^-$ with the y-intercept log $*\beta_{(1,1)}$ can be formulated:

$$log\frac{[NpO_2[B(OH)_4]]}{[NpO_2^+][B(OH)_4^-]} = log *\beta_{(1,1)} + log[B(OH)_4] \quad (7.3)$$

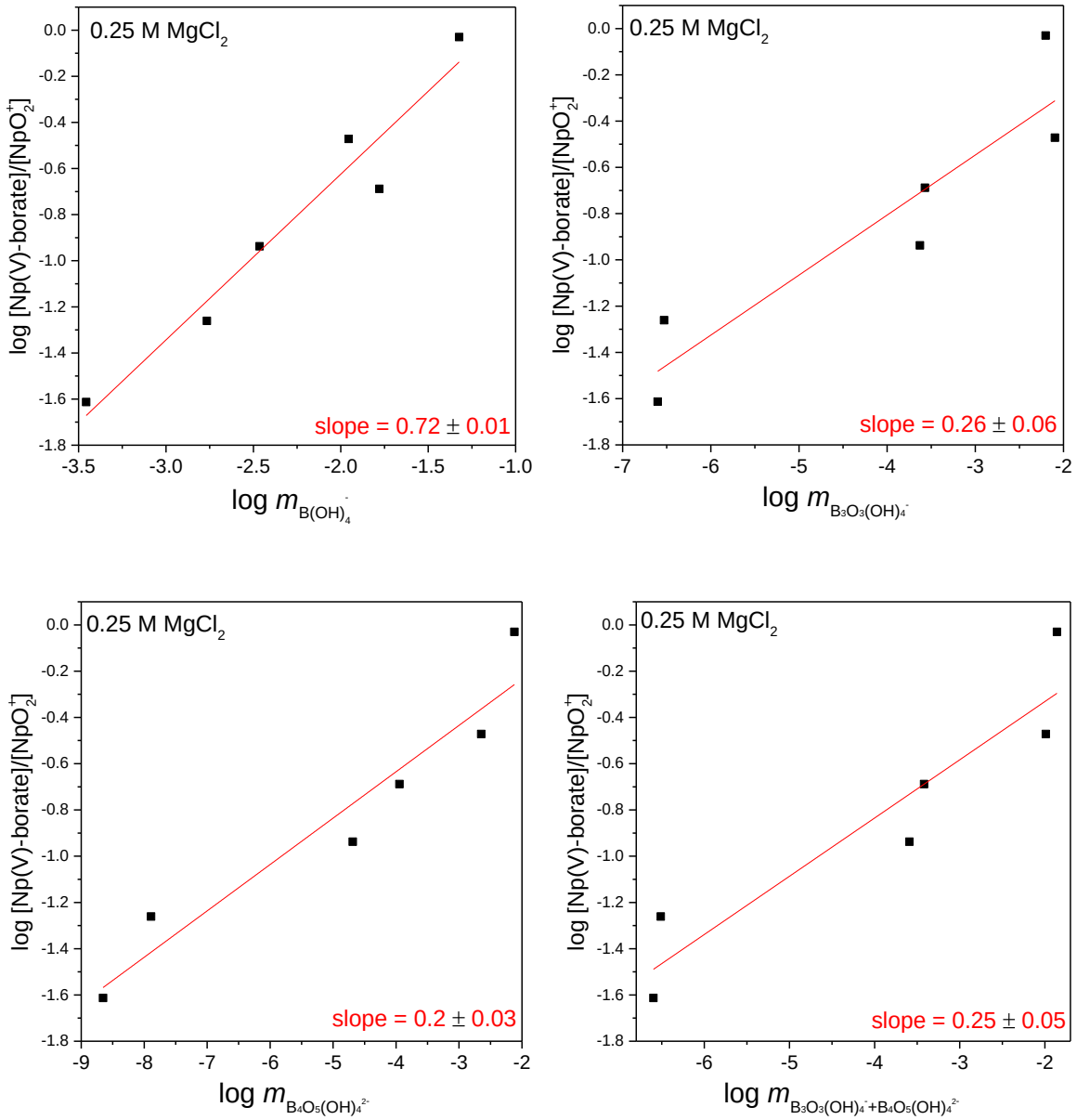

Figure 7.12. *Linear correlation of the spectroscopically determined log (Np(V)–borate] / $[NpO_2^+]$) ratio with log $[B(OH)_4^-]$ in 0.25 M $MgCl_2$ solution. For comparison the correlations of the spectroscopically determined log ($[Np(V)–borate]/[NpO_2^+]$) ratio with log $[B_3O_3(OH)_4^-]$, log $[B_4O_5(OH)_4^{2-}]$ and log $[B_3O_3(OH)_4^- + B_4O_5(OH)_4^{2-}]$ together with the fitted slopes are shown.*

According to equation 7.3, a slope of ~ 1 is expected for the plot of log ([$NpO_2[B(OH)_4](aq)$] / [NpO_2^+]) *vs.* log [$B(OH)_4^-$]. The slope of 0.72 obtained in Fig. 7.12 does not allow a reliable estimation of log $*\beta_{(1,1)}$ for the investigated Np(V)–borate system. Note that a key point in this linear correlation is the $[B(OH)_4^-]_{free}$, which in the present work was calculated with the thermodynamic and activity models reported by Felmy and co-workers [81]. Hence, uncertainties affecting the borate speciation in this model will lead to deviations in the linear plot (and consequently in the slope) shown in Fig. 7.12.

7.2 Conclusions

Solubility studies with $NpO_2OH(am)$ combined with accurate solid phase characterization and UV-Vis/NIR investigations confirm that the presence of borate strongly affects both the aqueous and solid speciation of Np(V)) in dilute to concentrated NaCl and $MgCl_2$ solutions at pH_m = 8 and 9 and $[B]_{tot} \geq 0.04$ M. UV–Vis/NIR investigations confirm the formation of at least one Np(V)–borate complex in $MgCl_2$ solutions. A much weaker interaction is observed in concentrated $MgCl_2$ solutions, as a result of the competition between Mg^{2+} and NpO_2^+ for borate complexation. The evaluation of the spectroscopic data collected suggests $B(OH)_4^-$ as most probable complexing borate species in the aqueous phase, although the exact stoichiometry of the complexation reaction and the determination of a formation constant was not feasible in this work. A similar trend in borate complexation was observed for Cm(III) in NaCl, $CaCl_2$ and $MgCl_2$ solutions with comparable $[B]_{tot}$ using TRLFS (see chapter 4).

In spite of the clear formation of Np(V)–borate aqueous species in solution at moderate pH_m, no significant increase in the solubility of NpO_2OH(am, fresh) is observed in the presence of $[B]_{tot} \leq 0.4$ M. On the contrary and similarly to Nd(III), a clear drop in the Np(V) solubility occurs in borate-bearing NaCl and $MgCl_2$ solutions with $pH_m \leq 9$. The drop in solubility is accompanied by a visible change of the initial solid (from green to white-gray), confirming the formation of a new solid phase. The formation of this previously unreported Np(V)–borate solid phase is further confirmed by XRD, XPS, SEM–EDS and EXAFS analysis. This solid phase transformation constitutes a previously unreported retention mechanism for the highly mobile Np(V). A first thermodynamic description and model of the Np(V) interactions in the presence of borate in NaCl and $MgCl_2$ systems is proposed in chapter 9.

8 Solubility of U(VI) in the presence of borate

The solubility of U(VI) was studied from undersaturation conditions in the presence of $0\ M \leq [B]_{tot} \leq 0.16\ M$ with $4.5 \leq pH_m \leq 9.3$ in 0.1 M and 5.0 M NaCl and 0.25 and 3.5 M $MgCl_2$ solutions. Samples in 0.1 M and 5.0 M NaCl systems with $pH_m \geq 7.5$ were prepared with $Na_2U_2O_7 \cdot H_2O(cr)$ as initial solid phase. In all samples in 0.25 and 3.5 M $MgCl_2$ systems and in 0.1 M and 5.0 M NaCl systems with $pH_m < 7.5$ freshly prepared meta-schoepite $UO_3 \cdot 2H_2O(cr)$ was added as initial solid phase. For comparison purposes, samples with U(VI) in the same pH_m and ionic strength conditions but without borate were prepared and measured following the same experimental approach. The U(VI) concentration was regularly quantified in combination with the measurement of pH_m for up to 380 days. Solid samples from selected solubility experiments were characterized by XRD after attaining equilibrium conditions.

8.1 Solubility of U(VI) in NaCl and $MgCl_2$ solutions

The solubility of U(VI) in 0.1 M, 5.0 M NaCl, 0.25 M $MgCl_2$ and 3.5 M $MgCl_2$ solutions with $0\ M \leq [B]_{tot} \leq 0.16\ M$ is shown in Fig. 8.1 and Fig. 8.2. The figures also show the solubility of $UO_3 \cdot 2H_2O(cr)$ and $Na_2U_2O_7 \cdot H_2O(cr)$ in NaCl and $MgCl_2$ solutions as calculated using the thermodynamic and (SIT) activity models reported elsewhere [53].

No effect of borate on the solubility of U(VI) is observed in dilute to concentrated NaCl solutions at $pH_m \leq 6.5$ (solubility control by $UO_3 \cdot 2H_2O(cr)$). The weak complexation capacity of borate is not sufficient to outcompete the cationic hydrolysis species of U(VI) prevailing in this pH region. Note also that in this pH_m region the non-complexing $B(OH)_3(aq)$ species is dominating the aqueous chemistry of boron. These data are also in excellent agreement with the solubility of $UO_3 \cdot 2H_2O(cr)$ as calculated in the absence of borate. In 0.1 M and 5.0 M NaCl solutions at $pH_m \geq 7.5$, a solubility increase with increasing $[B]_{tot}$ is observed. This effect is more pronounced in 5.0 M NaCl solution with an increase in U(VI) solubility of about 1.5 orders of magnitude, rather than in 0.1 M NaCl solution where a slight increase of ~ ½ order of magnitude is seen. This solubility increase unequivocally hints towards the formation of U(VI)–borate aqueous complexes within the pH-range 7.5–9. Lucchini et al. investigated the solubility of U(VI) in a synthetic brine solution (2.2-4.2 M NaCl and ~ 0.01 M $[B]_{tot}$) and found no effect of borate on the U(V) solubility at pH_m ~8.9 but the used $[B]_{tot}$ are significantly lower compared to the present experiments [157].

In contrast to the observations made for Nd(III) and Np(V), no decrease in the solubility of U(VI) is observed in NaCl solutions within the timeframe of the experiment (380 days). Hence, in spite of the observed U(VI)–borate interaction in the aqueous phase, such interaction did not progress further

towards the formation of a secondary U(VI)–borate solid phase. It is worth mentioning that [U(VI)] in equilibrium with $Na_2U_2O_7 \cdot H_2O$(cr) at pH_m = 7.5 is significantly lower than the solubility-limit set by $Nd(OH)_3$(am) and NpO_2OH(am), and thus that the solubility product of a potentially-forming U(VI)–borate solid phase is not exceeded. Although not evaluated in the present work, the formation of a U(VI)–borate solid phase at pH_m ≈9 and absence of Na^+ ($I \rightarrow 0$) cannot be completely ruled out. In these conditions, $UO_3 \cdot 2H_2O$(cr) allows significantly higher [U(VI)] in solution compared to $Na_2U_2O_7 \cdot H_2O$(cr) (1 to 2 log-units difference, see dashed lines in Fig. 8.1), which may lead to the formation of a secondary U(VI)–borate solid phase.

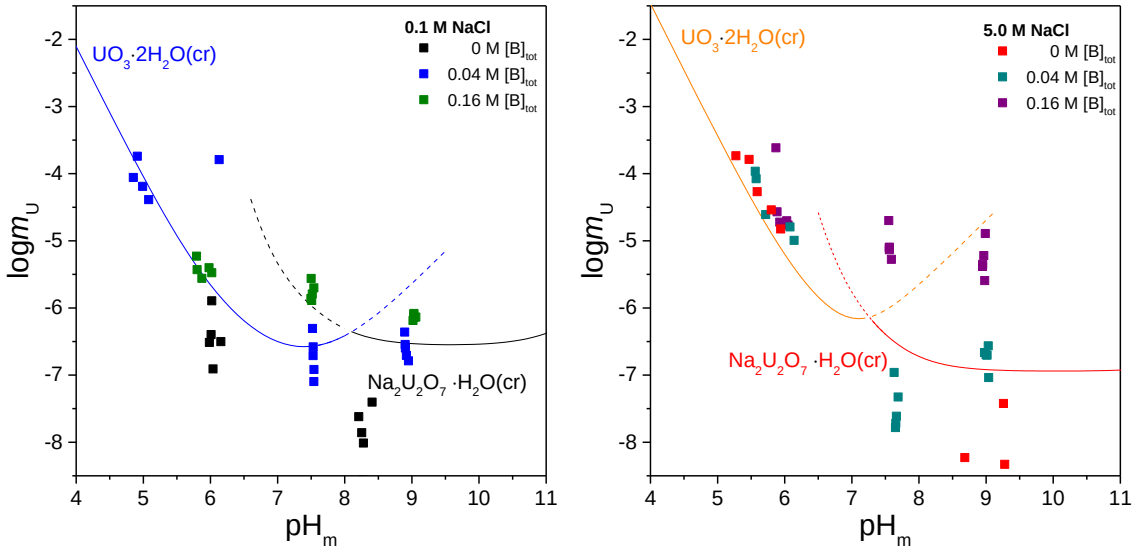

Figure 8.1. *Solubility of $UO_3 \cdot 2H_2O$(cr) and $Na_2U_2O_7 \cdot H_2O$ (cr) in the presence of 0 M ≤ $[B]_{tot}$ ≤ 0.16 M in 0.1 M and 5.0 M NaCl solutions. Comparison with calculated solubility of $UO_3 \cdot 2H_2O$(cr) (blue line) and $Na_2U_2O_7 \cdot H_2O$ (cr) (black line) in the absence of borate as reported in Altmaier et al. [53].*

A weaker effect of borate (compared to the NaCl system) on the U(VI) solubility can be observed for dilute to concentrated $MgCl_2$ systems. This effect is especially visible at pH_m = 7.5 and $[B]_{tot}$ = 0.16 M. As already observed in the Np(V) solubility studies, actinide borate interactions in $MgCl_2$ solutions are less pronounced than in NaCl solutions at comparable pH_m and ionic strength conditions. This effect is likely caused by a changed boron speciation in $MgCl_2$ media due to an interaction of Mg^{2+} with borate species in solution. This effect was also hinted in ^{11}B-NMR experiments (see chapter 3).

In $MgCl_2$ systems, the solubility data in the borate-free systems is partly scattered and lower than the expected solubility reported in the literature [53]. The lower solubility is likely caused by differences in the crystallinity and particle size of the initial solid phase controlling the solubility of U(VI).

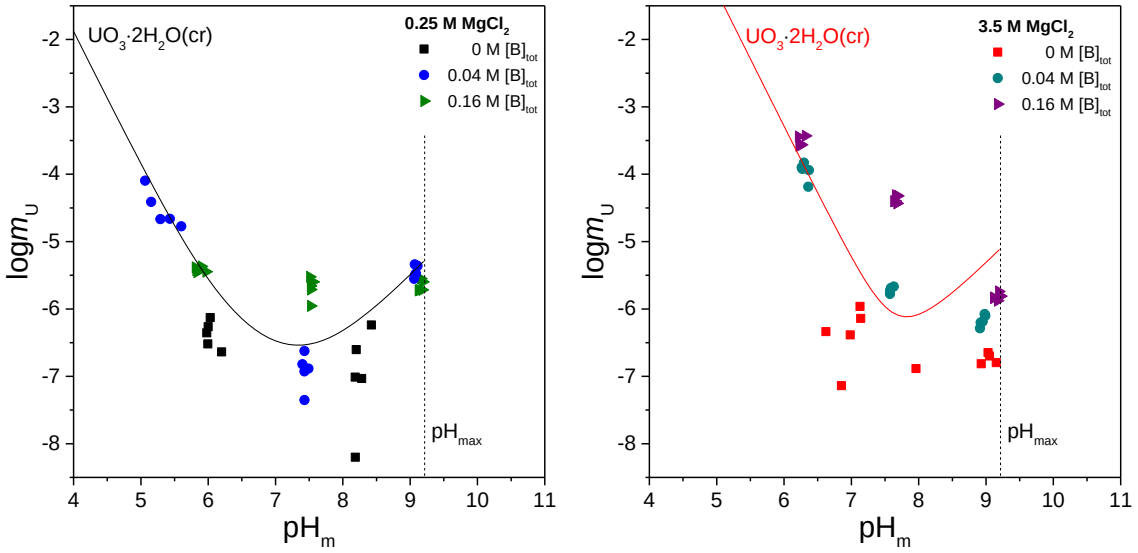

Figure 8.2. *Solubility of $UO_3{\cdot}2H_2O$(cr) in the presence of 0 M ≤ [B]$_{tot}$ ≤ 0.16 M in 0.25 M and 3.5 M $MgCl_2$ solutions. Comparison with calculated solubility of $UO_3{\cdot}2H_2O$(cr) in the absence of borate (solid line) as reported in Altmaier et al. [53].*

8.2 Solid phase characterization

XRD diffractograms obtained for selected solid phases are shown in Fig. 8.3. In all cases the measured patterns agree very well with those reported for $UO_3{\cdot}2H_2O$ (cr) JCPDF file No: 43-0364 [137] and $Na_2U_2O_7{\cdot}H_2O$(cr) [53], indicating that the bulk U(VI) controlling solid phase in all investigated samples is not affected by the presence of borate. Chernorukov et al. prepared several solid uranoborates with Na^+ and Mg^{2+} and investigated their stability [88-91, 93, 94]. Since high temperatures (T ≥ 870°C) are needed to synthesize these solid phases, it is very unlikely that similar uranoborates are forming under the investigated conditions.

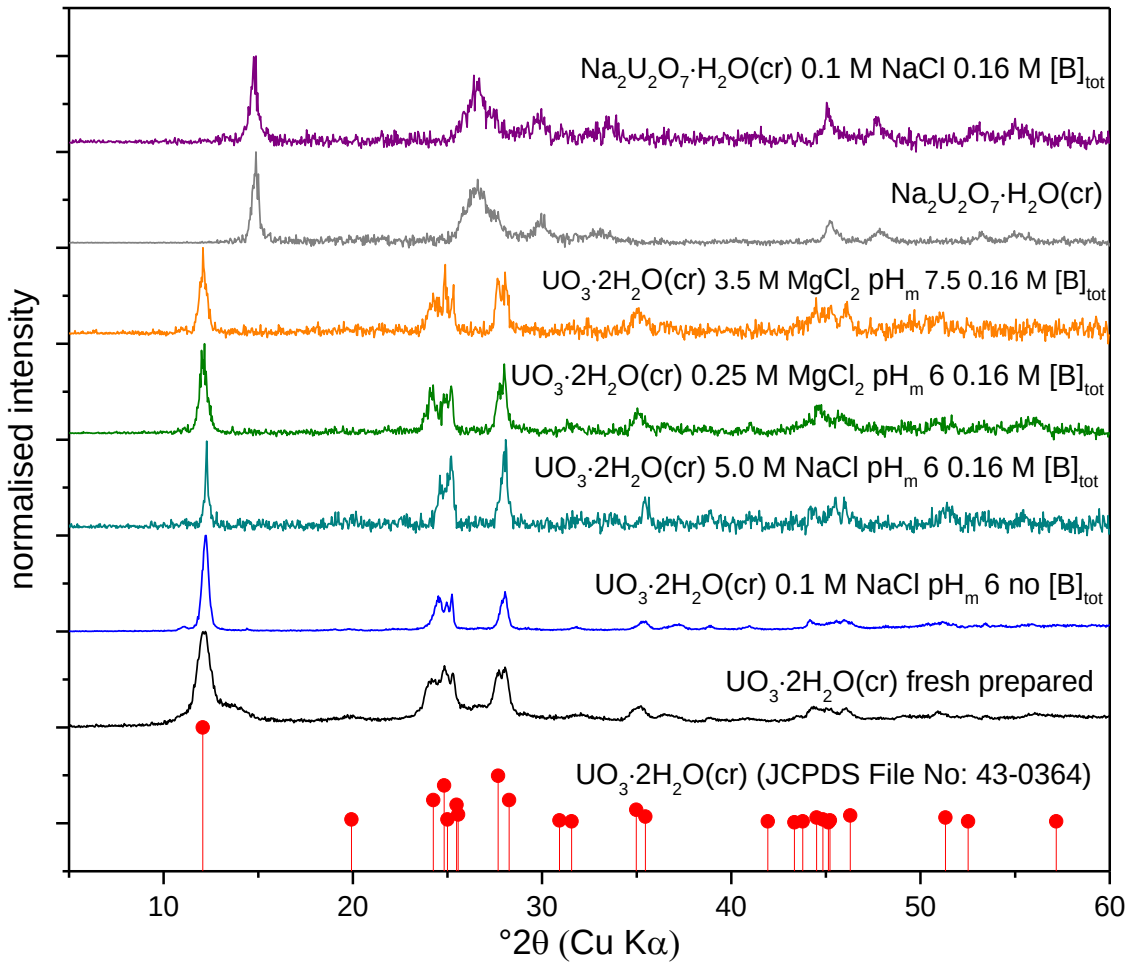

Figure 8.3. *XRD pattern of freshly prepared initial $UO_3{\cdot}2H_2O$(cr), $UO_3{\cdot}2H_2O$(cr) reference [137] and $UO_3{\cdot}2H_2O$(cr) alteration phases from solubility experiments in NaCl and $MgCl_2$ systems with 0 M ≤ $[B]_{tot}$ ≤ 0.16 M at pH_m 6–7.5 and initial $Na_2U_2O_2{\cdot}H_2O$ (cr) and $Na_2U_2O_2{\cdot}H_2O$ (cr) alteration phases from solubility experiment in 0.1 M NaCl and $[B]_{tot}$ = 0.16 M.*

8.3 Conclusions

Experimental data from U(VI) solubility studies in the presence of borate showed an increase in U(VI) solubility in NaCl systems at $7.5 \leq pH_m \leq 9$ for $[B]_{tot} \geq 0.04$ M likely caused by the formation of aqueous U(VI)-borate complexes. A weaker effect of borate is observed in dilute to concentrated $MgCl_2$ solutions, where a slight solubility increase at pH_m = 7.5 and $[B]_{tot}$ = 0.16 M can be seen. No drop in U(VI) solubility caused by the transformation of the initial solid phase as observed in Nd(III) (see chapter 4) and Np(V) systems (see chapter 7) is found in NaCl and $MgCl_2$ solutions under the investigated conditions. This behavior is likely related with the very low uranium concentration imposed by $Na_2U_2O_7{\cdot}H_2O$(cr) as solubility controlling-phase in NaCl media under weakly alkaline

conditions, although it could also be due to slow kinetics. In very dilute systems (absence of Na^+), the higher uranium concentrations under weakly alkaline conditions set by $UO_3 \cdot 2H_2O$(cr) may lead to the formation of secondary U(VI)–borate solid phases. The observations collected in this work allow neither confirming nor rejecting the latter hypothesis, and thus provide room for additional studies.

9 Chemical and thermodynamic model

Experimental solubility data and speciation information described in chapters 4 and 7 are jointly evaluated in the following with the aim of deriving comprehensive chemical, thermodynamic and (SIT) activity models for Nd(III)/Cm(III) and Np(V). The thermodynamic and activity models reported in Felmy and Weare for the system Na–K–Ca–Mg–H–CI–SO_4–CO_2–$B(OH)_4$–H_2O have been used to calculate the speciation of borate in dilute to concentrated NaCl and $MgCl_2$ solutions [81]. The Pitzer approach is used in the latter publication to calculate activity coefficients, and thus these have been converted to the SIT formulism using the approach described elsewhere [158]. A short description of the borate model derived by Felmy and Weare is provided in the following section.

9.1 Chemical and thermodynamic models reported by Felmy and Weare (1986)

Felmy and Weare derived thermodynamic and Pitzer activity models for the system Na–K–Ca–Mg–H–CI–SO_4–CO_2–$B(OH)_4$–H_2O at 25°C based on previous experimental studies by Ingri et al., among others [69, 70]. The authors coupled their model to the previously reported thermodynamic and Pitzer activity models by Harvie et al. describing the system Na–K–Ca–Mg–H–CI–SO_4–CO_2–H_2O at 25°C, and included the proposed borate aqueous species and solid compounds [159]. Stability constants for the different borate species were evaluated from various studies on aqueous borate chemistry, including solubility, emf and isopiestic studies performed under a large variety of experimental conditions [69, 70, 160]. The stability constants for the different borate species and the estimated activity coefficients by the authors are summarized in Tables 9.1, 9.2 and 9.3.

Table 9.1. *Borate equilibria selected in the chemical and thermodynamic model reported by Felmy and Weare (1986).*

Reactions	**$\Delta_r G°_m$ (kJ/mol)**	**log K°**
$B(OH)_3(aq) + H_2O \leftrightharpoons B(OH)_4^- + H^+$	52.74	-9.24
$B(OH)_3(aq) + Mg^{2+} + H_2O \leftrightharpoons MgB(OH)_4^+ + H^+$	44.75	-7.84
$3\ B(OH)_3(aq) \leftrightharpoons B_3O_3(OH)_4^- + 2H_2O + H^+$	42.97	-7.53
$4\ B(OH)_3(aq) \leftrightharpoons B_4O_5(OH)_4^{2-} + 3H_2O + 2H^+$	92.09	-16.13

Table 9.2. *Cation-anion interaction parameters estimated by Felmy and Weare for aqueous borate species.*

Cation	Anion	$\beta^{(0)}$	$\beta^{(1)}$	$C^{(\phi)}$
Na^+	$B(OH)_4^-$	-0.0427	0.089	0.0114
Na^+	$B_3O_3(OH)_4^-$	-0.056	0.91	-
Na^+	$B_4O_5(OH)_4^{2-}$	-0.11	-0.4	-
$MgB(OH)_4^+$	Cl^-	0.16	-	-
$CaB(OH)_4^+$	Cl^-	0.12	-	-

Table 9.3. *Anion-anion interaction parameters estimated by Felmy and Weare for aqueous borate species.*

Anion	Anion	Θ	ψ_{Na+}
$B(OH)_4^-$	Cl^-	-0.065	-0.0073
$B_3O_3(OH)_4^-$	Cl^-	0.12	-0.024
$B_4O_5(OH)_4^{2-}$	Cl^-	0.074	0.026

The Pitzer ion interaction parameters estimated by Felmy and Weare are converted to the SIT formulism as described in [161, 162], and are summarized in Table 9.4. The SIT ion interaction coefficient for the ion pair $B(OH)_4^-/Mg^{2+}$ was estimated based on charge analogies, as described in [163]. All ion interaction coefficients ε_{ij} used in the thermodynamic calculations are shown in Table 9.4. No ion interaction coefficients for the ion pairs $B_3O_3(OH)_4^-/Mg^{2+}$ and $B_4O_5(OH)_4^{2-}/Mg^{2+}$ were used in the calculations.

Table 9.4. *SIT ion interaction coefficients used in the model calculations.*

Species i	j	ε_{ij}	Reference
H^+	Cl^-	0.12	[22]
Na^+	Cl^-	0.03	[22]
Mg^{2+}	Cl^-	0.19	[22]
$B(OH)_4^-$	Na^+	-0.07	[81]
$B(OH)_4^-$	Mg^{2+}	0.15	Charge analogy
$B_3O_3(OH)_4^-$	Na^+	-0.08	[81]
$B_4O_5(OH)_4^{2-}$	Na^+	-0.23	[81]
$MgB(OH)_4^+$	Cl^-	0.05	[81]

9.2 Chemical, thermodynamic and activity models derived in this work for Ln/An(III) and Np(V) borate interactions

In order to derive correct thermodynamic data it is essential to refer to a complete and correct chemical model. Only if there is an unambiguous model for the relevant chemical equilibrium reactions controlling an aqueous system established, it is possible to explicitly quantify these processes within the concepts of equilibrium thermodynamics. In this chapter, a first preliminary thermodynamic description is proposed for the assessment of Ln/An(III) and Np(V) borate interactions. Note that following the discussions in previous chapters of this work there still are significant uncertainties related to key aspects which are required to allow for a comprehensive thermodynamic treatment. For instance, uncertainties related to borate speciation, the composition of aqueous actinide–borate complexes, the stability and exact composition of solubility limiting solid phases, or overall kinetic effects remain to be considered. In spite of these shortcomings which preclude a final thermodynamic description, the present PhD study nevertheless tries to explore to which extend preliminary thermodynamic data and models can be derived, based upon the new experimental evidence derived in this work. It is to note that in view of the several assumptions required in this process, the proposed chemical and thermodynamic models can serve only as a first starting point and rough thermodynamic

estimation of an-borate interactions in waste disposal scenarios. It will be required to verify and most likely improve these models and data in future studies.

In the following, a thermodynamic description for the systems Ln(III)/Cm(III)–Na–Mg–H–Cl–H_2O and Np(V)–Na–Mg–H–Cl–H_2O is developed based on the experimental solubility data, solid phase characterization and aqueous speciation data gained in this work. Note that a more accurate picture is obtained for Np(V), due to the appropriate knowledge of the Np(V)–borate solid phase stoichiometry and the simplified hydrolysis and consequent interpretation of the aqueous chemistry in the presence of borate. A much incomplete insight is achieved for Ln/An(III) because of the limited information on the stoichiometry of the solid phases and a more complex aqueous chemistry, both in the absence and presence of borate.

The SIT approach has been used in this work to account for ion interaction processes. The decision to use the SIT approach is based upon the need to estimate model parameter for ion-interaction processes based on a limited number of experimental data (log $^*K'_s$). The number of parameters to be fitted in the thermodynamic modelling with Pitzer is significantly larger than for SIT, and thus consequently larger data sets are required. The thermodynamic model reported by Felmy and Weare (1986) is used in the present study to describe the aqueous borate speciation in dilute to concentrated NaCl and $MgCl_2$ solutions.

9.2.1 Thermodynamic description of the Np(V)–borate system

The experimental data obtained in solubility studies with Np(V) in NaCl and $MgCl_2$ solutions with $[B]_{tot}$ = 0.16 M (chapter 7) showed a significant decrease of the Np(V) concentration at $pH_m \leq 9$ in NaCl and dilute $MgCl_2$ solutions. Solid phase characterization by XPS, XRD, SEM–EDS and EXAFS clearly confirmed the transformation of the initial solid NpO_2OH(am,fresh) to a hitherto unknown borate bearing Np(V) solid phase. Note that strong kinetics were observed in all the cases. This has relevant implications in the process of deriving the chemical and thermodynamic models, and only those samples with longer equilibration times have been considered in the thermodynamic interpretation of this system. These are properly marked in the corresponding figures and accordingly discussed in the text.

XPS and EXAFS analyses confirmed that the most crystalline Np(V)-borate solid phase formed in dilute NaCl solutions (see section 7.1.1). Kinetics of solid phase transformation in 5.0 M NaCl were faster, and resulted in a significantly amorphous solid phase, which is expectedly more soluble than such obtained in 0.1 M NaCl. No accurate data on the stoichiometry of the Np(V)–borate solid phase forming in 5.0 M NaCl was obtained by XPS or SEM–EDS, and thus these data have been disregarded in the thermodynamic interpretation. Regarding $MgCl_2$ systems, a solid phase transformation was only observed in dilute solutions. As discussed in chapter 3, a strong interaction of aqueous borate species

and Mg^{2+} takes place in concentrated $MgCl_2$ solutions according to the model of Felmy et al., potentially outcompeting the interaction of borate with actinides. Based on the experimental evidences collected in this work, stoichiometries of the Np(V)–borate solid phases forming in dilute NaCl and $MgCl_2$ solutions are considered as $NpO_2[B_5O_6(OH)_4]\cdot 2NaOH(cr)$ and $(NpO_2)_2[B_5O_6(OH)_4]_2\cdot 3Mg(OH)_2(cr)$, respectively.

UV–Vis/NIR spectroscopy confirmed the formation of a Np(V)–borate complex in $MgCl_2$ solutions with $[B]_{tot} \geq 0.04$ M and $pH_m = 8–9$ .The $[NpO_2^+]$ and [Np(V)–borate] could be determined based on the peak deconvolution of the UV–Vis/NIR spectra. The knowledge of $[NpO_2^+]_{free}$ is of great importance in the determination of the log $*K°_{s,0}$ of the Np(V)–borate solid phases formed in this system. Since no UV–Vis/NIR spectra were collected in 0.1 M NaCl solutions, it is assumed that the same aqueous speciation as for dilute $MgCl_2$ systems is retained.

Evaluation of the UV–Vis/NIR spectra collected in 0.25 M $MgCl_2$ pointed to $B(OH)_4^-$ as the most likely ligand complexing NpO_2^+ in solution. Unfortunately, no accurate stability constant for the formation of the $NpO_2B(OH)_4(aq)$ complex could be determined from the spectroscopic data due to inconsistencies with the slope of log ([Np(V)–borate] / $[NpO_2^+]$) *vs.* log $[B(OH)_4^-]$. In spite of this and as a qualitative exercise, an estimate of log $*\beta°_{(1,1)}$ for the complex $NpO_2B(OH)_4(aq)$ has been calculated, and its impact on the solubility of Np(V) evaluated in a second iteration process.

The assumptions made in the development of the thermodynamic and activity models are hence summarized in the following:

- Not all the solubility data collected for the Np(V) system were in thermodynamic equilibrium. Only those experiments with longer equilibration times have been considered for the calculation of log $*K°_{s,0}$.
- The stoichiometries quantified by XPS and SEM–EDS for the Np(V)–borate solid phases ($NpO_2[B_5O_6(OH)_4]\cdot 2NaOH(cr)$ and $(NpO_2)_2[B_5O_6(OH)_4]_2\cdot 3Mg(OH)_2(cr)$) are representative of the complete pH-range evaluated in this study.
- The Np(V)–borate solid phase controlling the solubility in concentrated NaCl solutions (within the timeframe of this study) is of amorphous nature and thus holds greater solubilities than the crystalline counterpart forming in dilute systems.
- The Np(V)–borate aqueous speciation in dilute NaCl and $MgCl_2$ systems is the same. Hence, $[NpO_2^+]_{free}$ experimentally determined for dilute $MgCl_2$ systems has been also considered in the determination of log $*K°_{s,0}$ in dilute NaCl systems.
- Only one aqueous Np(V)-borate complex forms, with the stoichiometry $NpO_2B(OH)_4(aq)$.

The steps followed in the development of the thermodynamic and activity model are:

- Chemical model is taken from the inputs by XPS and SEM–EDS (Np(V)–borate solid phase) and UV–Vis/NIR (Np(V)–borate aqueous species), in combination with the speciation model of Np(V) in the absence of borate selected in the NEA–TDB.
- Based on the chemical model derived and on the solubility data under equilibrium conditions, determination of log $*K'_{s,0}$ for the ternary Na/Mg–Np(V)–borate solid phases forming in dilute NaCl and $MgCl_2$ systems. Quantification based on $[NpO_2^+]_{free}$ determined experimentally, without specifically accounting for the complex $NpO_2B(OH)_4(aq)$.
- Extrapolation of log $*K'_{s,0}$ to $I = 0$ using the SIT ion interaction coefficients described in section 9.1.
- Comparison of calculated solubility of Na/Mg–Np(V)–borate solid phases with available experimental data. Assessment of the role of Np(V)–borate aqueous complex, using an estimated value of log $*\beta^\circ_{(1,1)}$ for the complex $NpO_2B(OH)_4(aq)$.

Based on the assumptions summarized above, the solubility of Np(V) in dilute NaCl solutions can be described as:

$$NpO_2[B_5O_6(OH)_4]\cdot 2\,NaOH(cr) + 8\,H_2O \rightleftharpoons NpO_2^+ + 5\,B(OH)_4^- + 2\,Na^+ + 2\,H^+ \quad (9.1)$$

with

$$log*K'_{(s,0)} = log[NpO_2^+] + 5\,log[B(OH)_4^-] + 2\,log[Na^+] + 2\,log[H^+] \quad (9.1a)$$

$$log*K^\circ_{(s,0)} = log*K'_{(s,0)} + log\ \gamma_{NpO_2^+} + 5\,log\ \gamma_{B(OH)_4^-} + 2\,log\ \gamma_{Na^+} + 2\,log\ \gamma_{H^+} - 8\ log\ a_w \quad (9.1b)$$

Analogously, the solubility of Np(V) in dilute $MgCl_2$ solutions can be described as:

$$\tfrac{1}{2}(NpO_2)_2[B_5O_6(OH)_4]_2\cdot 3\,Mg(OH)_2(cr) + 7\,H_2O \rightleftharpoons NpO_2^+ + 5\,B(OH)_4^- + \tfrac{3}{2}\,Mg^{2+} + H^+ \quad (9.2)$$

with

$$log*K'_{(s,0)} = log[NpO_2^+] + 5\,log[B(OH)_4^-] + \tfrac{3}{2}log[Mg^{2+}] + log[H^+] \quad (9.2a)$$

$$log*K^\circ_{(s,0)} = log*K'_{(s,0)} + log\ \gamma_{NpO_2^+} + 5\,log\ \gamma_{B(OH)_4^-} + \tfrac{3}{2}log\ \gamma_{Mg^{2+}} + log\ \gamma_{H^+} - 7\ log\ a_w \quad (9.2b)$$

The conditional stability constants for reaction 9.1 and 9.2 are determined from experimental solubility data in 0.1 M NaCl and 0.25 M $MgCl_2$ solutions and $[B]_{tot}$ = 0.16 M, respectively. Only data marked with (*) have been assumed to be in thermodynamic equilibrium, and thus have been used for the calculation of log $*K'_{s,0}$. The resulting values are the unweighted average of the considered data. In a final step, the value of log $*K°_{s,0}$ is determined by extrapolating the calculated conditional constants to I = 0 using Eqs 9.1b and 9.2b for NaCl and $MgCl_2$, respectively. The assigned uncertainty accounts for the relevant assumptions made in the development of the thermodynamic model.

Table 9.5. *log $*K°_{s,0}$ values derived in this work for $NpO_2[B_5O_6(OH)_4]\cdot 2NaOH(cr)$ and $(NpO_2)_2[B_5O_6(OH)_4]_2\cdot 3Mg(OH)_2(cr)$ solid phases.*

Reaction	**log $*K°_{s,0}$**
$NpO_2[B_5O_6(OH)_4]\cdot 2\,NaOH(cr) + 8\,H_2O \rightleftharpoons NpO_2^+ + 5\,B(OH)_4^- + 2\,Na^+ + 2\,H^+$	–34.1 ± 0.7
$\frac{1}{2}(NpO_2)_2[B_5O_6(OH)_4]_2\cdot 3\,Mg(OH)_2(cr) + 7\,H_2O \rightleftharpoons NpO_2^+ + 5\,B(OH)_4^- + \frac{3}{2}\,Mg^{2+} + H^+$	–26.0 ± 0.7

The formation of the aqueous complex $NpO_2B(OH)_4(aq)$ can be described as:

$$NpO_2^+ + B(OH)_4^- \rightleftharpoons NpO_2B(OH)_4 \quad (9.3)$$

$$log\beta'_{(1,1)} = log[NpO_2\,B(OH)_4] - log[NpO_2^+] - log[\,B(OH)_4^-] \quad (9.3a)$$

$$log\beta^{\circ}_{(1,1)} = log{*}\beta'_{(1,1)} + log\,\gamma_{NpO_2B(OH)_4} - log\,\gamma_{NpO_2^+} - log\,\gamma_{B(OH)_4^-} \quad (9.3b)$$

In spite of the inconsistencies with the slope of log ([Np(V)–borate] / $[NpO_2^+]$) *vs.* log $[B(OH)_4^-]$, the stability constant for the formation of this complex has been calculated as unweighted average of all the experimental points in Fig. 7.12a. The extrapolation to I = 0 is done based on Eq. 9.3b using the SIT approach, and results in log $\beta°_{(1,1)}$ = 1.6 ± 0.3. The reader should be cautioned that this value should be only considered in scoping calculations, and in the following is used to assess the impact of borate aqueous complexes on the solubility of Np(V). Figs. 9.1 and 9.2 show the calculated solubility of $NpO_2[B_5O_6(OH)_4]\cdot 2NaOH(cr)$ in 0.1 M and 5.0 M NaCl with $[B]_{tot}$ = 0.04 M and 0.16 M, together with experimental data obtained in this work under the same boundary conditions. The measured low Np(V) concentrations at $[B]_{tot}$ = 0.16 M and pH_m = 8 and 8.5 in 0.1 M NaCl are well described by the model. The high Np(V) concentrations measured at pH_m = 9 clearly correspond to metastable conditions; longer equilibration times would be needed to attain thermodynamic equilibrium from

oversaturation conditions. As expected, the Np(V)–borate complexation is very weak and the formation of the estimated Np(V) borate complex $NpO_2B(OH)_4(aq)$ is only slightly affecting the Np(V) solubility at $7.5 \leq pH_m \leq 10$. At lower boron concentrations ($[B]_{tot} = 0.04$ M), the calculated solubility of $NpO_2[B_5O_6(OH)_4]\cdot 2NaOH(cr)$ is higher, but still lies below the solubility of $NpO_2OH(am,fresh)$. It is evident that because of the smaller driving force for the transformation of $NpO_2OH(am,fresh)$ into $NpO_2[B_5O_6(OH)_4]\cdot 2NaOH(cr)$, longer equilibration times are needed.

The calculated solubility of $NpO_2[B_5O_6(OH)_4]\cdot 2NaOH(cr)$ in 5.0 M NaCl and $[B]_{tot} = 0.16$ M is several orders of magnitude lower than the experimentally measured concentration of Np under same conditions. Such discrepancies are clearly explained by the presence of an amorphous Na–Np(V)–borate solid phase. Based on the thermodynamic calculations using the log $*K°_{s,0}$ determined in this work for $NpO_2[B_5O_6(OH)_4]\cdot 2NaOH(cr)$, it can be hypothesized that the Np(V) solubility in concentrated NaCl solutions will further decrease with longer equilibration times due to the transformation of the amorphous solid to the thermodynamically more stable crystalline phase.

The calculated solubility of $(NpO_2)_2[B_5O_6(OH)_4]_2\cdot 3Mg(OH)_2(cr)$ in 0.25 M $MgCl_2$ solution with $[B]_{tot} = 0.04$ M and 0.16 M is shown in Fig. 9.3 in combination with experimental solubility data determined in this work under analogous boundary conditions. As for the 0.1 M NaCl system, the distinct decrease of more than 3 orders of magnitude in the Np(V) solubility at pH_m = 8-9 is well described with the thermodynamic and activity models derived in this work. Note that experimental solubility data at $pH_m = 9.3$ are largely underestimated by the thermodynamic model, basically due to the incomplete solid phase transformation in this sample and consequent solubility control by $NpO_2OH(am,hyd)$. Np(V)–borate complexation has a slight influence on the Np(V) solubility. The effect is greater at $pH_m \sim 9$, in good agreement with the UV–Vis/NIR spectra collected at $pH_m = 8$ and 9. Note that the measured [Np(V)] at $pH_m \sim 8.8$ was still decreasing slowly and probably will reach the calculated level with longer equilibration times. As in the case of dilute NaCl systems, the newly formed Mg–Np(V)–borate solid phase shows significantly greater solubility at lower borate concentrations ($[B]_{tot} = 0.04$ M). Although still below the solubility limit of $NpO_2OH(am,hyd)$, longer equilibration times are needed to achieve a complete solid phase transformation in these experimental conditions. Also, it is definitely necessary to perform larger pH variation in the transformation phases in order to establish a clear pH dependence of solubility.

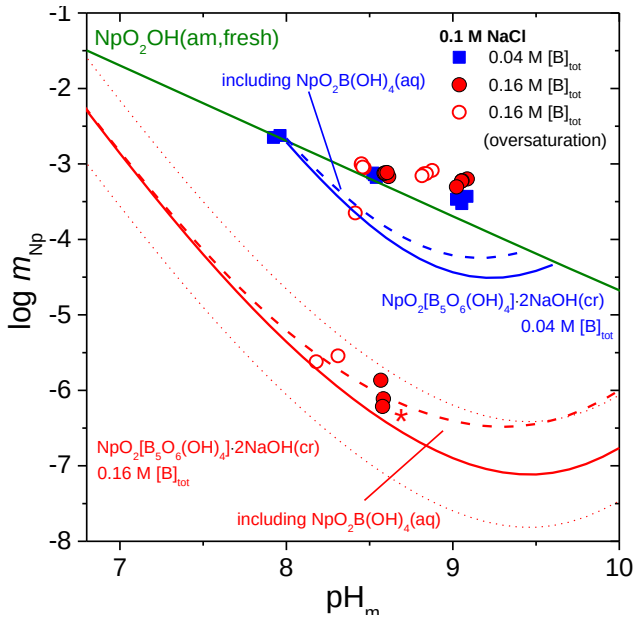

Figure 9.1. *Comparison of experimental solubility data determined in this work for Np(V) in borate-bearing 0.1 M NaCl solutions and model calculations using log *K'$_{s,0}$ values derived in this work for $NpO_2[B_5O_6(OH)_4]\cdot 2NaOH(cr)$. Dotted lines corresponding to the upper and lower solubility limits calculated with the uncertainty assigned to log*K°$_{s,O}$. Solid and dashed lines indicate the calculated solubility in the absence and presence of $NpO_2B(OH)_4(aq)$, respectively.*

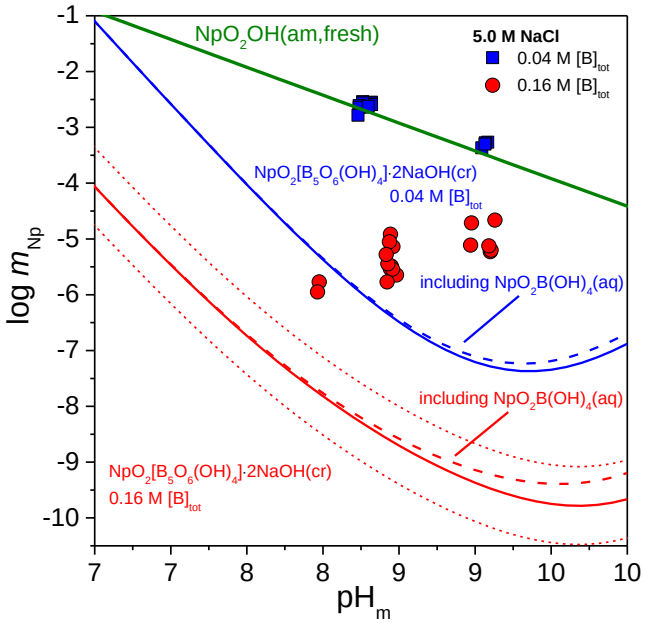

Figure 9.2. *Comparison of experimental solubility data determined in this work for Np(V) in borate-bearing 5.0 M NaCl solutions and model calculations using log *K'$_{s,0}$ values derived in this work for $NpO_2[B_5O_6(OH)_4]\cdot 2NaOH(cr)$. Dotted lines corresponding to the upper and lower solubility limits calculated with the uncertainty assigned to log*K°$_{s,O}$. Solid and dashed lines indicate the calculated solubility in the absence and presence of $NpO_2B(OH)_4(aq)$ in the calculations.*

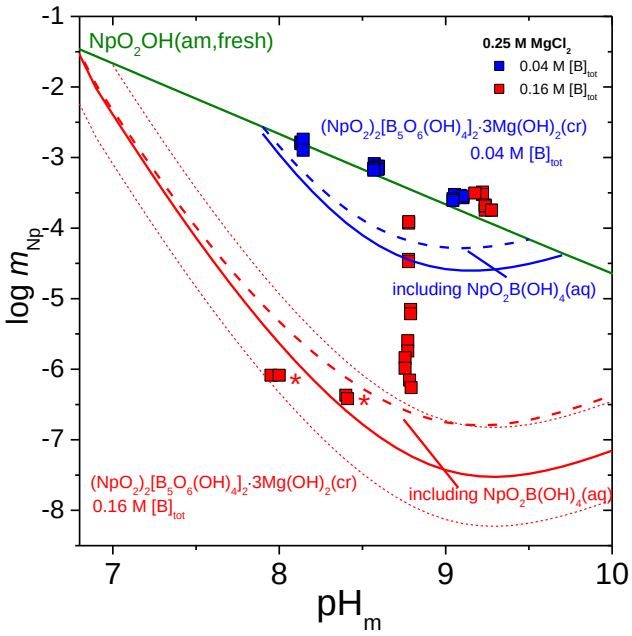

Figure 9.3. *Comparison of experimental solubility data determined in this work for Np(V) in borate-bearing 0.25 M $MgCl_2$ solutions and model calculations using log $*K'_{s,0}$ values derived in this work for $(NpO_2)_2[B_5O_6(OH)_4]_2{\cdot}3Mg(OH)_2$(cr). Dotted lines corresponding to the upper and lower solubility limits calculated with the uncertainty assigned to log$*K°_{s,O}$. Solid and dashed lines indicate the calculated solubility in the absence and presence of $NpO_2B(OH)_4$(aq) in the calculations.*

9.2.2 Thermodynamic description of the Nd(III)–borate system

Solubility studies performed in this work with $Nd(OH)_3$(am) (see chapter 4) showed a distinct drop in the Nd(III) solubility in NaCl and $MgCl_2$ solutions with $[B]_{tot} \geq 0.16$ M. In contrast to similar findings in the Np(V) system, no complete solid phase transformation but rather the formation of a Nd(III)–borate coating on the surface of $Nd(OH)_3$(am) was confirmed by XPS. Based on the outcome of the XPS analyses, the stoichiometry of the Nd(III)–borate solid phase forming in 0.1 M NaCl solutions has been defined as $NaNd[B_3O_4(OH)_3]_2$(am). On the other hand, XPS provided no conclusive results on the stoichiometry of the solid phases forming in $MgCl_2$ systems, and thus the latter have been disregarded in the thermodynamic evaluation carried out in this section.

Similar to observations made for the Np(V)–borate system, the formation of Cm(III)–borate complexes at $pH_m = 8$ in NaCl and $MgCl_2$ systems is confirmed by TRLFS. No quantitative evaluation of the spectra could be performed for the reasons detailed in section 4.3. Similarly to the Np(V) case, the formation of Ln/An(III)–borate complexes has a very minor impact on the overall Nd(III) solubility. In this framework, a complex between Ln/An(III) and $B(OH)_4^-$ has been postulated in

analogy to Np(V). The approach has the same limitations as discussed in the Np(V) case, although Nd(III) shows even a more limited experimental database, higher degree of complexity (because of the hydrolysis of Ln(III)/An(III) within this pH range), and consequently higher uncertainty. A more detailed description is provided below.

The assumptions made in the development of the thermodynamic and activity models are hence summarized in the following:

- The stoichiometry quantified by XPS for the Nd(III)–borate solid phase ($NaNd[B_3O_4(OH)_3]_2(am)$) in 0.1 M NaCl is representative of dilute to concentrated NaCl systems and of the complete pH-range evaluated in this study.
- The Nd(III)–borate aqueous species have no impact on the solubility of Nd(III). Hence, log $*K°_{s,0}$ of $NaNd[B_3O_4(OH)_3]_2(am)$ has been determined considering only the equilibrium between this solid phase and $Nd(OH)_n^{3-n}$ species.
- The formation of the species $NdB(OH)_4^{2+}(aq)$ has been postulated based on the confirmed role of $B(OH)_4^-$ as ligand in the Np(V) studies. An upper limit of log $*\beta°_{(1,1)}$ has been provided, so that the formation of this species has no effect on the solubility of $NaNd[B_3O_4(OH)_3]_2(am)$.

The steps followed in the development of the thermodynamic and activity model are:

- Chemical model is taken from the inputs by XPS (Nd(III)–borate solid phase) and TRLFS, in combination with the speciation model of Nd(III) in the absence of borate derived in Neck et al. [24].
- Based on the chemical model derived and on the solubility data under equilibrium conditions, determination of log $*K'_{s,0}$ for the ternary Na–Nd(III)–borate solid phase forming in dilute to concentrated NaCl systems. Quantification based on the assumption that aqueous Nd(III)–borate complexes have no impact on Nd(III) solubility.
- Extrapolation of log $*K'_{s,0}$ to $I = 0$ using the SIT ion interaction coefficients described in section 9.1.
- Comparison of calculated solubility of Na–Nd(III)–borate solid phase with available experimental data. Assessment of the role of Nd(III)–borate aqueous complexes, using an upper limit of log $*\beta°_{(1,1)}$ for the complex $NdB(OH)_4^{2+}$.

According with the assumptions described above, the solubility of $NaNd[B_3O_4(OH)_3]_2$(am) is postulated according to

$$NaNd[B_3O_4(OH)_3]_2 + 10\,H_2O \rightleftharpoons Nd^{3+} + 6\,B(OH)_4^- + Na^+ + 2\,H^+ \quad (9.4)$$

with

$$log\,{}^*K'_{(s,0)} = log[Nd^{3+}] + 6\,log[B(OH)_4^-] + log[Na^+] + 2\,log[H^+] \quad (9.4a)$$

$$log\,{}^*K^\circ_{(s,0)} = log\,{}^*K'_{(s,0)} + log\,\gamma_{Nd^{3+}} + 6\,log\,\gamma_{B(OH)_4^-} + log\,\gamma_{Na^+} + 2\,log\,\gamma_{H^+} - 10\,log\,a_w \quad (9.4b)$$

The conditional stability constant for reaction 9.4 is determined from the experimentally obtained Nd(III) solubility data in dilute to concentrated NaCl solutions with $[B]_{tot}$ = 0.16 M. The value for log $^*K^\circ_{s,0}$ was determined by extrapolating the calculated conditional constant log $^*K'_{s,0}$ to I = 0 using Eq 9.4b and the SIT approach. The value selected for log $^*K^\circ_{s,0}$ in this work is provided in Table 9.6 and corresponds to the unweighted average of the values obtained for all NaCl systems. The assigned uncertainty accounts for the relevant assumptions made in the development of the thermodynamic model.

Table 9.6. *log $^*K'_{s,0}$ values derived in this work for the $NaNd[B_3O_4(OH)_3]_2$(am) solid phase.*

Reaction	**log $^*K^\circ_{s,0}$**
$NaNd[B_3O_4(OH)_3]_2(am) + 10\,H_2O \rightleftharpoons Nd^{3+} + 6\,B(OH)_4^- + Na^+ + 2\,H^+$	–38.3 ± 1.2

The formation of Cm(III)–borate complexes has been confirmed by TRLFS studies at pH_m = 8 in NaCl and $MgCl_2$ solutions, although no quantitative evaluation of the spectra was achieved in the present work. Ln(III) complexes with aqueous borate species in comparable conditions are reported in the literature. Borkowski et al. postulated the formation of the complex $NdHB_4O_7^{2+}$, with a stability constant of log β = 4.55 ± 0.06 [6]. Note that the stoichiometry of the complex remains hypothetical, especially considering that experiments were performed at a single pH value and that the species $HB_4O_4^-$ does not belong to the standard speciation scheme of boron in aqueous solution. Recently, Schott et al. reported a weak borate complexation with Eu(III) in aqueous solution at rather high boron concentrations (0.3M ≤ $[B]_{tot}$ ≤ 0.7 M) at pH_m ~6. The authors defined a Eu(III)-polyborate complex assuming that all polyborate species present in solution have the same tendency to complex Eu^{3+}(aq)

[83]. For the complex $EuB(OR)_4^{2+}$ (R = H and or $[BO_3]$ units) a formation constant of log β = 2 was calculated.

For the Np(V)–borate system investigated in this work, a very weak Np(V) borate complex with a formation constant of log $\beta°_{(1,1)}$ = 1.6 was estimated. In contrast to the complexes reported in the literature for the system Ln(III)–borate, the evaluation of the UV–Vis/NIR spectra of Np(V) in the presence of borate identified the monomeric $B(OH)_4^-$ as most probable ligand rather than a polyborate species. Hence, $B(OH)_4^-$ is also postulated as complexing ligand in the Ln/An(III) system. Based on the absence of a manifest impact of the complex formation on the solubility of Nd(III), only an upper limit for the stability constant of $NdB(OH)_4^{2+}$ has been estimated (log $\beta° \leq 3$). Both the stoichiometry and stability of the postulated complex are to be considered only for scoping calculations.

$$Nd^{3+} + B(OH)_4^- \rightleftharpoons NdB(OH)_4^{2+} \tag{9.5}$$

$$log{*}\beta'_{(1,1)} = log[NdB(OH)_4^{2+}] - log[Nd^{3+}] - log[B(OH)_4^-] \tag{9.5a}$$

$$log{*}\beta°_{(1,1)} = log{*}\beta'_{(I,I)} + log\,\gamma_{NdB(OH)_4^{2+}} - log\,\gamma_{Nd^{3+}} - log\,\gamma_{B(OH)_4^-} \tag{9.5b}$$

The calculated solubility of $NaNd[B_3O_4(OH)_3]_2$(am) in 0.1 M , 1.0 M and 5.0 M NaCl solutions with $[B]_{tot}$ = 0.16 M is shown together with experimental data obtained in this work under analogous conditions in Fig. 9.4 – 9.6. In 5.0 M NaCl solution the calculated solubility of $NaNd[B_3O_4(OH)_3]_2$(am) additional is shown for $[B]_{tot}$ = 0.04 M. In 0.1 M and 1.0 M NaCl with $[B]_{tot} \leq 0.04$ M and 5.0 M NaCl with $[B]_{tot} < 0.04$ M $NaNd[B_3O_4(OH)_3]_2$(am) is less stable than $Nd(OH)_3$(am) according to the calculations and therefore not shown in the corresponding graphs.

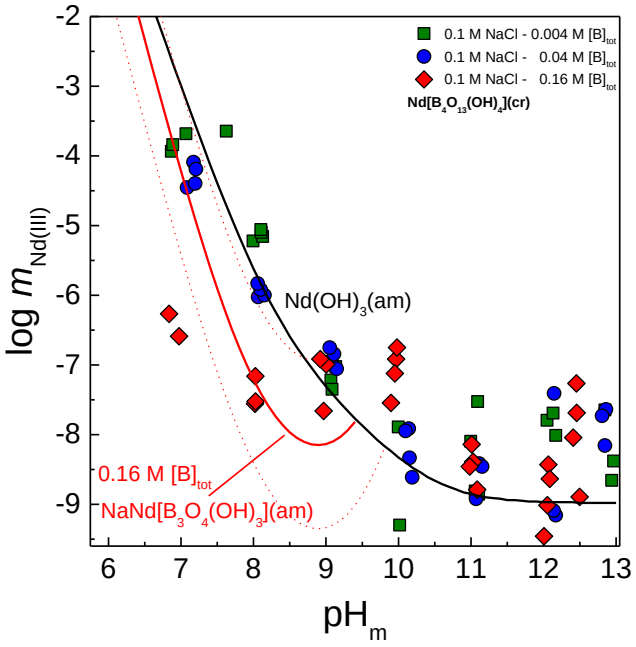

Figure 9.4. *Comparison of experimental solubility data determined in this work for Nd(III) in borate-bearing 0.1 M NaCl solutions and model calculations using log *K'$_{s,0}$ values derived in this work for NaNd[B$_3$O$_4$(OH)$_3$]$_2$(am). Dotted lines corresponding to the upper and lower solubility limits calculated with the uncertainty assigned to log*K°$_{s,O}$.*

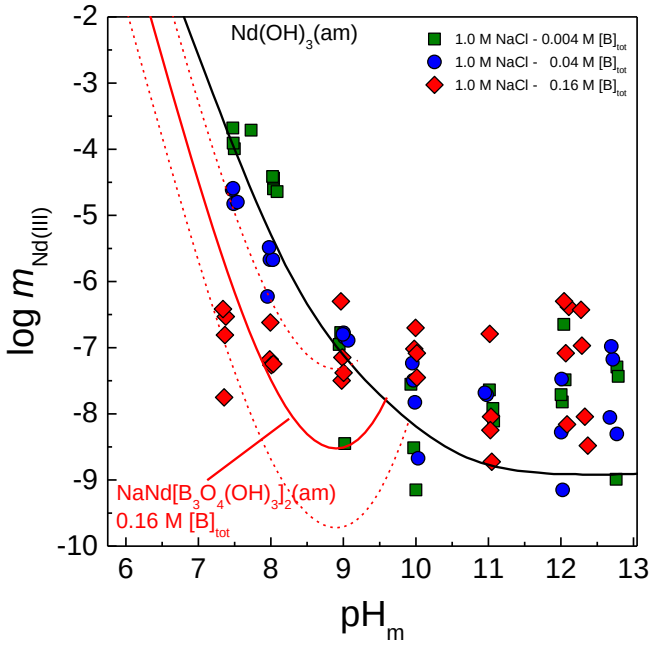

Figure 9.5. *Comparison of experimental solubility data determined in this work for Nd(III) in borate-bearing 1.0 M NaCl solutions and model calculations using log *K'$_{s,0}$ values derived in this work for NaNd[B$_3$O$_4$(OH)$_3$]$_2$(am). Dotted lines corresponding to the upper and lower solubility limits calculated with the uncertainty assigned to log*K°$_{s,O}$.*

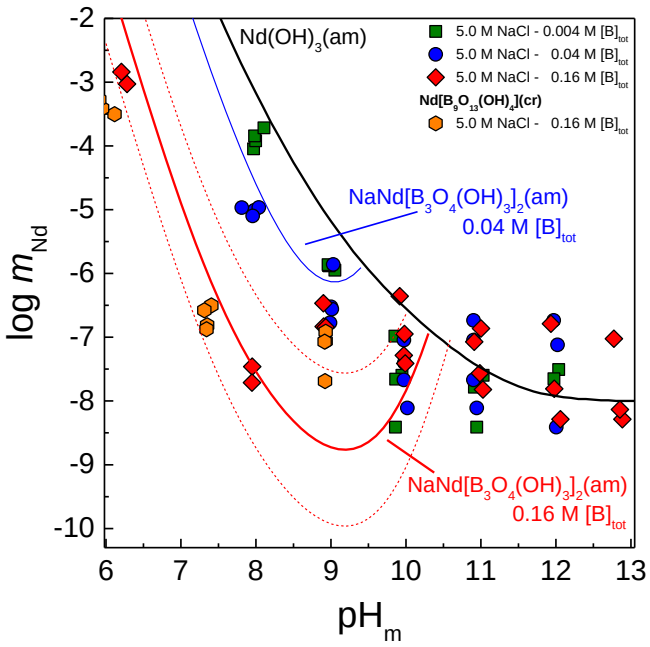

Figure 9.6. *Comparison of experimental solubility data determined in this work for Nd(III) in borate-bearing 5.0 M NaCl solutions and model calculations using log *K'$_{s,0}$ values derived in this work for NaNd[B$_3$O$_4$(OH)$_3$]$_2$(am). Dotted lines corresponding to the upper and lower solubility limits calculated with the uncertainty assigned to log*K°$_{s,O}$.*

The calculated solubility curves for the system Nd(III)–borate at $[B]_{tot}$ = 0.16 M are in moderate agreement with the experimental data at pH_m = 8 in all three NaCl systems. The model derived is strongly hindered by the large dispersion of the solubility data experimentally determined. Based on the experience gained for the Np(V)–borate system, and considering that the equilibration times allowed in the latter system were significantly longer than for the Nd(III) case (300 *vs.* 90–150 days), it can be also hypothesized that not all the experiments were in thermodynamic equilibrium at the time of the completion of the experiment. Above pH_m ~9.3, thermodynamic calculations predict that NaNd[$B_3O_4(OH)_3]_2$(am) becomes less stable than $Nd(OH)_3$(am), and the latter phase is thus responsible for the solubility control in the Nd(III)–borate system. Note further that the crystallinity of the Na–Nd(III)–borate solid phase coating the original $Nd(OH)_3$(am) may be susceptible to become more crystalline as thus decrease its solubility, as already observed for the Na/Mg–Np(V)–borate systems.

9.3 Conclusions

Preliminary thermodynamic and activity models for the systems Ln(III)/Cm(III)–Na–Mg–H–Cl–H_2O and Np(V)–Na–Mg–H–Cl–H_2O have been derived based on the experimental data generated in the present work (solubility, spectroscopy, solid phase characterization) in combination with the model for Na–K–Ca–Mg–H–CI–SO_4–CO_2–$B(OH)_4$–H_2O previously reported by Felmy and Weare. The main trends observed experimentally are reasonably well reproduced by the proposed model, especially for the Np(V) system. The need for these data are very relevant, as the formation of ternary Na/Mg–An(III)/An(V)–borate solid phases represent a previously unknown mechanism for the immobilization of these radionuclides.

However, a number of key uncertainties remain, and thus these models must be considered as a preliminary working tool in the process of deriving comprehensive and self-consistent chemical, thermodynamic and activity models for the actinide–borate systems. Hence, the aqueous An–borate complexes remain ill-defined for the investigated actinide systems (+III to +VI), also reflecting the complexity of the borate speciation in dilute to concentrated saline systems. In spite of the existing models on the borate speciation in saline systems, there is a clear need for improvement in this respect. The complexity of the borate system is also mirrored in the An–borate solid phases forming in the investigated systems. Although a number of well-defined stoichiometries for An–borate compounds have been identified (mainly based on XPS data), the existence of a relatively broad spectra of stoichiometries and degrees of crystallinity is suspected. Furthermore, these processes are strongly kinetically hindered, and consequently pose important difficulties for their evaluation within the context of a PhD thesis.

10 Summary and Conclusions

This PhD thesis has successfully addressed the impact of borate on the chemical behaviour of actinides under repository-relevant conditions, with special emphasis on complexation reactions, solubility phenomena and partly also on redox processes. The study extends from dilute to concentrated saline systems and from reduced (+III) to oxidized (+VI) actinide redox states, thus covering a wide spectrum of waste disposal concepts and scenarios. The newly generated experimental data provides key inputs for the assessment of the source term (maximum expected solubility) for actinides (III, IV, V, VI) in borate-bearing systems. In the case of Ln/An(III) and Np(V) where the strongest impact of borate has been observed, solubility data in combination with solid and aqueous phase characterization have been described and quantified in terms of equilibrium thermodynamics of aqueous systems using the SIT formulism. The derived preliminary thermodynamic models may represent a starting point for the quantitative modelling of the main processes observed for Ln/An(III) and Np(V) in borate-bearing repository-relevant conditions, which needs to be validated in subsequent future studies.

The interaction of Ln/An(III) was systematically investigated in the presence of borate at $6 \leq pH_m \leq 13$ in dilute to concentrated NaCl, $MgCl_2$ and $CaCl_2$ solutions with a series of comprehensive Nd(III) solubility experiments and Cm(III) TRLFS studies. TRLFS spectra confirmed the formation of weak Cm(III)–borate complexes under weakly alkaline conditions and $[B]_{tot} \geq 0.04$ M. No increase in the solubility of $Nd(OH)_3(am)$ was observed in the presence of borate, but instead a clear drop in the concentration of Nd(III) (2–4 orders of magnitude) took place at $pH_m \leq 9$ and $[B]_{tot} \geq 0.04$ M. XPS and SEM–EDS confirmed the presence of a previously unreported Nd(III)–borate solid phase, which formed as a coating of the unreacted $Nd(OH)_3(am)$ core. The strong hydrolysis of Ln(III) and An(III) under hyperalkaline pH conditions (≥ 10, predominance of $Ln/An(OH)_3(aq)$ in the aqueous phase) outcompetes any interaction of borate in this pH-range, both in the aqueous and solid phases.

The solubility of $NpO_2OH(am,fresh)$ was studied in dilute to concentrated NaCl and $MgCl_2$ solutions in the presence of borate under weakly alkaline pH conditions. This study was complemented with a comprehensive series of UV–Vis/NIR measurements under analogous experimental conditions to assess the interaction of Np(V) with borate in the aqueous phase. Spectroscopic data confirmed the formation of at least one Np(V)–borate complex, with $B(OH)_4^-$ being the most likely boron species participating in the complexation reaction. As for Nd(III), a very significant decrease of the Np(V) solubility accompanied by a change in the colour of the solid phase indicated the transformation of the original $NpO_2OH(am,fresh)$ into a secondary Np(V)–borate phase. Solid phase characterization achieved with XRD, XPS, SEM–EDS and EXAFS confirmed the formation of hitherto unknown Np(V)–borate forming in NaCl and dilute $MgCl_2$, with a likely stoichiometry of $NpO_2[B_5O_6(OH)_4]\cdot 2NaOH(cr)$ and $(NpO_2)_2[B_5O_6(OH)_4]_2\cdot 3Mg(OH)_2(cr)$.

The solubility of U(VI), Th(IV) and Pu(III/IV) was exemplarily investigated in dilute to concentrated NaCl and $MgCl_2$ systems in the presence of borate at $6.5 \leq pH_m \leq 9$. Borate shows no clear impact on the solubility of Th(IV) in dilute NaCl and $MgCl_2$ solutions. On the other hand, a slight increase of the Th(IV) solubility was found in concentrated NaCl and $MgCl_2$ solutions with pH_m = 7.5-9 and $[B]_{tot}$ = 0.16 M, which could be attributed to a weak Th(IV)–borate complex formation. The weaker interaction between Th(IV) and borate compared to An(III) and An(V) is related with the very strong tendency of Th(IV) (and tetravalent actinides in general) towards hydrolysis, which competes with the interaction of Th(IV) with borate under near-neutral to hyperalkaline pH conditions. Solubility studies with $UO_3 \cdot 2H_2O$(cr) and $Na_2U_2O_7 \cdot H_2O$(cr) performed in the presence of borate confirmed the formation of U(VI)–borate aqueous complexes under weakly alkaline conditions with $[B]_{tot} \geq 0.04$ M. No U(VI)–borate interaction was observed at $pH_m \leq 6.5$, likely due to the predominance of $B(OH)_3$(aq) in this pH-range and the poor complexing character of this boron species. In contrast to Nd(III) and Np(V), no decrease in the U(VI) solubility was observed in the presence of borate. This finding may be explained by the significantly lower solubility of $Na_2U_2O_7 \cdot H_2O$(cr), compared to $Nd(OH)_3$(am) and NpO_2OH(am,fresh) under weakly alkaline conditions. Solubility studies with Pu(III/IV) in dilute NaCl solutions showed only a slight effect of borate in redox conditions where Pu(IV) prevails. Under the very reducing conditions imposed by $Na_2S_2O_4$, XPS confirmed the predominance of a Pu(III) solid phase with a slightly decreased solubility with respect to $Pu(OH)_3$(s). As for Nd(III), this observation is likely linked to the solubility-control by a Pu(III)–borate solid phase.

This PhD thesis represents a key contribution for understanding and predicting the so-far largely unknown role of borate on the aquatic chemistry of actinides under repository relevant conditions. The strength of the actinide–borate interaction can be rationalized in terms of the effective charge of the actinide cation and corresponding competition with hydrolysis reactions: An(V) (Z_{eff} = 2.3) > An(III) (Z_{eff} = 3) > An(VI) (Z_{eff} = 3.2) > An(IV) (Z_{eff} = 4). The formation of sparingly soluble Ln/An(III)– and An(V)–borate solid phases represents a so-far unknown retention mechanism for these redox states, and it is especially relevant for the highly mobile Np(V). These results highlight the need of accounting for borate interactions for the correct assessment of actinide behaviour under repository conditions.

References:

1. Geckeis, H., Röhlig, K.-J., Mengel, K.: Endlagerung radioaktiver Abfälle. Chemie in unserer Zeit **46**, 282-293 (2012).
2. Mengel, K., Röhlig, K.-J., Geckeis, H.: Endlagerung radioaktiver Abfälle. Chemie in unserer Zeit **46**, 208-217 (2012).
3. Röhlig, K.-J., Geckeis, H., Mengel, K.: Endlagerung radioaktiver Abfälle. Chemie in unserer Zeit **46**, 140-149 (2012).
4. Bube, C., Metz, V., Bohnert, E., Garbev, K., Schild, D., Kienzler, B.: Long-term cement corrosion in chloride-rich solutions relevant to radioactive waste disposal in rock salt – Leaching experiments and thermodynamic simulations. Physics and Chemistry of the Earth, Parts A/B/C **64**, 87-94 (2013).
5. Altmaier, M., Metz, V., Neck, V., Muller, R., Fanghänel, T.: Solid-liquid equilibria of $Mg(OH)_2$(cr) and $Mg_2(OH)_3Cl*4H_2O$(cr) in the system Mg-Na-H-OH-O-Cl-H_2O at 25 °C. Geochimica Et Cosmochimica Acta **67**, 3595-3601 (2003).
6. Borkowski, M., Richmann, M., Reed, D. T., Xiong, Y.: Complexation of Nd(III) with tetraborate ion and its effect on actinide(III) solubility in WIPP brine. Radiochimica Acta **98**, 577-582 (2010).
7. Altmaier, M., Gaona, X., Fanghänel, T.: Recent Advances in Aqueous Actinide Chemistry and Thermodynamics. Chemical reviews **113**, 901-943 (2013).
8. Geckeis, H., Lützenkirchen, J., Polly, R., Rabung, T., Schmidt, M.: Mineral–water interface reactions of actinides. Chemical reviews **113**, 1016-1062 (2013).
9. Fanghänel, T., Neck, V.: Aquatic chemistry and solubility phenomena of actinide oxides/hydroxides. Pure and Applied Chemistry **74**, 1895-1907 (2002).
10. Choppin, G. R.: Actinide speciation in the environment. Journal of Radioanalytical and Nuclear Chemistry **273**, 695-703 (2007).
11. Le Naour, C., Trubert, D., Di Giandomenico, M. V., Fillaux, C., Den Auwer, C., Moisy, P., Hennig, C.: First structural characterization of a protactinium (V) single oxo bond in aqueous media. Inorganic chemistry **44**, 9542-9546 (2005).
12. Trubert, D., Le Naour, C., Jaussaud, C.: Hydrolysis of Protactinium(V). I. Equilibrium Constants at 25°C: A Solvent Extraction Study with TTA in the Aqueous System $Pa(V)/H_2O/H^+/Na^+/ClO_4^-$. Journal of solution chemistry **31**, 261-277 (2002).
13. Choppin, G. R.: Utility of oxidation state analogs in the study of plutonium behavior. Radiochimica Acta **85**, 89-96 (1999).
14. Choppin, G. R., Rao, L. F.: Complexation of pentavalent and hexavalent actinides by fluoride. Radiochimca Acta **37**, 143-146 (1984).

15. Pearson, R. G.: The HSAB principle - More quantitative aspects. Inorganica Chimica Acta **240**, 93-98 (1995).
16. Runde, W.: Zum chemischen Verhalten von drei-und fünfwertigem Americium in salinen NaCl-Lösungen. PhD Thesis, Technische Universität München München (1993).
17. Nelson, F., Kraus, K. A.: Chemistry of Aqueous Uranium (V) Solutions. III. The Uranium (IV)-(V)-(VI) Equilibrium in Perchlorate and Chloride Solutions1. Journal of the American Chemical Society **73**, 2157-2161 (1951).
18. Newton, T., Baker, F.: A uranium (V)-uranium (VI) complex and its effect on the uranium (V) disproportionation rate. Inorganic chemistry **4**, 1166-1170 (1965).
19. Heal, H.: Electrochemistry of uranium. Nature **157**, 225 (1946).
20. Ilton, E. S., Pacheco, J. S. L., Bargar, J. R., Shi, Z., Liu, J., Kovarik, L., Engelhard, M. H., Felmy, A. R.: Reduction of U (VI) Incorporated in the Structure of Hematite. Environmental science & technology **46**, 9428-9436 (2012).
21. Grenthe, I., Fuger, J., Konings, R., Lemire, R., Muller, A., Nguyen-Trung, C.: Chemical Thermodynamics 1; Chemical Thermodynamics of Uranium Elsevier, Amsterdam (1992).
22. Guillaumont, R., Fanghänel, T., Fuger, J., Grenthe, I., Neck, V., Palmer, D. A., Rand, M. H.: *Update on the chemical thermodynamics of uranium, neptunium, plutonium, americium and technetium*. Elsevier, Amsterdam (2003).
23. Felmy, A. R., Rai, D., Schramke, J. A., Ryan, J. L.: The solubility of plutonium hydroxide in dilute solution and in high-ionic-strength chloride brines. Radiochimca Acta **48**, 29-36 (1989).
24. Neck, V., Altmaier, M., Rabung, T., Lutzenkirchen, J., Fanghanel, T.: Thermodynamics of trivalent actinides and neodymium in NaCl, $MgCl_2$, and $CaCl_2$ solutions: Solubility, hydrolysis, and ternary Ca-M(III)-OH complexes. Pure and Applied Chemistry **81**, 1555-1568 (2009).
25. Rabung, T., Altmaier, M., Neck, V., Fanghänel, T.: A TRLFS study of Cm(III) hydroxide complexes in alkaline $CaCl_2$ solutions. Radiochimica Acta **96**, 551-559 (2008).
26. Wood, S. A., Palmer, D. A., Wesolowski, D. J., Bénézeth, P.: The aqueous geochemistry of the rare earth elements and yttrium. Part XI. The solubility of $Nd(OH)_3$ and hydrolysis of Nd^{3+} from 30 to 290°C at saturated water vapor pressure with in-situ pH_m measurement. Water–rock interactions, ore deposits, and environmental geochemistry: a tribute to David Crerar, Special Publication **7**, 229-256 (2002).
27. Rand, M. H., Fuger, J., Grenthe, I., Neck, V., Rai, D.: *Chemical thermodynamics of thorium*. Organization for Economic, (2008).
28. Neck, V., Kim, J.: Solubility and hydrolysis of tetravalent actinides. Radiochimica Acta International journal for chemical aspects of nuclear science and technology **89**, 1 (2001).

29. Altmaier, M., Neck, V., Fanghanel, T.: Solubility and colloid formation of Th(IV) in concentrated NaCl and $MgCl_2$ solution. Radiochimica Acta **92**, 537-543 (2004).
30. Brendebach, B., Altmaier, M., Rothe, J., Neck, V., Denecke, M.: EXAFS study of aqueous ZrIV and ThIV complexes in alkaline $CaCl_2$ solutions: $Ca_3[Zr(OH)_6]^{4+}$ and $Ca_4[Th(OH)_8]^{4+}$. Inorganic chemistry **46**, 6804-6810 (2007).
31. Altmaier, M., Neck, V., Fanghanel, T.: Solubility of Zr(IV), Th(IV) and Pu(IV) hydrous oxides in $CaCl_2$ solutions and the formation of ternary Ca-M(IV)-OH complexes. Radiochimica Acta **96**, 541-550 (2008).
32. Fellhauer, D., Neck, V., Altmaier, M., Lutzenkirchen, J., Fanghanel, T.: Solubility of tetravalent actinides in alkaline $CaCl_2$ solutions and formation of $Ca_4[An(OH)_8]^{4+}$ complexes: A study of Np(IV) and Pu(IV) under reducing conditions and the systematic trend in the An(IV) series. Radiochimica Acta **98**, 541-548 (2010).
33. Higashi, S.: Determination of the solubility of thorium hydroxide. Bull. Inst. Phys. Chem. Res.(Toyko) **37**, 200-206 (1959).
34. Runde, W., Kim, J.: Report RCM 01094, (1994).
35. Lierse, C., Treiber, W., Kim, J.: Hydrolysis reactions of neptunium (V). Radiochimca Acta **38**, 27-28 (1985).
36. Neck, V., Kim, J., Kanellakopulos, B.: Solubility and hydrolysis behaviour of neptunium (V). Radiochimca Acta **56**, 25-30 (1992).
37. Rao, L., Srinivasan, T. G., Garnov, A. Y., Zanonato, P., Di Bernardo, P., Bismondo, A.: Hydrolysis of neptunium (V) at variable temperatures (10–85 C). Geochimica et Cosmochimica Acta **68**, 4821-4830 (2004).
38. Neck, V.: Comment on "Hydrolysis of neptunium (V) at variable temperatures (10–85° C)" by L. Rao, TG Srinivasan, A. Yu. Garnov, P. Zanonato, P. Di Bernardo, and A. Bismondo. Geochimica et Cosmochimica Acta **70**, 4551-4555 (2006).
39. Rao, L., Srinivasan, T. G., Garnov, A. Y., Zanonato, P., Bernardo, P. D., Bismondo, A.: Response to the comment by V. Neck on "Hydrolysis of neptunium(V) at variable temperatures (10–85° C)", Geochimica et Cosmochimica Acta 68, 4821–4830. Geochimica et Cosmochimica Acta **70**, 4556-4562 (2006).
40. Petrov, V. G., Gaona, X., Fellhauer, D., Dardenne, K., Kalmykov, S. N., Altmaier, M.: Np(V) Solubility and Solid Phase Transformation in dilute to concentrated NaCl Solutions. In: Migration Conference, Beijing, China (2011).
41. Neck, V., Runde, W., Kim, J. m., Kanellakopulos, B.: Solid-liquid equilibrium reactions of neptunium(V) in carbonate solution at different ionic strength. Radiochimica Acta **65**, 29-37 (1994).

42. Gaona, X., Tits, J., Dardenne, K., Liu, X., Rothe, J., Denecke, M. A., Wieland, E., Altmaier, M.: Spectroscopic investigations of Np (V/VI) redox speciation in hyperalkaline TMA-(OH, Cl) solutions. Radiochimica Acta International journal for chemical aspects of nuclear science and technology **100**, 759-770 (2012).
43. Gaona, X., Fellhauer, D., Altmaier, M.: Thermodynamic description of Np (VI) solubility, hydrolysis, and redox behavior in dilute to concentrated alkaline NaCl solutions. Pure and Applied Chemistry Pure Appl. Chem. **85**, 2027-2049 (2013).
44. Tasker, I., O'Hare, P., lewis, B. M., Johnson, G., Cordfunke, E.: Thermochemistry of uranium compounds. XVI. Calorimetric determination of the standard molar enthalpy of formation at 298.15 K, low-temperature heat capacity, and high-temperature enthalpy increments of UO_2 (OH_2) H_2O (schoepite). Canadian journal of chemistry **66**, 620-625 (1988).
45. Hoekstra, H., Siegel, S.: The uranium trioxide-water system. Journal of Inorganic and Nuclear Chemistry **35**, 761-779 (1973).
46. Sowder, A., Clark, S., Fjeld, R.: The transformation of uranyl oxide hydrates: the effect of dehydration on synthetic metaschoepite and its alteration to becquerelite. Environmental science & technology **33**, 3552-3557 (1999).
47. Finch, R. J., Hawthorne, F. C., Ewing, R. C.: Structural relations among schoepite, metaschoepite and" dehydrated schoepite". Canadian mineralogist **36**, 831-846 (1998).
48. Gorman-Lewis, D., Fein, J. B., Burns, P. C., Szymanowski, J. E., Converse, J.: Solubility measurements of the uranyl oxide hydrate phases metaschoepite, compreignacite, Na–compreignacite, becquerelite, and clarkeite. The Journal of Chemical Thermodynamics **40**, 980-990 (2008).
49. Altmaier, M., Neck, V., Müller, R., Fanghänel, T.: Solubility of U(VI) and formation of CaU_2O_7 $3H_2O$(cr) in alkaline $CaCl_2$ solutions In: Migration Avignon, France (2005).
50. Crea, F., De Stefano, C., Pettignano, A., Sammartano, S.: Hydrolysis of dioxouranium(VI): a calorimetric study in NaCl(aq) and $NaClO_4$ aq, at 25 °C. Thermochimica Acta **414**, 185-189 (2004).
51. Zanonato, P., Di Bernardo, P., Bismondo, A., Liu, G. K., Chen, X. Y., Rao, L. F.: Hydrolysis of uranium(VI) at variable temperatures (10-85 degrees C). Journal of the American Chemical Society **126**, 5515-5522 (2004).
52. Moll, H., Rossberg, A., Steudtner, R., Drobot, B. r., Müller, K., Tsushima, S.: Uranium (VI) Chemistry in Strong Alkaline Solution: Speciation and Oxygen Exchange Mechanism. Inorganic chemistry **53**, 1585-1593 (2014).
53. Altmaier, M., Neck, V., Metz, V., Müller, R., Schlieker, M., Fanghänel, T.: The solubility of U(VI) in NaCl and $MgCl_2$ solution. Proceedings of the Migration conference in Gyeongju (Korea) (2003).

54. Delahay, P., Pourbaix, M., Van Rysselberghe, P.: Potential-pH diagrams. Journal of chemical education **27**, 683 (1950).
55. Neck, V., Altmaier, M., Fanghänel, T.: Solubility of plutonium hydroxides/hydrous oxides under reducing conditions and in the presence of oxygen. Comptes Rendus Chimie **10**, 959-977 (2007).
56. Neck, V., Altmaier, M., Seibert, A., Yun, J. I., Marquardt, C. M., Fanghanel, T.: Solubility and redox reactions of Pu(IV) hydrous oxide: Evidence for the formation of PuO_2+x(s, hyd). Radiochimica Acta **95**, 193-207 (2007).
57. Neck, V., Altmaier, M., Fanghanel, T.: Thermodynamic data for hydrous and anhydrous PuO_2^+(s). Journal of Alloys and Compounds **444**, 464-469 (2007).
58. Newton, W.: The Kinetics of the Oxidation-Reduction Reactions of Uranium, Neptunium, Plutonium, and Americium in Solutions. (1975).
59. Fellhauer, D.: Untersuchungen zur Redoxchemie und Löslichkeit von Neptunium und Plutonium. PhD Thesis, Universität Heidelberg Heidelberg (2013).
60. Rai, D., Gorby, Y. A., Fredrickson, J. K., Moore, D. A., Yui, M.: Reductive dissolution of PuO_2 (am): The effect of Fe (II) and hydroquinone. Journal of solution chemistry **31**, 433-453 (2002).
61. Choppin, G. R., Jensen, M. P.: Actinides in solution: complexation and kinetics. In: *The Chemistry of the Actinide and Transactinide Elements* ed.). Springer, (2006).
62. Ciavatta, L.: The specific interaction theory in evaluating ionic equilibria. Ann. Chim.(Rome) **70**, 551-567 (1980).
63. Pitzer, K. S.: *Activity coefficients in electrolyte solutions*. CRC press, Boca Raton (1991).
64. Woods, W. G.: An introduction to boron: history, sources, uses, and chemistry. Environmental Health Perspectives **102**, 5-11 (1994).
65. Garrett, D. E.: *Borates: handbook of deposits, processing, properties, and use*. Academic Press, (1998).
66. Kistler, R. B., Helvaci, C.: Boron and borates. Industrial minerals and rocks **6**, 171-186 (1994).
67. Burns, P. C.: Borate clusters and fundamental building blocks containing four polyhedra: why few clusters are utilized as fundamental building blocks of structures. Canadian mineralogist **33**, 1167-1176 (1995).
68. Grice, J. D., Burns, P. C., Hawthorne, F.: Borate minerals. II. A hierarchy of structures based upon the borate fundamental building block. Canadian mineralogist **37**, 731-762 (1999).
69. Ingri, N., Lagerstrom, G., Frydman, M., Sillen, L. G.: Equilibrium studies of polyanions .2. polyborates in $NaClO_4$ medium. Acta Chemica Scandinavica **11**, 1034-1058 (1957).

70. Ingri, N.: Equilibrium studies of polyanions .8. On the first equilibrium steps in the hydrolysis of boric acid, a comparison between equilibria in 0.1 M and 3.0 M $NACIO_4$. Acta Chemica Scandinavica **16**, 439-448 (1962).
71. Hirao, T., Kotaka, M., Kakihana, H.: Raman-spectra of polyborate ions in aqueous-solution. Journal of Inorganic & Nuclear Chemistry **41**, 1217-1220 (1979).
72. Salentine, C. G.: High-field B-11-NMR of alkali borates - aqueous polyborate equilibria. Inorganic Chemistry **22**, 3920-3924 (1983).
73. Heller, G., Janda, R., Mathieu, J.: Investigations of the polyborate equilibria in aqueous-solutions by B-11-NMR and raman-spectroscopy. Inorganica Chimica Acta-Articles **40**, X107-X108 (1980).
74. Momii, R. K., Nachtrie.Nh: Nuclear magnetic resonance study of borate-polyborate equilibria in aqueous solution. Inorganic Chemistry **6**, 1189-1192 (1967).
75. Ishihara, K., Nagasawa, A., Umemoto, K., Ito, H., Saito, K.: Kinetic-study of boric acid-borate interchange in aqueous-solution by B-11 NMR-spectroscopy. Inorganic Chemistry **33**, 3811-3816 (1994).
76. Nies, N. P., Hulbert, R. W.: Solubility isotherms in the system sodium oxide-boric oxide-water. Revised solubility-temperature curves of boric acid, borax, sodium pentaborate, and sodium metaborate. Journal of Chemical and Engineering Data **12**, 303-313 (1967).
77. Owen, B. B.: The dissociation constant of boric acid from 10 to 50. Journal of the American Chemical Society **56**, 1695-1697 (1934).
78. Apelblat, A., Manzurola, E.: Solubilities and vapour pressures of saturated aqueous solutions of sodium tetraborate, sodium carbonate, and magnesium sulfate and freezing-temperature lowerings of sodium tetraborate and sodium carbonate solutions. Journal of Chemical Thermodynamics **35**, 221-238 (2003).
79. Nikolaev, A., Chelischeva, A.: The 25 C isotherm of the system: $CaO-B_2O_3-H_2O$ and $MgO-B_2O_3-H_2O$. Comp. Rend. Acad. Sci USSR **28**, 127-130 (1940).
80. Kurnakova, A. G.: Physicochemical study of calcium and magnesium borates. Izvest. Sektora Fiz. Khim. Anal., Inst. Obshchei i Neorg., Akad. Nauk SSSR **15**, 125 (1947).
81. Felmy, A. R., Weare, J. H.: The prediction of borate mineral equilibria in natural waters: Application to Searles Lake, California. Geochimica et Cosmochimica Acta **50**, 2771-2783 (1986).
82. Holleman, A. F., Wiberg, E.: *Lehrbuch der anorganischen Chemie*. Walter de Gruyter, (1995).
83. Schott, J., Kretzschmar, J., Acker, M., Eidner, S., Kumke, M. U., Drobot, B., Barkleit, A., Taut, S., Brendler, V., Stumpf, T.: Formation of a Eu(iii) borate solid species from a weak Eu(iii) borate complex in aqueous solution. Dalton Transactions **43**, 11516-11528 (2014).

84. Zhihong, L., Bo, G., Shuni, L., Mancheng, H., Shuping, X.: Raman spectroscopic analysis of supersaturated aqueous solution of $MgO.B_2O_3$-32%$MgCl_2$-H_2O during acidification and dilution. Spectrochimica acta. Part A, Molecular and biomolecular spectroscopy **60**, 3125-3128 (2004).

85. Wang, P., Kosinski, J. J., Lencka, M. M., Anderko, A., Springer, R. D.: Thermodynamic modeling of boric acid and selected metal borate systems. Pure and Applied Chemistry **85**, 2117-2144 (2013).

86. Kienzler, B., Luckscheiter, B., Wilhelm, S.: Waste form corrosion modeling: comparison with experimental results. Waste Management **21**, 741-752 (2001).

87. Chernorukov, N. G., Knyazev, A. V., Khomyakova, V. O., Nipruk, O. V.: Heterogeneous equilibria in the system uranoborate $MII(BUO_5)_2 \cdot nH_2O$-aqueous solution (MII=Mn, Co, Ni, Zn). Radiochemistry **48**, 18-23 (2006).

88. Chernorukov, N. G., Knyazev, A. V., Kortikova, O. V.: Thermochemistry of Alkaline-Earth Metal Uranoborates. Radiochemistry **45**, 475-479 (2003).

89. Chernorukov, N. G., Knyazev, A. V., Kortikova, O. V., Sergacheva, I. V.: Synthesis, Structure, and Thermochemical Properties of Alkali Metal Uranoborates. Russian Journal of General Chemistry **73**, 1167-1173 (2003).

90. Chernorukov, N. G., Knyazev, A. V., Sergacheva, I. V., Ershova, A. V.: Synthesis and Physicochemical Study of Compounds in UO_3-AkOk/(Ak= B, Si, Ge)-HO Systems. Radiochemistry **46**, 218-223 (2004).

91. Chernorukov, N. G., Nipruk, O. V., Knyazev, A. V., Khomyakova, V. O.: Solubility and Thermodynamic Properties of Alkali Metal Unanoborates. Radiochemistry **45**, 273-275 (2003).

92. Chernorukov, N. G., Smirnova, N. N., Knyazev, A. V., Marochkina, M. N., Bykova, T. A., Ershova, A. V.: The thermodynamic properties of calcium uranoborate. Russian Journal of Physical Chemistry **80**, 37-41 (2006).

93. Chernorukov, N. G., Smirnova, N. N., Knyazev, A. V., Marochkina, M. N., Ershova, A. V.: The thermodynamic properties of magnesium uranoborate tetrahydrate. Russian Journal of Physical Chemistry **80**, 1205-1209 (2006).

94. Chernorukov, N. G., Smirnova, N. N., Knyazev, A. V., Marochkina, M. N., Ershova, A. V.: The thermodynamic properties of uranyl metaborate. Russian Journal of Physical Chemistry **80**, 1915-1919 (2006).

95. Chernorukov, N. G., Smirnova, N. N., Knyazev, A. V., Marochkina, M. N., Ershova, A. V.: The thermodynamic properties of magnesium uranoborate. Russian Journal of Physical Chemistry A **81**, 683-687 (2007).

96. Karyakin, N. V., Chernorukov, N. G., Knyazev, A. V., Khomyakova, V. O., Smirnova, N. N.: Thermodynamics of Alkali Metal Uranoborates. Radiochemistry **47**, 136-149 (2005).

97. Karyakin, N., Chernorukov, N., Knyazev, A., Kortikova, O.: The thermodynamic characteristics of lithium uranoborate. Russian Journal of Physical Chemistry **77**, 1925-1928 (2003).

98. Behm, H.: Hexapotassium (Cyclo-Octahydroxotetracosaoxohexadecaborato)Dioxouranate(VI) Dodecahydrate, $K_6UO_2(B_{16}O_{24}(OH)_8)\cdot 12H_2O$. Acta Crystallographica Section C-Crystal Structure Communications **41**, 642-645 (1985).

99. Cousson, A., Gasperin, M.: Synthese et structure du borate de thorium: ThB_2O_5. Acta Crystallographica Section C **47**, 10-12 (1991).

100. Gasperin, M.: Synthese et structure du diborouranate de magnesium, MgB_2UO_7. Acta Crystallographica Section C **43**, 2264-2266 (1987).

101. Gasperin, M.: Synthesis and structure of sodium borouranate, $NaBUO_5$. Acta Crystallographica Section C-Crystal Structure Communications **44**, 415-416 (1988).

102. Li, L. Y., Jin, X. L., Li, G. B., Wang, Y. X., Liao, F. H., Yao, G. Q., Lin, J. H.: Novel rare earth polyborates. 2. Syntheses and structures. Chemistry of Materials **15**, 2253-2260 (2003).

103. Lu, P. C., Wang, Y. X., Lin, J. H., You, L. P.: A novel synthesis route to rare earth polyborates. Chemical Communications 1178-1179 (2001).

104. Wang, S. A., Alekseev, E. V., Depmeier, W., Albrecht-Schmitt, T. E.: Recent progress in actinide borate chemistry. Chemical Communications **47**, 10874-10885 (2011).

105. Polinski, M. J., Wang, S. A., Alekseev, E. V., Depmeier, W., Albrecht-Schmitt, T. E.: Bonding Changes in Plutonium(III) and Americium(III) Borates. Angewandte Chemie-International Edition **50**, 8891-8894 (2011).

106. Wang, S., Alekseev, E. V., Depmeier, W., Albrecht-Schmitt, T. E.: Surprising Coordination for Plutonium in the First Plutonium(III) Borate. Inorganic Chemistry **50**, 2079-2081 (2011).

107. Wang, S., Alekseev, E. V., Ling, J., Liu, G., Depmeier, W., Albrecht-Schmitt, T. E.: Polarity and chirality in uranyl borates: insights into understanding the vitrification of nuclear waste and the development of nonlinear optical materials. Chemistry of Materials **22**, 2155-2163 (2010).

108. Rabinowitch, E., Belford, R.: *Spectroscopy and Photophysics of Uranyl Compounds*. Pergamon Press Oxford (1964).

109. Beitz, J. V., Wester, D. W., Williams, C. W.: 5f state interaction with inner coordination sphere ligands: Es 3+ ion fluorescence in aqueous and organic phases. Journal of the Less Common Metals **93**, 331-338 (1983).

110. Nugent, L. J., Baybarz, R., Burnett, J.: Electron-transfer spectra and the II-III oxidation potentials of some lanthanide and actinide halides in solution. The Journal of Physical Chemistry **73**, 1177-1178 (1969).

111. Carnall, W., Goodman, G., Rajnak, K., Rana, R.: Report ANL-88-8. Argonne National Laboratory (1988).

112. Carnall, W., Beitz, J., Crosswhite, H.: Electronic energy level and intensity correlations in the spectra of the trivalent actinide aquo ions. III. Bk^{3+}. The Journal of chemical physics **80**, 2301-2308 (1984).

113. Fanghänel, T., Kim, J. I., Paviet, P., Klenze, R., Hauser, W.: Thermodynamics of radioactive trace-elements in concentrated electrolyte-solutions - hydrolysis of Cm^{3+} in NaCl-solutions. Radiochimica Acta **66-7**, 81-87 (1994).

114. Matsika, S., Pitzer, R. M.: Electronic spectrum of the NpO_2^{2+} and NpO_2^{+} ions. The Journal of Physical Chemistry A **104**, 4064-4068 (2000).

115. Atkins, E., Atkins, P. W., De Paula, J.: *Physikalische chemie*. John Wiley & Sons, (2013).

116. Hagan, P., Cleveland, J.: The absorption spectra of neptunium ions in perchloric acid solution. Journal of Inorganic and Nuclear Chemistry **28**, 2905-2909 (1966).

117. Rao, P. V., Gudi, N., Bagawde, S., Patil, S.: The complexing of Np (V) by some inorganic ligands. Journal of Inorganic and Nuclear Chemistry **41**, 235-239 (1979).

118. Matsika, S., Zhang, Z., Brozell, S., Blaudeau, J.-P., Wang, Q., Pitzer, R.: Electronic structure and spectra of actinyl ions. The Journal of Physical Chemistry A **105**, 3825-3828 (2001).

119. Diakonov, I., Tagirov, B., Ragnarsdottir, K.: Standard Thermodynamic Properties and Heat Capacity Equations for Rare Earth Element Hydroxides. Radiochimca Acta **81**, 107-116 (1998).

120. Jackson, N., Short, J.: The Separation of Neptunium and Plutonium by Ion Exchange. United Kingdom Atomic Energy Authority. Research Group. Atomic Energy Research Establishment, Harwell, Berks, England, (1959).

121. Sørensen, S., Linderstrøm-Lang, K.: On the determination and value of π 0 in electrometric measurements of hydrogen ion concentrations. Compt. rend. du Lab. Carlsberg **15**, 1-40 (1924).

122. Bates, R. G.: Definitions of pH scales. Chemical reviews **42**, 1-61 (1948).

123. Buck, R., Rondinini, S., Covington, A., Baucke, F., Brett, C., Camoes, M., Milton, M., Mussini, T., Naumann, R., Pratt, K.: Measurement of pH. Definition, standards, and procedures (IUPAC Recommendations 2002). Pure and Applied Chemistry **74**, 2169-2200 (2002).

124. Butler, J., Cogley, D.: *Ionic Equilibrium: Solubility and pH Calculations*. John Willey and Sons, New York (1998).

125. Knauss, K. G., Wolery, T. J., Jackson, K. J.: A new approach to measuring pH in brines and other concentrated electrolytes. Geochimica et Cosmochimica Acta **54**, 1519-1523 (1990).

126. Keller, C.: *Grundlagen der Radiochemie*. Otto Salle Verlag, Frankfurt am Main (1993).

127. Seah, M., Gilmore, I., Beamson, G.: XPS: binding energy calibration of electron spectrometers 5—re-evaluation of the reference energies. Surface and Interface Analysis **26**, 642-649 (1998).

128. Ravel, á., Newville, M.: ATHENA, ARTEMIS, HEPHAESTUS: data analysis for X-ray absorption spectroscopy using IFEFFIT. Journal of synchrotron radiation **12**, 537-541 (2005).

129. Ankudinov, A., Bouldin, C., Rehr, J., Sims, J., Hung, H.: Parallel calculation of electron multiple scattering using Lanczos algorithms. Physical Review B **65**, 104107 (2002).

130. Heberling, F., Scheinost, A. C., Bosbach, D.: Formation of a ternary neptunyl(V) biscarbonato inner-sphere sorption complex inhibits calcite growth rate. Journal of Contaminant Hydrology **124**, 50-56 (2011).

131. Coddington, J., Taylor, M.: High Field ^{11}B and ^{13}C Nmr Investigations of Aqueous Borate Solutions and Borate-Diol Complexes. Journal of coordination chemistry **20**, 27-38 (1989).

132. Müller, D., Grimmer, A. R., Timper, U., Heller, G., Shakibaie-Moghadam, M.: ^{11}B-MAS-NMR-Untersuchungen zur Anionenstruktur von Boraten. Zeitschrift für anorganische und allgemeine Chemie **619**, 1262-1268 (1993).

133. How, M., Kennedy, G., Mooney, E.: The pH dependence of the boron-11 chemical-shift of borate–boric acid solutions. Journal of the Chemical Society D: Chemical Communications 267-268 (1969).

134. Onak, T., Landesman, H., Williams, R., Shapiro, I.: The B-11 nuclear magnetic resonance chemical shifts and spin coupling values for various compounds. The Journal of Physical Chemistry **63**, 1533-1535 (1959).

135. Hertam, A.: ^{11}B-NMR spektroskopische Untersuchungen zum Lösungszustand von Boraten in konzentrierten Salzlösungen. Diplomarbeit, Technische Universität Bergakademie Freiberg (2011).

136. Borkowski, M., Richmann, M., Kalanke, S., Reed, D. T.: Borate chemistry and interactions with Actinides in high ionic strength solutions at moderate pH. In: Proceedings of the international workshop ABC-Salt in Karlsruhe (Germany), (2011).

137. JCPDS: Powder diffraction files, Joint Commitee on Powder Diffraction Standards. USA Swarthmore (2001).

138. Kimura, T., Choppin, G. R., Kato, Y., Yoshida, Z.: Determination of the hydration number of Cm(III) in various aqueous solutions. Radiochimica Acta **72**, 61-64 (1996).

139. Kim, J. I., Klenze, R., Wimmer, H., Runde, W., Hauser, W.: A study of the carbonate complexation of CmIII and EuIII by time-resolved laser fluorescence spectroscopy. Journal of Alloys and Compounds **213–214**, 333-340 (1994).

140. Fanghänel, T., Kim, J. I.: Spectroscopic evaluation of thermodynamics of trivalent actinides in brines. Journal of Alloys and Compounds **271–273**, 728-737 (1998).

141. Herm, M.: Untersuchung der Löslichkeit und Speziation von drei- und sechswertigen Actiniden in nitrathaltigen salinaren Lösungen. Diploma Thesis, Karlsruher Institute of Technology Karlsruhe (2012).

142. Wimmer, H., Klenze, R., Kim, J. I.: A study of Hydrolysis reaction of Curium(III) by Time Resolved Laser Fluorescence Spectroscopy. Radiochimica Acta **56**, 79-83 (1992).

143. Altmaier, M., Neck, V., Müller, R., Fanghänel, T.: Solubility of ThO_2 xH_2O (am) in carbonate solution and the formation of ternary Th (IV) hydroxide-carbonate complexes. Radiochimica Acta/International journal for chemical aspects of nuclear science and technology **93**, 83-92 (2005).

144. Altmaier, M., Neck, V., Denecke, M. A., Yin, R., Fanghanel, T.: Solubility of ThO_2xH_2O(am) and the formation of ternary Th(IV) hydroxide-carbonate complexes in $NaHCO_3$-Na_2CO_3 solutions containing 0-4 M NaCl. Radiochimica Acta **94**, 495-500 (2006).

145. Tits, J., Wieland, E., Bradbury, M.: The effect of isosaccharinic acid and gluconic acid on the retention of Eu (III), Am (III) and Th (IV) by calcite. Applied geochemistry **20**, 2082-2096 (2005).

146. Gaona, X., Montoya, V., Colàs, E., Grivé, M., Duro, L.: Review of the complexation of tetravalent actinides by ISA and gluconate under alkaline to hyperalkaline conditions. Journal of Contaminant Hydrology **102**, 217-227 (2008).

147. Yamaguchi, T., Sakamoto, Y., Ohnuki, T.: Effect of the complexation on solubility of Pu (IV) in aqueous carbonate system. Radiochimca Acta **66**, 9-14 (1994).

148. Rai, D., Hess, N. J., Felmy, A. R., Moore, D. A., Yui, M., Vitorge, P.: A thermodynamic model for the solubility of PuO_2(am) in the aqueous K^+-HCO_3^--CO_3^{2-}-OH^--H_2O system. Radiochimca Acta **86**, 89-100 (1999).

149. Larson, D., Haschke, J. M.: XPS-AES characterization of plutonium oxides and oxide carbide. The existence of plutonium monoxide. Inorganic Chemistry **20**, 1945-1950 (1981).

150. Larson, D., Motyl, K.: Detection of plutonium hydride using X-ray photoelectron spectroscopy. Journal of Electron Spectroscopy and Related Phenomena **50**, 67-76 (1990).

151. Holman, D. A., Bennett, D. W.: A multicomponent kinetics study of the anaerobic decomposition of aqueous sodium dithionite. The Journal of Physical Chemistry **98**, 13300-13307 (1994).

152. Münchow, V., Steudel, R.: The Decomposition of Aqueous Dithionite and its reactions with polythionates $SnO^{2-}{}_{6}$ (n= 3–5) studied by ion-pair chromatography. Zeitschrift für anorganische und allgemeine Chemie **620**, 121-126 (1994).

153. Fellhauer, D.: Personal Communication. (2015).

154. Rothe, J., Butorin, S., Dardenne, K., Denecke, M., Kienzler, B., Löble, M., Metz, V., Seibert, A., Steppert, M., Vitova, T.: The INE-Beamline for actinide science at ANKA. Review of Scientific Instruments **83**, 043105 (2012).

155. Wang, S., Alekseev, E. V., Ling, J., Skanthakumar, S., Soderholm, L., Depmeier, W., Albrecht-Schmitt, T. E.: Neptunium Diverges Sharply from Uranium and Plutonium in Crystalline Borate Matrixes: Insights into the Complex Behavior of the Early Actinides Relevant to Nuclear Waste Storage Angewandte Chemie **122**, 1190-1190 (2010).

156. Neck, V., Fanghänel, T., Rudolph, G., Kim, J.: Thermodynamics of Neptunium (V) in Concentrated Salt Solutions: Chloride Complexation and Ion Interaction (Pitzer) Parameters for the NpO_2^+ Ion. Radiochimca Acta **69**, 39-48 (1995).

157. Lucchini, J.-F., Borkowski, M., Richmann, M. K., Ballard, S., Reed, D. T.: Solubility of Nd^{3+} and UO_2^{2+} in WIPP brine as oxidation-state invariant analogs for plutonium. Journal of Alloys and Compounds **444**, 506-511 (2007).

158. Grenthe, I., Puigdomènech, I., Allard, B.: *Modelling in Aquatic Chemistry*. Nuclear Energy Agency, Organisation for Economic Co-operation and Development, Paris (1997).

159. Harvie, C. E., Møller, N., Weare, J. H.: The prediction of mineral solubilities in natural waters: The Na-K-Mg-Ca-H-Cl-SO_4-OH-HCO_3-CO_3-CO_2-H_2O system to high ionic strengths at 25°C. Geochimica et Cosmochimica Acta **48**, 723-751 (1984).

160. Hershey, J. P., Fernandez, M., Milne, P. J., Millero, F. J.: The ionization of boric acid in NaCl, Na-Ca-Cl and Na-Mg-Cl solutions at 25° C. Geochimica et Cosmochimica Acta **50**, 143-148 (1986).

161. Grenthe, I., Plyasunov, A.: On the use of semiempirical electrolyte theories for modeling of solution chemical data. Pure and applied chemistry **69**, 951-958 (1997).

162. Plyasunov, A., Fanghanel, T., Grenthe, I.: Estimation of the Pitzer Equation Parameters for Aqueous Complexes. A Case Study for Uranium at 298.15 K and 1 atm. Acta Chemica Scandinavica **52**, 250-260 (1998).

163. Hummel, W.: *Ionic strength corrections and estimations of SIT ion interaction coefficients*. PSI Report TM-44-09-01, Paul Scherrer Institut, Villigen (Switzerland) (2009).

Peer Reviewed Publikationen:

Hinz, K., Altmaier, M., Gaona, X., Rabung, Th., Schild, D., Richmann, M., Reed, D., Alekseev, E., Geckeis, H. (2015) Interaction of Nd(III) and Cm(III) with borate in dilute to concentrated alkaline NaCl, $MgCl_2$ and $CaCl_2$ solutions: solubility and TRLFS studies, New Journal of Chemistry, **39**, 849-859.

Vorträge:

Hinz, K., Altmaier, M., Rabung, Th., Geckeis, H. (2013) Complexation of An(III/IV) with borate in dilute to concentrated alkaline NaCl, $CaCl_2$ and $MgCl_2$ solutions. ABC-Salt Workshop ’13, Santa Fe (New Mexico, USA), April 15-17.

Hinz, K., Altmaier, M., Rabung, Th., Geckeis, (2013) H. Boratkomplexierung drei- und vierwertiger Actiniden in alkalischen NaCl, $CaCl_2$ und $MgCl_2$ Lösungen. GDCh Wissenschaftsforum Chemie 2013, Darmstadt (Germany), September 01-04.

Hinz, K., Altmaier, M., Gaona, X., Rabung, Th., Schild, D., Adam, C., Geckeis, H. (2013) Complexation of Nd(III)/Cm(III) with borate in dilute to concentrated alkaline NaCl, $MgCl_2$ and $CaCl_2$ solutions: solubility and TRLFS studies. 14^{th} International Conference on the Chemistry and Migration Behaviour of Actinides and Fission Products in the Geosphere (MIGRATION), Brighton (UK), September 08-13.

Hinz, K., Altmaier, M., Gaona, X., Rabung, Th., Alekseev, E., Schild, D., Geckeis, H. (2014) Interaction of An(III/IV/V and VI) with borate in dilute to concentrated NaCl, $CaCl_2$ and $MgCl_2$ solutions. 248^{th} ACS National Meeting, San Francisco (California, USA), August 10-14.

Hinz, K., Altmaier, M., Gaona, X., Rabung, Th., Alekseev, E., Schild, D., Geckeis, H. (2014) Interaction of An(III/IV/V and VI) with Borate in Dilute to Concentrated NaCl, $CaCl_2$ and $MgCl_2$ Solutions, Plutonium Futures – the Science 2014, September 7-12, Las Vegas, USA, 2014

Hinz, K., Gaona, X., Rabung, Fellhauer, D., Vespa, M., Schild, D., Dardenne, K., Altmaier, M., Geckeis, H. (2015) Interaction of Ln(III) and An(III/IV/V and VI) with borate in dilute to concentrated NaCl, $CaCl_2$ and $MgCl_2$ Solutions, ABC-Salt IV workshop, Heidelberg, April, 14-15.

Poster:

Hinz, K., Altmaier, M., Rabung, Th., Geckeis, H. (2011) Complexation of Nd(III)/Cm(III) with borate in dilute to concentrated alkaline NaCl and $CaCl_2$ solutions, ABC-Salt II workshop "Actinide Brine Chemistry in a Salt-Based Repository“, Karlsruhe (Germany), November 7-8.

Hinz, K., Altmaier, M., Rabung, Th., Richmann, M., Reed, D., Geckeis, H. (2012) Solubility and Speciation of Cm(III) and Nd(III) in borate rich NaCl and $CaCl_2$ solutions. Plutonium Futures “The Science” 2012, Cambridge (UK), July 15-20.

Hinz, K., Altmaier, M., Gaona, X., Rabung, Th., Alekseev, E., Schild, D., Geckeis, H. (2014) Interaction of An(III/IV/V and VI) with borate in dilute to concentrated NaCl, $CaCl_2$ and $MgCl_2$ solutions. 16th International Symposium on Solubility Phenomena and Related Equilibrium Processes (ISSP), Karlsruhe (Germany), July 21-25.

Hinz, K., Altmaier, M., Gaona, X., Fellhauer, D., Schild, D., Vespa, M., Dardenne, K., Geckeis, H. (2015) Interaction of Np(V) with borate in dilute to concentrated NaCl and $MgCl_2$ solutions. 15^{th} International Conference on the Chemistry and Migration Behaviour of Actinides and Fission Products in the Geosphere, Santa Fe, NM, USA, September, 13-18